Studies of Reaction Processes for Voloxidation Methods

A Dissertation
Presented for the
Doctor of Philosophy
Degree
The University of Tennessee, Knoxville

Jared Allen Johnson
May 2013

DEDICATION

I wish to dedicate this work to my parents, Mark and Karen Johnson, who instilled in me the traits that enabled me to complete this endeavor.

ACKNOWLEDGEMENTS

I would like to thank all those who have contributed in part to this research and my scientific and professional development. I would like to thank Dr. Pete Counce first and foremost for introducing me to research in the nuclear fuel cycle field and for always being available as a counselor for all matters. Your constant encouragement through my development has driven me. I would also like to thank Dr. Barry Spencer, Dr. Bill Del Cul, Dr. Rodney Hunt, and Emory Collins for passing their knowledge to the extent I have been capable of absorbing. You each have been influential mentors, and I aspire to one day hold the respect of the community you possess. I would also like to express my gratitude to Dr. Claudia Rawn for her advising on all parts diffraction and her encouragement and optimism that has rejuvenated my motivation countless times. I also express my appreciation to my other committee members, Dr. Jack Watson, Dr. David Keffer, and Dr. Tom Meek. Lastly, I would like to thank all those who aided me in the development of the proposal that made this research possible, especially Dr. David DePaoli.

ABSTRACT

Various facets of the voloxidation process and processes that have been derived from the voloxidation process have been investigated since its development over four decades ago. Despite the numerous studies performed, gaps remain in understanding of particular fundamental aspects of the reaction processes. In this work, several of these specific aspects of the oxidation processes for standard voloxidation and NO_2 [nitrogen dioxide] voloxidation are studied experimentally and modeled.

In the case of standard voloxidation, the oxidation rates of simulant UO_2 [uranium dioxide] pressurized water reactor pellets in oxygen-rich environments were studied with an emphasis on the controlling phenomena for the reaction and the influence of cladding on these phenomena. Parametric isolation experiments for the oxidation of UO_2 pellets using thermogravimetric analysis were employed in which oxidant concentration, temperature, gas flow rate, and effect of cladding were studied. To supplement the thermogravimetric experiments, the reaction interface was characterized using neutron diffraction to validate assumptions for model development. From these experiments, a model approach is derived for the oxidation of clad UO_2 pellets during voloxidation. This work provides needed insight into the influence of various parameters on oxidation rate and reveals the potential controlling phenomena and their parameter dependencies to allow for improved process design.

Advanced NO_2 voloxidation, unlike standard voloxidation, is a novel process only recently proposed and thus there is much to investigate. The NO_2 voloxidation experiments and reaction models presented focus on the oxidation process of U_3O_8

[triuranium octoxide] to UO_3 [uranium trioxide]. A structure for the ε [epsilon]-UO_3 polymorph is proposed and employed for *in situ* X-ray diffraction studies for quantitative analysis to determine reaction rates and reaction mechanism. The data collected were modeled using a phenomena-based approach to propose the controlling mechanism for reaction. From the findings of the research presented, a better understanding of the oxidation process of U_3O_8 to UO_3 by NO_2 was achieved.

TABLE OF CONTENTS

Introduction 1
Oxygen Voloxidation 3
NO_2 Voloxidation 5
References 8
Chapter 1 Literature Review 10
Abstract 11
1.1 Voloxidation Processes 11
1.2 Oxidation of Uranium Oxides by O_2 13
1.2.1 Oxidation Processes and Phases 14
1.3 Additional Variables Influencing Oxidation 22
1.4 Uranium Oxide Oxidation Models 26
1.4.1 Oxidation to U_3O_8 26
1.4.2 Voloxidation Modeling 29
1.5 Diffusion through Uranium Oxides 31
1.6 Structure of Uranium Oxides: Crystalline and Microscopic 39
1.7 Oxidation of Uranium Oxides by NO_2 42
References 46
Chapter 2 Oxidation of Surrogate and Used Nuclear Fuel Pellets 53
Abstract 54
2.1 Introduction 54
2.2 Experimental 57
2.2.1 Surrogate Materials 57
2.2.2 Experimental Equipment and Procedure 58
2.3 Results 61
2.3.1 Reaction Rates of Surrogates 61
2.3.2 Used Fuel Reaction Rate 68
2.4 Model and Discussion of Results 70
2.4.1 Model Approach 70
2.5 Model/Data Comparison 75
2.6 Conclusions 79
Acknowledgments 80
References 81
Chapter 3 Phase Mapping of Uranium Oxides Using Neutron Diffraction 83
Abstract 84
3.1 Introduction 84
3.2 Experimental 87
3.2.1 Sample Preparation 87
3.3 Diffraction Measurements 88
3.4 Results and Discussion 90
3.4.1 Neutron Diffraction Results 90
3.5 Comparison of Images to Diffraction Data 93
3.6 Conclusion 94

Acknowledgments 95
References 96
Chapter 4 Measurements Of Oxidation Kinetics for U_3O_8 to ε-UO_3 with NO_2 98
Abstract 99
4.1 Introduction 99
4.2 Experimental 102
4.3 Results and Discussion 104
4.4 Conclusions 112
Acknowledgments 112
References 113
Conclusions and Recommendations 115
Conclusions 116
Recommendations 118
Vita 120

LIST OF TABLES

Table 1.1. Proposed uranium oxide phases [69]. 40
Table 2.1. Average particle size and surface area of U_3O_8. 62
Table 3.1. Sample listing with reaction conditions. 88
Table 4.1. Model equations for surface and diffusion-controlled reaction. 109
Table 4.2. Effective diffusivities and front progression rates estimated by step-wise model approach. 110

LIST OF FIGURES

Figure i.1. Schematic of the oxidation clad UO_2 pellets. 5
Figure 1.1. Reaction curve character for three observed cases: (a) diffusion, (b) nucleation and growth, and (c) hybrid [10]. 16
Figure 1.2. Calculated U/O phase diagram with experimental data comparison [19, 20, 23-34]. 17
Figure 1.3. Cross-section of pellet oxidized at 400˚C [13]. 18
Figure 1.4. Sketch of proposed oxidation process [13]. 19
Figure 1.5. Oxidation of UO_2 particle at 300°C in He/O_2 (80/20) (50 μm scale shown) [37]. 21
Figure 1.6. Activation energy for atomic movement in a lattice [66]. 34
Figure 1.7. Schematic of grain oxidation [17]. 37
Figure 1.8. Cubic fluorite crystalline structure [66]. 40
Figure 1.9. Proposed UO_2 and U_3O_8 structures (not all oxygen atoms shown for clarity) [69]. 41
Figure 1.10. Equilibrium ratio of NO_x components at 1 atmosphere. 43
Figure 2.1. Scanning electron microscope image of cross-sectioned UO_2 pellet at 600x magnification. 58
Figure 2.2. Sketch of macro-thermogravimetric analysis system for unagitated samples. 59
Figure 2.3. Sketch of macro-thermogravimetric system for agitated samples. 60
Figure 2.4. Reaction kinetics for unclad UO_2 pellet oxidation to U_3O_8. 61
Figure 2.5. Scanning electron microscope images of U_3O_8 product from reaction temperatures of (a) 450°C, (b) 525°C, and (c) 600°C. 63
Figure 2.6. U_3O_8 product growing out of cladding. 64
Figure 2.7. Oxidation of clad UO_2 pellet exposed to air at 525°C. 65
Figure 2.8. Cross-section of partially reacted pellet, which plateaued during reaction. ... 66
Figure 2.9. Cross-section of clad pellet, which was reacted with agitation. 67
Figure 2.10. Conversion rate for clad UO_2 pellets to U_3O_8. 67
Figure 2.11. Conversion rate for a 2-in. clad Dresden fuel segment at 525°C in air (no agitation). 68
Figure 2.12. Swollen Dresden used nuclear fuel segment, post reaction. 69
Figure 2.13. Schematic of clad UO_2 oxidation system with potential controlling reaction phenomena. 71
Figure 2.14. Diffusion model for gas layer diffusion reaction control at 525°C and 1 atm air. 74
Figure 2.15. Schematic of clad UO_2 oxidation system with two product phases. 76
Figure 2.16. Reaction character of diffusion, reaction control, and hybrid. 78
Figure 3.1. Clad, partially reacted, depleted uranium oxide samples in aluminum tubes loaded for neutron diffraction measurements. 89
Figure 3.2(a-e). Neutron counts per minute summed for seven detectors for five partially reacted pellets as a function of height for the (220) peak for UO_2. 91
Figure 3.3. Raw data for 40-minute count times of "Pellet 3." 92

Figure 3.4. “Pellet 3” – U_3O_8 (002) reflection intensity as a function of distance. 93
Figure 3.5. “Pellet 5” cross-sectioned post reaction and measurement. 94
Figure 4.1. Custom designed environmental sample stage. 103
Figure 4.2. Scanning electron microscope image of ε-UO_3 product (200x). 104
Figure 4.3. X-ray powder diffraction data showing the reaction of U_3O_8 to UO_3 at 195°C. 105
Figure 4.4. Refined UO_3 phase fractions at 195, 210, 235, and 250°C. 106
Figure 4.5. Semi-log plot to test for model plot for first-order kinetics for data collected. 107
Figure 4.6. Refined amount of conversion as a function of time along with the model prediction for oxidation of U_3O_8 to UO_3 at 195°C. 111

INTRODUCTION

Introduction

Two of the greatest challenges for the prospect of reprocessing used nuclear fuel (UNF) in the U.S. are the development of processes that will reduce the release of particular volatile and semi-volatile fission products to meet permitted limits and reduce the costs associated with current fuel reprocessing technologies. Voloxidation methods can aid in overcoming these challenges and have been studied to a limited extent over the past few decades after research into reprocessing UNF in the U.S. was curtailed. With the ending of development of the Yucca Mountain nuclear waste repository and the ever-growing inventory of UNF being stored by the utility companies, the problem of dealing with UNF is nearing crisis proportions. A potential option for reducing quantities of nuclear waste, while allowing for reuse of fissile material, is a modified open nuclear fuel cycle. The modified open cycle is a hybrid between those described as closed and open cycles. In the closed process, almost all components are separated and all fissile materials are recovered. In an open cycle process, there is no recycle of material. The modified open cycle aims to reuse remaining fissile material to some extent but without the extensive processing required for a closed cycle. Countries that currently reprocess UNF use some form of modified open cycle for technical and economic reasons. New or improved separation methods are needed to meet the goal of safe, economical reprocessing in both the U.S. and other countries.

In almost all modified open and closed recycle processes, the first step requires the removal of the fuel from Zircaloy cladding. A voloxidation step enables this removal and provides the capability to separate and capture a variety of troublesome volatile and semi-volatile radionuclides prior to other separation processes that remove non-volatile fission products. Variations of the voloxidation process have been proposed for specific applications which will

each be discussed in greater detail. Some form of gas-solid thermal processing is likely to be included in any future reprocessing scheme whether it be a head-end step or the sole separation process. In any case, there is insufficient understanding of the fundamental science of the controlling phenomena and even less expertise has been developed for new advanced voloxidation techniques, specifically for NO_2 voloxidation.

This document provides a review of the relevant research for standard O_2 voloxidation as well as NO_2 voloxidation and identifies specific areas related to these processes which require further consideration and research. Following the review, there are three chapters that address specific gaps in our current understanding of these oxidation techniques. Two of these chapters (Chapters 2 and 3) specifically relate to standard voloxidation in which the influence of varied oxidation parameters and the influence of cladding is examined and modeled. To verify some assumptions used in these models and to characterize the reaction interface and oxide phase distribution, neutron diffraction interrogation of partially reacted clad pellets was employed. The third chapter (Chapter 4) is aimed at improving understanding of potential voloxidation techniques by investigating the kinetics and mechanism of NO_2 oxidation of U_3O_8 powder.

The sections forthcoming in this chapter provide a brief introduction to both O_2 and NO_2 voloxidation of UNF.

Oxygen Voloxidation

The original voloxidation process was developed at Oak Ridge National Laboratory (ORNL) as a method to remove tritium from UNF in the form of tritiated water by heating the fuel to ~450°C–600°C in air after being segmented into 2–7 cm lengths [1-5]. The original UNF, mainly monolithic cubic UO_2 (10.96 gm/cm^3), is converted to orthorhombic U_3O_8 (8.3 g/cm^3) powder under these conditions and undergoes a ~36% crystalline volume increase resulting in

comminution of the fuel [6]. Previous work found that a fraction of other fission products including ruthenium, iodine, carbon, xenon, and krypton are released during the process [1-5]. Since the original development of the voloxidation process, advanced voloxidation methods have been proposed and investigated in order to release more of the volatile and semi-volatile fission products and form a product with advantageous properties for subsequent processing. In addition to the potential use as a head-end process for reprocessing UNF for a variety of proposed schemes, the voloxidation methods are also under consideration as a preconditioning process for the removal of the fuel from Zircaloy cladding for safe storage. Voloxidation techniques have even been considered as a sole process in a modified open reprocessing cycle.

Following the literature review provided in Chapter 1, Chapters 2 and 3 of this work provide new insight into the reaction of clad fuel with O_2 in standard voloxidation processes. These chapters provide novel qualitative and quantitative insight into the phenomena occurring and controlling reactions. It was believed that there could be five phenomena occurring during the voloxidation process; however, it had yet to be determined conclusively which of these, or combination thereof, control or limit the rate of the reaction under particular conditions. The diffusion of the oxidant through a stagnant gas, if present, would be the first potentially controlling process followed by the diffusion of the oxidant through the unspalled “ash” or product layer, whether it is U_3O_8 or intermediates such as U_3O_7 and U_4O_9 (Figure i.1.). The extent to which these intermediates are present is debated in Chapter 3, which also includes results of experiments using neutron diffraction [7, 8]. The actual kinetics of the oxidation are then considered and finally, the diffusion of nonoxidizing gases through the bulk gas phase is considered.

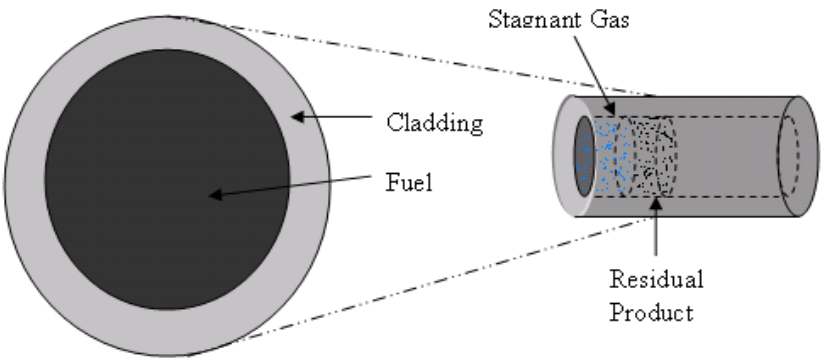


Figure i.1. Schematic of the oxidation clad UO_2 pellets.

Other phenomena can influence the model of the previously described processes such as the rate a product ash builds or falls away as it is comminuted or density changes of the product layer.

While other attempts to model these phenomena based solely on conventional theory have been performed, it is necessary to couple modeling with experiments to determine to what extent variables such as temperature, oxidant concentration, and cladding influence the behavior and to extract other potentially unforeseen phenomena in this complex process. This work is meant to gain a better understanding of the conversion of clad UO_2 pellets to U_3O_8 powder and to develop a base model in which the most influential parameters of a given voloxidation process are deduced.

NO_2 Voloxidation

An alternate voloxidation method using NO_2 as an oxidant at temperatures lower than standard voloxidation has recently been proposed at ORNL for which a provisional patent has been granted [9]. The final oxide product of the reaction of UO_2 with NO_2 is ε-UO_3 after intermediate formation of U_3O_8. It has been proposed that the desired reaction be achieved by a

two-step process. Based on preliminary studies, the initial reaction of UO_2 to U_3O_8 is proposed to be performed at ~350°C where UO_3 formation from UO_2 pellets has been observed to be slow. The cooling of the system to a temperature of ~250°C has been recommended for the second oxidation reaction [9]. The reaction can be performed at lower temperatures (185°C) but with slower kinetics [10]. Further reduction of the temperature after oxide formation results in the formation of $UO_2(NO_3)_3NO$ (uranyl nitrosyl nitrate) which decomposes to $UO_2(NO_3)_2$ (uranyl nitrate salt) [9].

The volatile component release rates using NO_2 have not yet been studied; however, preliminary studies suggest oxidation rates greater than those in air. An increase in fission product release is likely due to several processes. The additional phase change will increase surface area reducing the diffusion path length for volatiles and semi-volatiles to escape. The higher oxidation potential of NO_2 has been observed to liberate iodide from CsI, the chemical form which most iodine is found in UNF, by reaction to form $CsNO_3$ [11, 12]. The removal and trapping of ^{129}I is a significant challenge for reprocessing fuel due to its low release limit and resulting need for decontamination factors greater than 1000 for the majority of UNF [13]. While the bulk of iodine (~95–99%) can be released during dissolution, those countries currently reprocessing are forced to attempt to trap the remaining iodine at a number of points in subsequent processes as it distributes to both organic and aqueous phases. Therefore, the ability to release and trap ^{129}I in a head-end process could allow reprocessing to be more attractive in the U.S. as it would enable compliance with the low release limit while eliminating the expense of multiple subsequent trapping systems. Potential optimized designs featuring recycle of NO_x with regeneration of NO_2 from NO via addition of O_2 limit quantities of off-gas needing treatment as well as concentrate the volatile and semi-volatile fission products for trapping. The solubility

properties of a UO_3 product are also advantageous to reprocessing as UO_3 readily dissolves in dilute nitric acid (0.3 *M* or greater) with little to no NO_x evolution. The dissolution in a low-acid system is ideal for solvent extraction processes such as UREX, and the great reduction of dissolver off-gas impacts both vessel design size and off-gas handling [9].

While numerous proof-of-principle experiments have been conducted in recent years with surrogate and actual used fuel at ORNL to validate a number of the components of the proposed NO_2 process, many aspects are not fully understood [9]. The NO_2 voloxidation relevant research presented in Chapter 4 provides fundamental information on the structure of ε-UO_3 and the kinetics of its formation from U_3O_8 by reaction with NO_2. A structure of the UO_3 polymorph of interest is proposed from data analysis of neutron and X-ray diffraction (XRD) patterns collected at the Spallation Neutron Source (SNS) POWGEN, the High Flux Isotope Reactor (HFIR) HB-2A, and at the High Temperature Materials Laboratory (HTML) X-ray diffractometers. Additionally, experiments to measure reaction kinetics were performed by means of *in situ* XRD measurements using a custom sample stage. The kinetic data generated from quantitative analysis by refinement of the data using the proposed ε-UO_3 structure was analyzed for reaction model development [14].

This work is intended to examine traditional and newly conceived advanced voloxidation methods and develop an understanding of the essential phenomena controlling the reaction of both standard voloxidation and NO_2 voloxidation, as these are both promising technologies for future UNF recycling applications.

References

1. Goode, J.H., *Voloxidation - Removal of Volatile Fission Products from Spent LMFBR Fuels.* ORNL-TM-3723, Union Carbide Corporation, Oak Ridge National Laboratory, January 1973.

2. Goode, J.H., R.G. Stacy, and V.C.A. Vaughen, *Head-End Reprocessing Studies with H. B. Robinson-2 Fuel.* ORNL-TM-6037, Union Carbide Corporation, Oak Ridge National Laboratory, June 1978.

3. Goode, J.H., *et al*., *Comparison Studies of Head-End Reprocessing Using Three LWR Fuels.* ORNL-TM-7103, Union Carbide Corporation, Oak Ridge National Laboratory, June 1980.

4. Spencer, B.B., *et al*., *GNEP Coupled End-to-End Demonstration Project: Head-End Processing and Tritium Removal using Voloxidation*. in *32nd Annual Actinide Separations Conference*. 2008. Park City, Utah.

5. Spencer, B.B., *et al*., *Voloxidation Processing of Kilogram Quantities of Used Nuclear Fuel*. in *Sixteenth Symposium on Separation Science and Technology for Energy Applications*. 2009. Gatlinburg, Tennessee.

6. McEachern, R.J. and P. Taylor, *A review of the oxidation of uranium dioxide at temperatures below 400°C.* Journal of Nuclear Materials, 1998. **254**(2-3): p. 87-121.

7. McCracken, D.R., *Oxidation of UO_2 at 400°C to 1000°C in Air and its Relevance to Fission Product Release.* AECL-8642, Chalk River Nuclear Laboratories, Atomic Energy of Canada Limited, July 1985.

8. McEachern, R.J., *et al*., *Determination of the activation energy for the formation of U_3O_8 on UO_2.* Journal of Nuclear Materials, 1997. **249**(1): p. 58-69.

9. Del Cul, G.D., *et al*., *Conceptual Design of a Simplified Head-End Process for the Recycling of Used Nuclear Fuel*. in *American Nuclear Society 2012 Annual Meeting*. 2012. Chicago, Illinois.

10. Kobets, L.V. and G.N. Klavsut, *Behavior of U_3O_8 in Dissociating Gaseous Dinitrogen Tetroxide.* Soviet Radiochemistry, 1986. **28**(6): p. 657-660.

11. Busker, G., R.W. Grimes, and M.R. Bradford, *The diffusion of iodine and caesium in the $UO_{2 +/- x}$ lattice.* Journal of Nuclear Materials, 2000. **279**(1): p. 46-50.

12. Grimes, R.W., R.G.J. Ball, and C.R.A. Catlow, *Site Preference and Binding of Iodine and Cesium in Uranium-Dioxide.* Journal of Physics and Chemistry of Solids, 1992. **53**(4): p. 475-484.

13. Jubin, R.T., *et al*., *Position Paper on Practicable Performance Criteria for the Removal Efficiency of Volatile Radionuclides.* INL/EXT-12-25410, Battelle Energy Alliance, Idaho National Laboratory, March 2012.

14. Johnson, J.A., *et al*., *Kinetic Studies of NO_2 Oxidation of Uranium Oxides by In Situ XRD and Neutron Diffraction*. in *American Nuclear Society inter Meeting*. 2012. San Diego, California.

CHAPTER 1

LITERATURE REVIEW

Abstract

The following literature review is intended to provide an analysis of the essential phenomena related to voloxidation processes and an evaluation of the extent to which they are currently understood. The review first describes the voloxidation process and its derivatives and then delves deeper into the oxidation reactions, variables effecting oxidation, and modeling approaches that have been employed or that are relevant to the oxidation process. Finally, the oxidation process of uranium oxides by NO_2 is examined and pertinent literature summarized.

1.1 Voloxidation Processes

There have been a number of variations of standard voloxidation proposed and demonstrated. The goal of these processes is increased release of volatile and semi-volatile fission products. One approach to achieving this is the control of oxide product properties such as surface area. With increases in oxidation temperature above ~500°C, U_3O_8 product particle size has been observed to increase and particle surface area decrease; therefore, voloxidation at temperatures of 400–480°C results in a product with a higher surface area reducing the path for diffusion of volatile and semi-volatile fission products. However, the lower temperature reduces the diffusion rate of the volatile components. The previously proposed techniques described below attempt to increase reaction rates by increasing the product surface area and/or by increasing diffusion rates and volatility of semi-volatiles using higher temperatures.

One voloxidation alternative is AIROX (Atomics International Reduction OXidation), which was proposed for a used nuclear fuel (UNF) recycle process in which light water reactor (LWR) fuel is treated by AIROX to remove volatile and semi-volatiles before enrichment of AIROX product by blending with highly enriched U/Pu oxide. The process involves puncturing

the fuel cladding before oxidation/reduction cycling of fuel using an oxygen-rich atmosphere for oxidation and a hydrogen/argon or nitrogen atmosphere for reduction. In this process, it is essential to remove as much of the volatile and semi-volatile fission products as possible because the treated fuel is to be reused without further separations. Demonstrations in which the fuel was heated to temperatures greater than the initially proposed 400–600°C (up to 1800°C) resulted in the release of all volatile and a large portion of semi-volatile fission products including C, Kr, Xe, I, Ru, and fractions of other components such as Mo, Rh, Te, and Cs. Experiments under reduced pressure showed an increase in the release of semi-volatiles. At temperatures above 875°C, the uranium oxide product from this reaction is the hexagonal β-U_3O_8 [1-4].

Another process designed to exploit fracturing of uranium oxide grains due to oxide crystalline structure changes caused by oxidation is OREOX (Oxidation and REduction of OXide fuel). This process is proposed to support the Direct Use of Pressurized water reactor spent fuel In the CANadian Deuterium Uranium reactor (DUPIC) process. Like the AIROX process, OREOX consists of cycling between oxidation and hydrogen reduction of fuel powder to increase surface area due to the expansion and contraction of the crystal structure. In this particular process, oxidation of fuel is conducted at 500°C in air with the reduction back to UO_2 at 700°C in Ar-4%H_2. Cycling the fuel up to three times has been proposed with a resulting total increase in surface area of up to a factor of five for simulated high-burnup nuclear fuel (SIMFUEL) [5, 6].

DEOX (DEclad via OXidation) is an oxidation process conducted at higher temperatures than standard voloxidation (up to1100°C). The process differs from AIROX and OREOX in the absence of oxidation/reduction cycling and that it is not intended as a sole separation process. Instead, it was designed to support further reprocessing, in particular, electrorefining. The fuel is

oxidized at the higher temperatures to produce an oxide product with a greater particle size to reduce dispersion issues as well as to increase the release of semi-volatiles [7-9].

While each of these processes has a unique name, all are intended to remove fuel from cladding for subsequent processing and to remove volatile and semi-volatile fission products. Though additional fission product release at elevated temperatures is often desired, treatment of UNF at these temperatures does have unfavorable consequences. Heating to these high temperatures (>600°C) requires reactors constructed of expensive materials, and the longevity is reduced resulting in the costly replacement and disposal of contaminated equipment. Additionally, the higher temperature treatment also reduces dissolution kinetics.

1.2 Oxidation of Uranium Oxides by O_2

The research reported to date for the oxidation of UO_2 to U_3O_8 is broad in both approach and motivation. In spite of the extensive studies in the field of uranium oxidation, there remain gaps in the understanding of the oxidation process and even more for the specific conditions typical for oxidation in a voloxidation process. Research on oxidation by O_2 has primarily been focused on reactions under 400°C. Fewer studies of higher temperature oxidation of UO_2 by O_2 are those of interest for the application of standard voloxidation. This section is intended to provide an overview of various approaches used to investigate the oxidation processes and the complexity of the system.

1.2.1 Oxidation Processes and Phases

The oxidation reaction relevant for voloxidation studies is the transformation of UO_2 to U_3O_8 in the temperature range of 450–600°C. While this is the range of interest, studies of the process at lower temperatures provide a more clear understanding of the steps in the transformation. The oxidation at temperatures below 350°C has been observed to proceed by two separate steps, each with differing controlling mechanisms, via Equation 1.1.

$$UO_2 \rightarrow U_4O_9 \,/\, U_3O_7 \rightarrow U_3O_8 \tag{1.1}$$

The first step in the reaction is the oxidation of UO_2 to the intermediates U_3O_7, U_4O_9, or sub- and hyperstoichiometric ratios of U_3O_7 and U_4O_9. The reaction to these intermediates which will be referred to here on as U_4O_9/U_3O_7 proceeds by a parabolic reaction curve indicative of diffusion control. The transition to these intermediate phases is accompanied by a slight crystalline volume reduction from that of UO_2 (~2%) which is thought to induce fracturing at the grain boundaries [10]. The presence and quantities of each of these phases is a function of temperature and other variables such as impurities, which will be discussed in Section 2.3. The formation of intermediate phases has been observed and is predicted by thermodynamic calculations [11]. However, there are conflicting reports of the formation of these phases under particular conditions. A majority of the studies report the absence of the intermediates above 350°C while others report the presence of these phases at temperatures exceeding 1000°C [10, 12-16].

Unlike the initial diffusion-controlled oxidation to the intermediates, the reaction to U_3O_8 displays a sigmoidal curve typical of nucleation and growth or an autocatalytic reaction. The product, U_3O_8, has been found to have a particle size similar to that of the initial UO_2 grains with

a “popcorn” type appearance, which is believed to be a result of the tensile forces generated when different regions within the grain expand due to phase change [10].

Examples of the reaction curves that characterize the three observed behaviors for the oxidation of UO_2 are shown in Figure 1.1 where (1.1a) is a reaction curve that corresponds to diffusion limited reaction (< ~300°C) while (1.1b) is typically observed in reactions that are occurring via nucleation and growth (> ~350°C). A hybrid of the two is shown in plot (1.1c) whose shape has been observed for reaction of UO_2 at intermediate temperatures around 300°C [17].

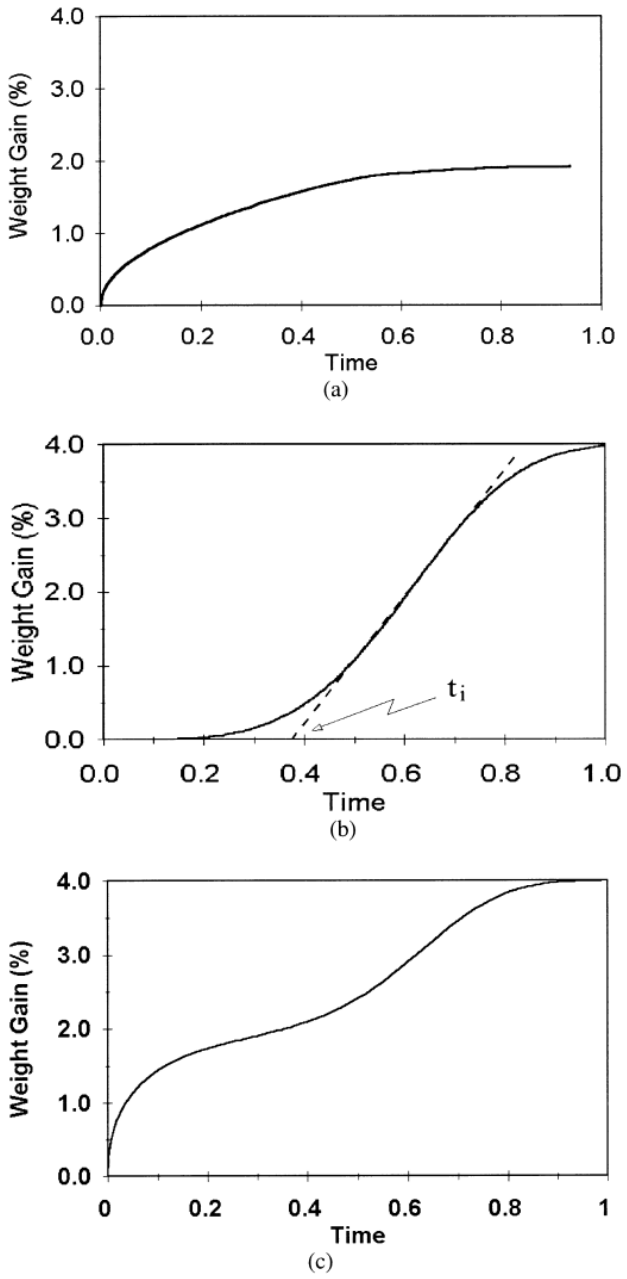
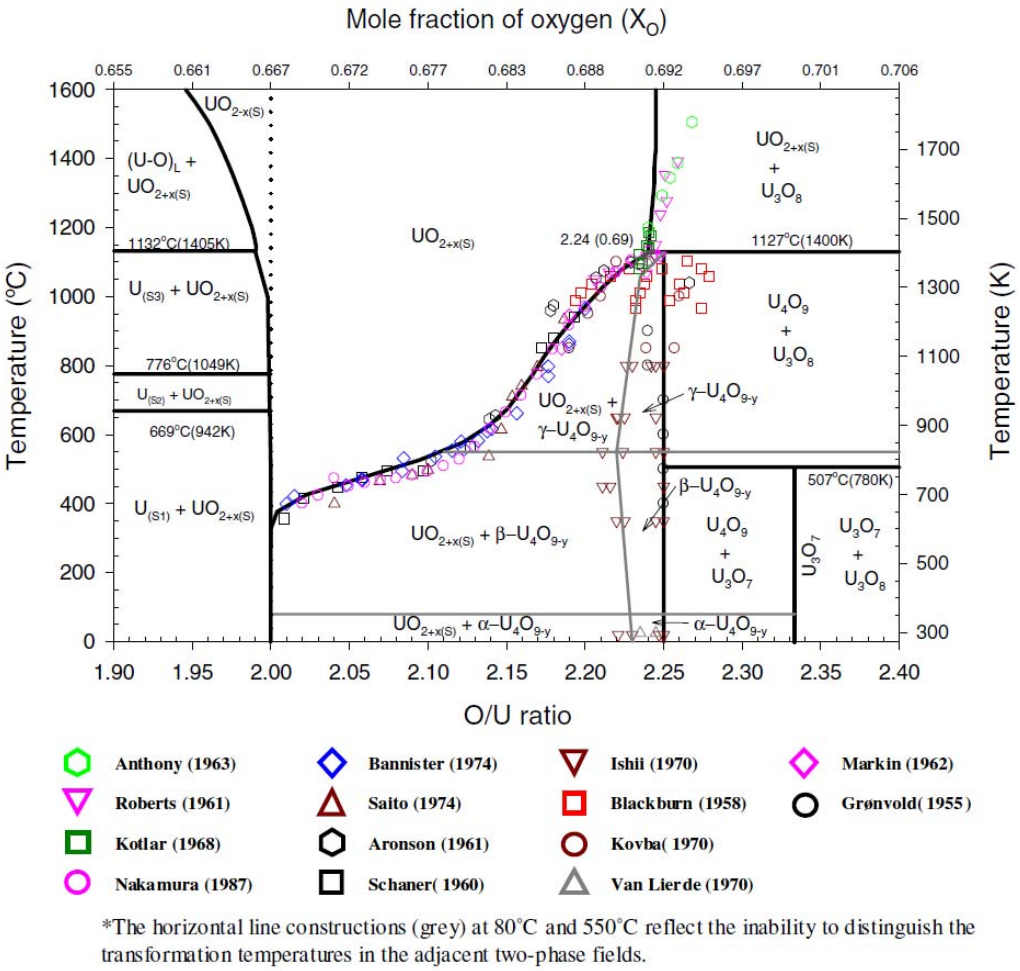


Figure 1.1. Reaction curve character for three observed cases: (a) diffusion, (b) nucleation and growth, and (c) hybrid [10].

The presence and quantity of each phase and other less stable transition U/O phases are a function of temperature as shown in the phase diagram for the U/O system in Figure 1.2. The phase diagram shown includes experimental data from various sources for the phase boundary of U_4O_{9-y} presented by Higgs *et al*. [11]. There have been a number of proposed phase diagrams for

the U/O system [18-24]. While the majority of proposed phase diagrams over the years are very similar, there are differences in predicted phases at particular conditions for the intermediates previously mentioned. However, the diagrams generated from thermodynamic data do suggest the presence of some fraction of intermediate at temperatures well above 1000°C even though, as previously mentioned, they have rarely been detected.



*The horizontal line constructions (grey) at 80°C and 550°C reflect the inability to distinguish the transformation temperatures in the adjacent two-phase fields.

Figure 1.2. Calculated U/O phase diagram with experimental data comparison [19, 20, 23-34].

While there has been substantial effort to understand the chemical reaction and phase transitions, there has been less effort aimed at understanding the process at a micro and macro

scale. Studies reported by Bae *et al*. elucidate the influence spallation of grains and associated intergranular and intragranular cracking on the reaction rate [13]. Unlike a majority of studies of reaction rate, this research was spawned from interest in a voloxidation type process. Therefore, their study focuses on higher reaction temperatures that few studies address. Unirradiated UO_2 pellets and granular UO_2 were oxidized in air at temperatures ranging from 350°C to 500°C and examined by microscopy. It was concluded that, at 400°C, intermediates such as U_4O_9 are formed. This contradicts other studies; however, the use of macro-XRD in a number of the year>1999</year></dates><pub-location>New York</pub-location><publisher>John Wiley suggested as the cause for the lack of identification of the intermediates [13]. A revealing image of the cracking process is shown in Figure 1.3 in which a cross-section of a pellet is shown where cracks of various sizes can be observed. An image of the cross-section of a pellet during the cracking process shown in Figure 1.3 illustrates how cracks of various sizes are formed.[13].

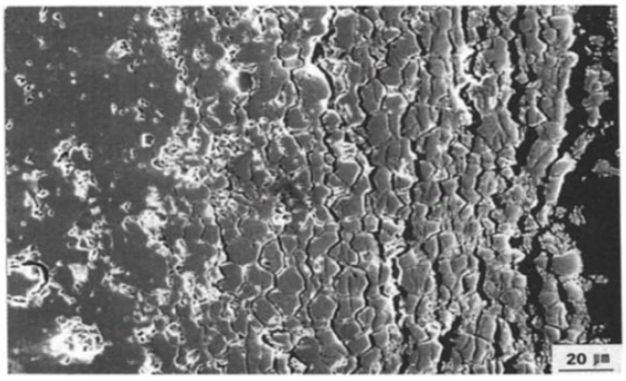


Figure 1.3. Cross-section of pellet oxidized at 400˚C [13].

The results of the Bae *et al*. study culminated in a proposed process for oxidation and spallation and was supported by the images taken throughout the oxidation process. It is believed the oxidation process begins with the reaction at the surface of UO_2 to form intermediate oxides

(U_4O_9/U_3O_7). The volume reduction due to the crystalline structure change causes grain boundary cracking which results in initial spallation of the oxides. As the oxidation progresses, U_3O_8 begins to form on the spalled grains as well as the unspalled grains at cracked grain boundaries, and this accelerates the spallation process. It is believed that spalling of grains mainly occurs along the intergranular cracks. This overall process mechanism is proposed specifically for temperatures around 400°C [13]. Below 400°C the formation of intermediates is thought to be more extensive before any U_3O_8 is formed, and at temperatures above 600°C the process is retarded by the induced plasticity of the material that slows the spallation rate [35]. A schematic of the proposed process is shown in Figure 1.4.

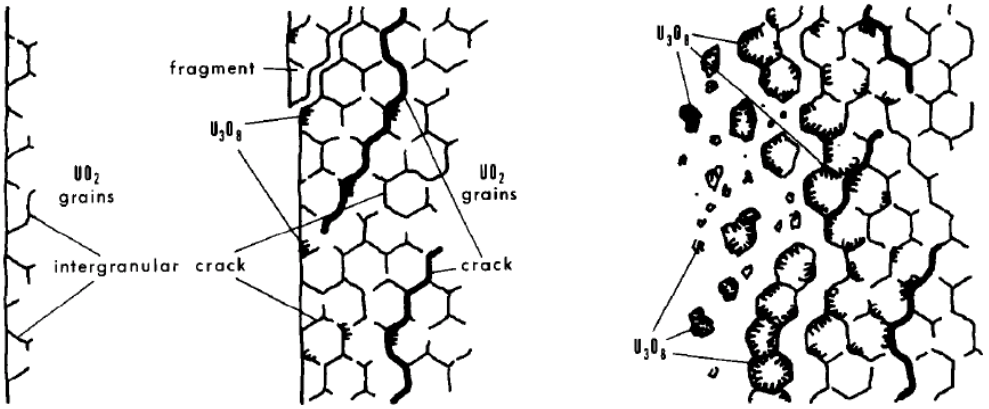


Figure 1.4. Sketch of proposed oxidation process [13].

Quemard *et al*. attempted to couple this mechanism to chemical reaction kinetics to give a better understanding of the phenomena occurring and how they correspond to the reaction rate curves for the oxidation of unirradiated UO_2 [13, 14, 36, 37]. From this work, it is hypothesized the reaction is controlled by the exposed surface caused by cracking of the uranium oxide upon phase transition. The authors point to the previous work in which a sigmoidal rate curve is

developed based on cracking induced reaction, but it is noted that the cracking of UO_2 is less understood when compared to that of cubic niobium, which was the focus of the reference work [38]. It is also concluded that a nucleation and growth model for the oxidation of UO_2 pellets is not physically representative of the process although the reaction curve character is sigmoidal [13, 37].

It was found by Quemard *et al*. and supported by Bae *et al*. that the initial incubation period observed in the reaction curve corresponds to the initial formation of U_4O_9/U_3O_7 leading to formation of macro-cracking at grain boundaries [13, 37]. After the macro-cracking, the reaction rate increases as there is a larger surface area exposed. It was also observed via XRD that the cracking of the intermediate oxides penetrates to fresh UO_2. It is proposed that the oxide layer thickness required for cracking to occur is less than 1 μm at the given conditions (300°C in air). Micro-cracking was found to then occur at the macro-crack surfaces. This cracking is likely evidence of the formation of U_3O_8. Based on these findings, the time to initial cracking and this time's dependence on such factors as temperature and environment are of great importance. It is believed the cracking begins at a given thickness for a given composition and that the temperature dependence is merely related to the diffusion rate for which oxygen penetrates the $UO_2/U_4O_9/U_3O_7$. An increase in volume due to cracking and expansion of up to 200% was observed for a particle under microscopy. Images taken of the particle being oxidized at 330°C correlated to the reaction conversion rate as shown in Figure 1.5 giving insight into the reaction at temperatures lower than those typical of voloxidation processes where "bulk area (%)" is the percent area increase from initial particle area observed by microscopy [37].

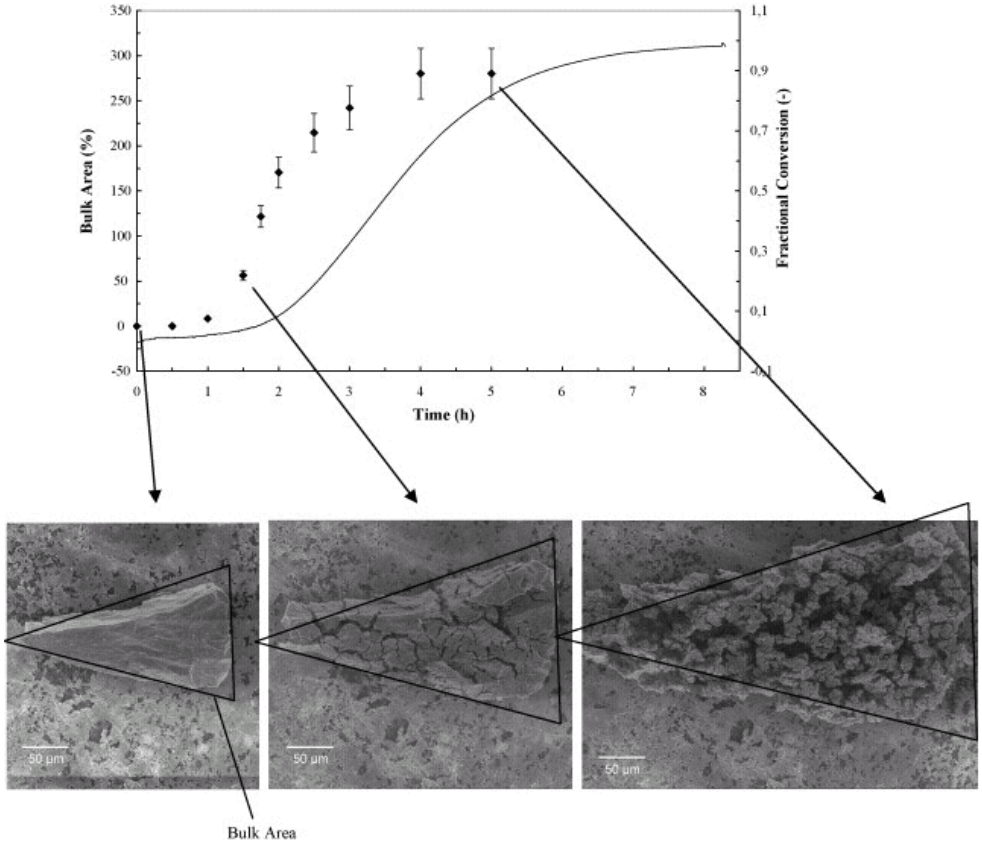


Figure 1.5. Oxidation of UO_2 particle at 300°C in He/O_2 (80/20) (50 µm scale shown) [37].

Based on the observations in their study, the authors suggest that a process is occurring in which initial cracking of the intermediate phases occurs after an incubation period. It is thought oxygen diffuses to create a critical thickness of oxide after which continued macro-cracking occurs with conversion of UO_2 to intermediates taking place simultaneously with nucleation and growth of U_3O_8. This conversion causes micro-fracturing until complete fracture takes place, corresponding to the initial leveling of the conversion curve. The reaction finishes with final nucleation and growth of U_3O_8 until all UO_2 is consumed. This mechanism was found to hold for both high and low temperatures even though at 400°C the metastable U_3O_7 phase was not observed but instead a UO_{2+x} phase was observed which also induces the initial cracking [37].

These studies probed the oxidation process at the micro-scale to propose a reaction mechanism. Several conclusions for the research to be presented in this dissertation can be drawn from these findings in this section. One of the most important conclusions is that the use of a nucleation and growth model for the oxidation UO_2 pellets is not a completely accurate representation of the process. Many have used such a model because it readily fits the observed sigmoidal reaction curve for oxidation of UO_2 pellets and the observation that at the reaction surface U_3O_8 does form by a nucleation and growth process. However, the basis of the frequently employed nucleation and growth models for oxidation of UO_2 pellets in gas-solid contact through the reaction volume which is not accurate for this case. Therefore, this model only has its place when examining surface reaction of the UO_2 pellets and will not be applied to the overall reaction of clad or unclad pellets. Another impactful conclusion from work performed by others is the "mechanical" mechanism by which the oxidation occurs. It is important to view the oxidation process as not a solely diffusive or chemical reaction process.

1.3 Additional Variables Influencing Oxidation

While oxidation temperature and oxidant concentration have been shown to be the most influential parameters for the oxidation of UO_2, studies have shown that other variables can affect the oxidation rates.

In gas-solid reactions, the thermodynamics of adsorption of the gas on the solid must be considered. Studies have been performed for the case of O_2 adsorbing onto UO_2 and have been found to be highly exothermic (-230 kJ/mol) with very low activation energy [39]. While this process occurs as part of the oxidation process, the details are of little interest in the current work

as it is apparent it does not serve as a rate-controlling process for reaction in the system of interest [10].

The influence of moisture or humidity on O_2 oxidation of UO_2 has been studied in some detail, with the results of the effects of H_2O on oxidation being somewhat varied and contradictory as to its effect on oxidation rate [10]. At elevated temperatures and atmospheric pressure, it has been found that steam alone cannot oxidize UO_2 to unhydrated forms past fluorite-type UO_{2+x}. It is possible that the presence of water can cause the formation of UO_3-xH_2O compounds such as schoepite and other oxide hydrates [40, 41]. Others have even found that water can enhance oxygen diffusion along grain boundaries in sintered pellets [42]. However, at relative humidity less than 40%, the products do not differ from that of dry air, while in the presence of higher humidity the UO_3-H_2O compounds can form [43].

The age of fuel pellets has been reported to affect the rate of oxidation. It has been observed that a thin layer of UO_3 or UO_3 hydrate can form on the surface over time, which has been found to inhibit further oxidation. The time to U_3O_8 powdering was also found to be significantly increased with age of the fuel or UO_2 simulant [44, 45].

It has been observed by researchers that impurities introduced during irradiation, such as rare earth species and plutonium, have an effect on the rate and mechanism of oxidation of the fuel. Fission products have been found to stabilize a U_4O_{9+y} phase that is preferentially formed over the U_3O_7 phase typically observed in the oxidation of UO_2, and the UO_2 has been found to hold its fluorite structure at higher temperatures and longer times than UO_2 absent of impurities for oxidation under 195°C [46-51]. The pathway by which UO_2 is oxidized has been reported to be quite different for irradiated versus unirradiated UO_2 fuels and, furthermore, there are observed differences in oxidation rates among irradiated fuels based on burnup, linear reactor

power, and gas release. For unirradiated UO_2, it has been found that the reaction occurs by Equation 1.1; however, the reaction for irradiated fuel is somewhat different due to the stabilization of U_4O_9, thought to be caused by fission products.

$$UO_2 \rightarrow U_4O_9 \rightarrow U_4O_{9+y} \rightarrow U_3O_8 \quad (1.2)$$

Another study specifically focused on examining the reaction of both irradiated and unirradiated UO_2 oxide fuel segments, taken from a pressurized water reactor (PWR) fuel manufacturer, to U_3O_8 under identical conditions at temperatures 150°C–375°C [50]. The initial weight gain was observed to be faster for irradiated fuel, but the complete reaction was much slower and in some cases, incomplete. This is believed to be a result of two main processes — the formation of fission products and changes in microstructure. Fission product gases are known to diffuse to grain boundaries and form "bubbles," which were observed in one study to range from 2–10 nm [52]. These gasses coalesce at the grain boundaries and are thought to create a somewhat interlinked pathway for the oxidant to diffuse through, thereby, increasing the overall reaction surface area. The inhibition of continued reaction is thought to be a result of microstructure effects as the temperatures reached during irradiation likely change the micro-structure [51]. The effect of irradiation-induced vacancies in the lattice increasing oxygen diffusion rates has been found to be negligible, as low burnup LWR fuel has shown annealing around 200°C to 300°C [53, 54]. Boase and Vandergraaf found an increase in oxidation rate with used CANDU fuel powder of 3 to 3.5 times at temperatures between 200°C and 300°C, while the oxidation rate for pellets in the range of 300°C to 460°C had no observable signifigant difference [55]. Although studies with impurities showed effects on intermediate formation and an overall slowed reaction

due to the stabilty of the cubic U_4O_{9+y} versus that of the tetragonal U_3O_7, experiments with irradiated UO_2 have shown varied results in oxidation rates with temperature. There have not been sufficient studies to be able to quantify the effects of irradiation on oxidation.

Another parameter with potential to influence oxidation rate and mechanism is the rate at which the oxidation temperature is increased [56]. It has been concluded that there is a definitive U_3O_7 phase formed in an oxygen atmosphere when the UO_2 is heated to temperatures above 200°C at a rate of 10°C/min. If the UO_2 is introduced to an environment of temperatures of 300°C or ramped to this temperature at rates of 20°C/min, a U_3O_7 phase was not observed by the experimenter [56]. The effects of annealing U_3O_7 have also been investigated by holding a temperature of 200°C for varying amounts of time. This annealing effect of the U_3O_7 was found to retard the subsequent oxidation to U_3O_8 upon an increase in temperature [56].

From the review presented in this section, it is clear that there are numerous variables that have been researched for the oxidation of UO_2, and in some cases, that have been observed to have a significant impact on oxidation rates. It is clear that these additional variables, coupled with the primary parameters (temperature, oxidant concentration, UO_2 density, and grain size), make the prediction of used fuel oxidation rates difficult at best. Therefore, the research presented in the following three chapters focuses on gaining a better understanding and the development of a basic model for the prediction of specific phenomena as opposed to attempting to develop an intricate universal model for the entire voloxidation process.

1.4 Uranium Oxide Oxidation Models

1.4.1 Oxidation to U_3O_8

The oxidation of UO_2 to U_3O_8 and intermediates has been modeled using a variety of methods. These approaches vary from diffusion to semi-empirical multi-parameter regressions attempting to account for a variety of phenomena.

Early work attempting to model the oxidation process of UO_2 to U_3O_8 displaying sigmoidal character has employed nucleation and growth models such as the Johnson-Mehl and Avrami equations [57, 58]. Ohashi and Aronson, specifically, modeled the oxidation to U_3O_8 with the Johnson-Mehl equation in their investigation of variables affecting oxidation [56, 59].

$$\log\left(\frac{1}{1-y}\right) = \frac{1}{2.303}k^n t^n \tag{1.3}$$

Where y is the extent of reaction, t is the reaction time, k is the reaction constant, and n is an empirical exponent factor. The model is based on two main assumptions: 1) the nuclei of U_3O_8 are formed all over the surface of the specimen in a random manner, the rate of nucleation being proportional to the area of the surface remaining untransformed, and 2) the nuclei grow at a constant linear rate of progression in all directions within the particle and along the surface until meeting another. The values of k and n were determined from experimental data for varying conditions. It was observed that the model was significantly dependent on many parameters, namely heating rate, temperature, and annealing effects, but the model fits the data well overall [56].

Building on this work, McEachern *et al*. employed a two-dimensional model for surface oxidation by a nucleation and growth process. The model was observed to fit well with X-ray diffraction oxidation data collected; the Arrhenius plot was linear with activation energy of 146±10 kJ mol^{-1}[14]. While such models may be accurate for surface oxidation, the application of a nucleation and growth model alone for oxidation of UO_2 pellets does not capture the additional phenomena that may influence reaction rate.

Valdivieso *et al*. use a more general approach to modeling the reaction of UO_2 to U_3O_8 at temperatures up to 500°C, with the main study being on the process at 370°C. The aim of this modeling effort was to address two important questions: 1) Is the reaction pseudo-steady state? and 2) Is there a rate-limiting step? Differential scanning calorimetry and thermogravimetric analysis (DSC/TGA) were performed to establish not only reaction rate but to determine if the process is pseudo-steady state, which it was determined to be. This conclusion was reached from the linear relationship found between weight gain and heat rate. Another important aspect of their work is the reaction of powdered UO_2 compared to that of sintered UO_2 pellets. The authors point to the error in assuming a nucleation and growth model such as that of Johnson-Mehl in the case of sintered pellets as these models assume the nucleation occurs throughout the volume of the existing phase versus just the surface of the grains. As in previous work, it was determined from X-ray diffraction analysis the reaction product at elevated temperatures (above 350°C) did not contain detectable quantities of U_3O_7 or other intermediates. This study also analyzed the effect of the partial pressure of O_2 up to 20 kPa, above which no effect was found. Oxidation of UO_2 was found to increase in rate with O_2 partial pressure, but increases were greater at lower pressures with a smaller change in rate from 10 to 20 kPa. A test for the existence of a rate-limiting step was performed based on the assumption that the rate of conversion can be described

by a general model consisting of the product of the term $\Phi(T, P_{O_2})$ and E(t) where Φ is only a function of temperature and/or partial pressure of oxygen, while E is a function of time. This allows one to test the existence of a rate-limiting step by inducing perturbations in temperature and pressure and taking the ratio of the respective Φs. If for different times of reaction, the ratios are constant, there exists a rate-limiting step, and this was found to be the case in the UO_2 to U_3O_8 oxidation. Then, by using the rate of reaction at different temperatures and assuming the Φ can be described by the product of the Arrhenius equation and a function of partial pressure of oxygen,

$$\Phi(T, P_{O_2}) = A_0 \exp(\frac{E_a}{RT}) f(P_{O_2}) \tag{1.4}$$

the activation energy can be determined by taking the ratio of $\Phi(T_1)$ and $\Phi(T_2)$. The mean activation energy was found to be 103 kJ/mol within this temperature range, which agrees with the majority of other literature, even though there is uncertainty as to how to decouple the activation energies of the two stages of oxidation if both actually occur at higher temperatures [60]. While this work suggests the existence of a rate-limiting step, it does little to identify the process that is rate-limiting.

While there have been numerous attempts to model the oxidation process (both to intermediates and U_3O_8), they vary in approach and conclusiveness. It is clear that at the surface oxidation to U_3O_8 proceeds by a nucleation and growth model, but for oxidation at a larger scale, the controlling phenomena have yet to be fully characterized.

1.4.2 Voloxidation Modeling

Although there have been some efforts to develop models specifically for voloxidation processes, improvement and refinement are needed. The models that have been developed vary in approach from the macro and empirical to those based on thermodynamics focused on minute details of the mechanism. None of the models developed thus far are believed to be sufficient and do not provide a combination of insight into the details of the process and a predictive capability from which to optimize and innovate. Both features are desired.

The majority of the phenomena-based modeling of the voloxidation reactions has been conducted by the Korean Atomic Energy Research Institute where a voloxidation type process is being considered for a head-end step for a pyroprocessing approach to reprocessing UNF. A shrinking core type model was employed in which the resistance to the various forms of mass transfer and reaction rate are summed as if they were in series. The model derived is as follows [61-64] :

$$t = \frac{\rho_s r}{2bC_{Ag}k_g}x + \frac{\rho_s r^2}{4bC_{Ag}D_e}[x + (1-x)\ln(1-x)] + \frac{\rho_s r}{bC_{Ag}k_s}[1-(1-x)^{1/2}] \tag{1.5}$$

where r is the radius of the pellet, x is conversion of oxide reactant, ρ_s is the molar density of the oxide reactant, C_{Ag} is the molar concentration of oxygen, D_e is an effective diffusivity coefficient, k_g is a mass transfer coefficient, and k_s is a chemical reaction rate constant. Based on the functional form above, it can be inferred that the equations were derived for unclad fuel segments [short bare cylinder of MO_2 (UO_2, PuO_2)]. The first term accounts for mass transfer through a gas layer surrounding the cylinder while the second term accounts for the diffusion of

the oxidant through the "ash" or product layer. The third and final term is the time associated with the chemical reaction of the MO_2.

Within this model, instead of the k'' reaction constant being present as the simple case described by Levenspiel, a reaction equation (third term) is presented that is believed to describe the reaction mechanism which is based on the Johnson-Mehl equation for nucleation and growth. The authors conclude that there are two main steps of the reaction, diffusion of oxidant through a product layer, and the chemical reactions. These steps are frequently not accounted for separately in an analysis of the reaction kinetics.

An inaccuracy for the model shown in Equation 1.5 is the assumption used that the particle is of constant size with a reaction interface moving toward the core of the particle or pellet. In actuality, the "ash" or U_3O_8/UO_3/intermediate oxide products spall away from the main mass with some remaining on the surface. The authors mention that the activation energy for the "ash" diffusion process is low and state this is likely due to the spalling of the product. However, the model equation assumes a constant volume and ever-growing product layer. This assumption is also relevant to the gas phase diffusion model in that the model assumes the gas layer begins at the initial volume and extends to the reaction interface. The first concern with this assumption is that typically the stagnant gas volume will initially be larger than the volume of the particle and, secondly, because of the previously mentioned spalling of the product, the gas layer is thought to likely shrink with the continual reduction in volume. In addition, with this approach, one is accounting for diffusion over the same volume twice when including an effective diffusivity and gas layer diffusion integrated over the same space. The effective diffusivity should account for all diffusive resistance within a given volume.

The parameters of the model in Equation 1.5 were determined by numerical regression when fitting the model to data gathered by Boase and Vandergraaf [55]. This method of obtaining parameters and modeling such systems was taken from the work of Jothimurugesan and Harrison who studied the reaction of H_2S and zinc oxide-titanium sorbents [65]. It is believed that this method is only valid if the mechanisms of the reaction are well understood and certain; however, they are not for the oxidation process of UO_2 pellets to U_3O_8. While the models fit quite well at high temperatures where the reaction is relatively fast, the models were less accurate at lower temperatures. It must also be noted that this procedure was only conducted for data gathered from unirradiated depleted uranium pellets. Without model validation being conducted successfully for irradiated fuel of various burn up and age, this model cannot be deemed useful as a predictive tool.

There have been varied approaches to model the oxidation process that occurs during voloxidation; however, it is believed that the shrinking core model is the most appropriate approach given the level of understanding of mechanisms and of their parametric sensitivity. Nevertheless, it is necessary that such a model be developed along with experiments in which specific potentially controlling phenomena are probed to create a model in which the parameters have verified physical significance rather than serving as fitting parameters.

1.5 Diffusion through Uranium Oxides

Diffusion of oxygen into the uranium oxide matrix is supposed to be the controlling mechanism of oxidation at temperatures under 300°C, but still occurs at elevated temperatures even though it does not appear to be the limiting phenomena. For diffusion-controlled reactions, the rate of diffusion of oxygen through a discrete layer of intermediate U_4O_9/U_3O_7 is thought to

be limiting rather than the diffusion into UO_2 [36]. At higher temperatures where U_3O_8 nucleates and grows much faster, the presence of U_4O_9/U_3O_7 is typically not observed, but an understanding of the diffusion rates through all uranium oxide is useful in understanding the overall system. It is also possible, upon the quick oxidation to U_3O_8, a finite layer of unspalled U_3O_8 remains on the surface of the UO_2, which in effect could be limiting further oxidation of covered UO_2. In this case, the diffusion of O_2 through the pores of U_3O_8 could control if the spalling rate is slow and the product is dense. This section, however, is focused on examining modeling approaches and results for diffusive processes within the uranium oxide matrix (atomic diffusion).

In any case of UO_2 oxidation by O_2, the process begins with the initial oxidation of exposed UO_2, which occurs by the diffusion of oxygen into the UO_2 matrix. The diffusion is found to be a thermally activated process. While Fick's first and second laws seem to be the most frequently employed when considering diffusion, this system is not merely concentration driven. Both models assume diffusion coefficients are constant with concentration and position (Equations 1.6 and 1.7).

$$J = -D\frac{\partial c}{\partial x} \tag{1.6}$$

$$\frac{\partial c}{\partial t} = -D\frac{\partial^2 c}{\partial x^2} \tag{1.7}$$

The system can, however, be modeled unidirectionally and as a system consisting of diffusion through a slab. Diffusion of oxygen into the matrix is driven by chemical potential or

molar free energy differences, yet the rate of reaction or diffusion can be modeled by an activated process much like chemical reactions [66]. In the diffusion of oxygen, there are oxygen-uranium affinities that must be overcome for oxygen movement to another energetically favorable position. In addition, there is a drastic structure change that occurs along the entire process. For the movement of oxygen atoms and overall structure changes, there is an activation energy that must be achieved to overcome the unfavorable transition state configuration while the oxygen is in between sites of lower energy or saddle points. Due to the model approach being analogous to that of chemical reaction, the rate can be described by Equations 1.8 and 1.9 [66].

$$A + B \rightarrow AB \tag{1.8}$$

$$\text{Reaction rate} = \nu C_{AB} = (\nu K) C_A C_B, \tag{1.9}$$

where ν is a frequency factor of the activated complex being transformed to product oxide and

$$K = \exp\left(-\frac{\Delta G}{RT}\right) = \exp\left(-\frac{\Delta H}{RT}\right)\exp\left(\frac{\Delta S}{R}\right) \tag{1.10}$$

The rate constant for the reaction is then:

$$k = \nu \exp\left(-\frac{\Delta H}{RT}\right)\exp\left(\frac{\Delta S}{R}\right) \tag{1.11}$$

The gradient in free energy per atom is described as:

$$\chi = -\frac{1}{N}\frac{dG}{dx} = -\frac{1}{N}\frac{d\mu}{dx} \tag{1.12}$$

Where μ is molal free energy, N is Avogadro's number, and x is distance. Therefore, for one jump of position (distance λ) or energy difference, as can be seen in Figure 1.6,

$$\Delta\mu = -N\lambda\chi \tag{1.13}$$

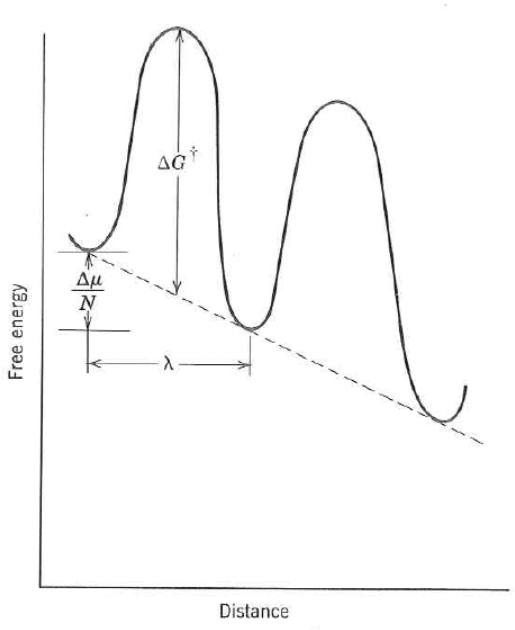


Figure 1.6. Activation energy for atomic movement in a lattice [66].

the overall reaction rate, $\mathbf{k_{net}}$, can be described as a difference in the rates or probability of the two different states, where k is the Boltzmann constant.

$$\mathbf{k}_{net} = \mathbf{k}_{forward} - \mathbf{k}_{back} = \nu \exp(-\frac{\Delta G}{kT})\left[\exp\left(\frac{\frac{1}{2}\chi\lambda}{kT}\right) - \exp\left(-\frac{\frac{1}{2}\chi\lambda}{kT}\right)\right] \tag{1.14}$$

In most cases, the thermal influence is much greater than that of the free energy; therefore, the expression can be reduced to,

$$\mathbf{k}_{net} = 2\nu \exp\left(-\frac{\Delta G}{kT}\right)\sinh\left(\frac{1}{2}\frac{\chi\lambda}{kT}\right) \tag{1.15}$$

$$\mathbf{k}_{net} = \nu \exp\left(-\frac{\Delta G}{kT}\right)\left(\frac{\chi\lambda}{kT}\right) \tag{1.16}$$

And by substitution,

$$\mathbf{k}_{net} = -\frac{\nu\lambda}{NkT}\exp\left(-\frac{\Delta G}{kT}\right)\left(\frac{d\mu}{dx}\right) \tag{1.17}$$

With this approach, the flux is described by,

$$J = \lambda \mathbf{k}_{net} c \tag{1.18}$$

When compared to Fick's first law, the diffusion coefficient of the following form is obtained.

$$D = \lambda^2 \nu \exp\left(-\frac{\Delta G}{kT}\right) \tag{1.19}$$

This approach does not account for vacant sites, but for UO_{2+x} the diffusivity is relatively insensitive to x showing that the effect of vacancies is not significant [67].

Numerous experimental studies have been performed to determine the diffusivity of oxygen into UO_2. Matzke reports the diffusivity to be ~1.5 × 10^{-7} cm^2 s^{-1} at 1000°K with an estimated activation energy of 96±8 kJ mol^{-1} [67]. The diffusivity, D^0, can be expressed as an Arrhenius equation,

$$D^O = D^O_{1000} e^{[(E_a / R1000) - (E_a / RT)]} \tag{1.20}$$

The case of diffusion of oxygen in U_3O_7 has also been studied. A parabolic rate has been observed for the formation of U_4O_9/U_3O_7. Therefore, a rate constant with units m^2s^{-1} has been proposed of the form:

$$k = 2V_{MO} D^O \Delta C \tag{1.21}$$

where V_{MO} is the volume of the metal oxide formed per mole of atomic oxygen and ΔC is the concentration gradient of "free oxygen" across the U_3O_7 layer (assuming a pure U_3O_7 layer) [10, 68].

Earlier experimental work of McEachern into the values of k resulted in the development of an expression of the form [36],

.

$$k = 2V_{MO} D^O \left(\frac{0.01}{V_{MO}} \right) \tag{1.22}$$

$$\ln(k) = -\frac{95.7 kJmol^{-1}}{R}\frac{1}{T} - 17.33 \tag{1.23}$$

From these equations and assumptions, a D^O value of 1.5×10^{-11} m^2 s^{-1} has been calculated which is identical to the diffusivity reported by Matzke previously mentioned for diffusion into UO_2 [10, 67]. It is not surprising then that the proposed models of diffusion through the UO_2 versus diffusion through a discrete layer of U_3O_7 yield almost identical results seeing that the diffusivities are comparable.

Another model for the oxidation of UNF focused on the initial oxidation to U_4O_9 or U_3O_7 in the induction and plateau region [17]. The developed model attempts to address both the rates of reaction/diffusion of oxygen into the grain as well as the progression of oxidation on a larger scale through grain boundaries. The intragranular model incorporates two non-stationary fronts for each of the two respective subsequent phases beyond UO_2 but does not include U_3O_8 as its formation is believed to occur through a nucleation and growth process.

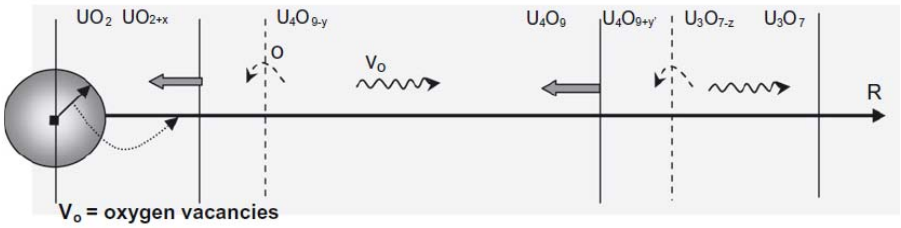


Figure 1.7. Schematic of grain oxidation [17].

The model is based on Fick's Law in spherical coordinates where D is the diffusivity, R is the initial particle radius, C is concentration, and r is the radius at time (t) greater than zero.

$$\frac{\partial C}{\partial t} = D\left(\frac{2}{R}\frac{\partial C}{\partial r} + \frac{\partial^2 C}{\partial r^2}\right) \tag{1.24}$$

The key parameters of this model are the diffusivities of each of the phases, and it was assumed that the initial surface was U_4O_9. Diffusivities were regressed from the model after the model was fit to data at different temperatures. The values of the diffusivities do not necessarily coincide with those found in other literature, but there is also no obvious consensus on these values. The authors do point out, however, that the activation energies for diffusion calculated from the model are comparable to that in other work [17]. The diffusion model previously described and presented in Equation 1.24 is combined with a model of the progression front of oxidation and is described by the following:

$$R_{adv} = R_{eq} - \frac{tR_{eq}}{t_o} \qquad \text{for } t = [0;t_o] \tag{1.25}$$

$$R_{eq} = V_{gb}t_o \tag{1.26}$$

Where R_{eq} is the radius of an equivalent sphere, t is time, and V_{gb} is the oxidation propagation at the grain boundaries.

While the case described in this work only examines the initial oxidation to intermediates, which are not as important at higher temperatures, the methods presented are not unique for studies of UO_2 oxidation and may be extended to the process at higher temperatures and possibly coupled with a model for U_3O_8 formation. [17].

In these cases, the direct implementation of the described models is not suitable for voloxidation modeling, but the concepts developed and approach are of great interest due to detail presented by the approach. For diffusion of oxygen in uranium oxides, whether that of UO_3, U_3O_8, U_3O_7/U_4O_9, or UO_2, the process is more complex than simple diffusion of oxygen into a plane of solid crystal (atomic diffusion). The effects of grain boundary area, porosity, and tortuosity must be accounted for to create an accurate representation of what is occurring, making modeling at this scale difficult due to material property variability. Factors such as the pore size associated with different oxidation states must also be taken into consideration as these influence the dominant diffusion mechanism occurring; namely, bulk, capillary, or Knudsen. These diffusion mechanisms are separate from the diffusion of oxygen into the uranium matrix.

1.6 Structure of Uranium Oxides: Crystalline and Microscopic

The change in crystalline structure upon oxidation of UO_2 to U_3O_8, resulting in a 36% crystalline volume increase, is the essential process of voloxidation. This drastic volume increase causes the uranium oxide to powderize and fall away, both removing the fuel from cladding and releasing trapped volatile fission products. The crystalline structure of UO_2 consists of the simple fluorite cubic structure, which is ideal for its use in nuclear fuel as vacant space in the middle of the unit cell allows for fission products to be located there with less stress on the structure than in other structures [66]. This fluorite structure, whose name comes from CaF_2, is shown in Figure 1.8.

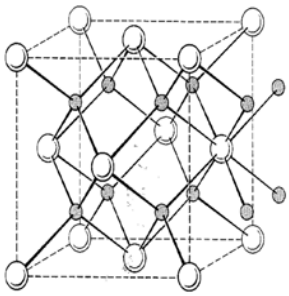


Figure 1.8. Cubic fluorite crystalline structure [66].

Like that of UO_2, all oxides up to α-U_2O_5 have the fluorite structure after which the uranium oxides exist in a layered structure [69]. A list of uranium oxides is presented in Table 1.1 along with their class and lattice parameters.

Table 1.1. Proposed uranium oxide phases [69].

Crystallographic data for the uranium oxides

Phase	O/U ratio	Structure	Crystal class	Unit cell (Å)
UO_2	2.00	Fluorite	Cubic	$a = 5.470$
UO_{2+x}	2.00 → 2.25	Fluorite	Cubic	$a = 5.470 \rightarrow 5.445$
α-U_4O_9	2.45 → 2.25	Fluorite	Rhombohedral	$a = 4 \times (5.441 \rightarrow 5.444)$; $\alpha = 90.078°$ ($T = 20°C$)
β-U_4O_9	2.25	Fluorite	Cubic	$a = 4 \times 5.438$ ($T = 65°C$)
γ-U_4O_9	2.25	Fluorite	Cubic	$a = 4 \times (5.47 \rightarrow 5.50)$ ($T > 600°C$)
α-U_3O_7	2.27 → 2.33	Fluorite	Tetragonal	$a = 5.472$; $c = 5.397$
β-U_3O_7	2.33	Fluorite	Tetragonal	$a = 5.363$; $c = 5.531$
$U_{16}O_{37}$ (γ-U_3O_7)	2.31	Fluorite	Tetragonal	$a = 5.407$; $c = 5.497$
U_8O_{19} (δ-U_3O_7)	2.375	Fluorite	Monoclinic	$a = 5.378$; $b = 5.559$; $c = 5.378$; $\beta = 90.29°$
γ-U_2O_5	2.50	Fluorite	Monoclinic	$a = 5.410$; $b = 5.481$; $c = 5.410$; $\beta = 90.49°$
α-U_2O_5	2.50	Layered	Hexagonal	$a = 3.885$; $c = 4.082$
β-U_2O_5	2.50	Layered	Hexagonal	$a = 3.813$; $c = 13.18$
U_2O_5	2.50	Layered	Orthorhombic	$a = 8.29$; $b = 31.71$; $c = 6.73$
α-U_3O_8	2.660 → 2.667	Layered	Orthorhombic	$a = 6.715$; $b = 11.96$; $c = 4.146$
β-U_3O_8	2.67	Layered	Orthorhombic	$a = 7.07$; $b = 11.45$; $c = 8.30$
$U_{12}O_{35}$	2.92	Layered	Orthorhombic	$a = 6.91$; $b = 3.92$; $c = 4.12$
α-UO_3	3.00	Layered	Orthorhombic	$a = 6.84$; $b = 43.45$; $c = 4.157$
β-UO_3	3.00	Layered	Monoclinic	$a = 10.34$; $b = 14.33$; $c = 3.91$; $\beta = 99.03°$
γ-UO_3	3.00		Tetragonal	$a = 6.013$; $c = 19.975$
δ-UO_3	3.00	ReO_3-type	Cubic	$a = 4.16$
ϵ-UO_3	3.00	Layered	Triclinic	$a = 4.002$; $\alpha = 98.10°$; $b = 3.841$; $\beta = 90.20°$; $c = 4.165$; $\gamma = 120.17°$
η-UO_3	3.00		Orthorhombic	$a = 7.511$; $b = 5.466$; $c = 5.224$

The process by which the crystalline structure changes by the introduction of additional oxygen has been studied extensively. The proposed processes by which structural changes occur are based on the observations of growth in particle planes as well as findings of preferential phase changes in particular planes. The observation that oxidation on the (111) face of UO_2 crystals occurs more readily than that of the (110) and (100) faces is useful in suggesting a mechanism. The two main crystals of interest are that of the fluorite cubic UO_2 and the layered orthorhombic α-U_3O_8. A comparison of these structures is displayed in Figure 1.9, in which the expansion accompanying this transformation is apparent. The fluorite structure occurs in ABCABC packing pattern, while the layered α-U_3O_8 has a pattern of AAA in which the uranium layers are stacked with another directly above and below. The analysis, which focuses on the movement of the uranium atoms as opposed to basing the transition mechanism on oxygen, is much more convoluted. Of particular interest, the (111) uranium plane in UO_2 and the (001) plane of α-U_3O_8 are almost identical, as can be seen in Figure 1.9 [69].

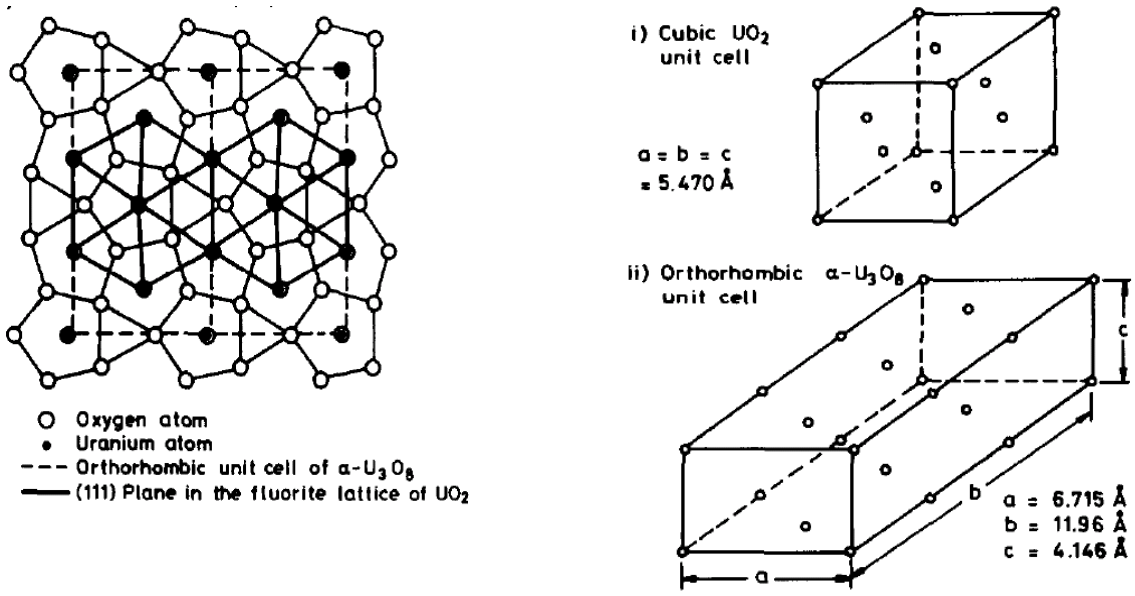


Figure 1.9. Proposed UO_2 and U_3O_8 structures (not all oxygen atoms shown for clarity) [69].

The simplest and most straightforward proposed mechanism involves the direct formation of U_3O_8 from UO_2 fluorite, in which the outermost (111) plane is displaced in the <112> direction to create a AA pattern with the uranium atoms aligned on top of one another and then stretched away to give the correct spacing that is found in U_3O_8. However, it is believed that intermediates such as U_3O_7 and U_4O_9 are formed at lower temperatures and possibly to some extent at higher temperatures [12, 70]. An additional explanation based on the formation of U_2O_5, which serves as the transition composition for the change from fluorite and layered is also proposed but is a bit more complicated, in which a ABC/ABAC/AA sequence is formed [69].

1.7 Oxidation of Uranium Oxides by NO_2

The use of NO_2 as an oxidant in a voloxidation system is being explored for potential increased fission product release as well as a number of other possible advantages over standard voloxidation, such as reduced oxidation temperatures. Earlier studies of the interactions of uranium oxides with N_2O_4/NO_2 have been somewhat limited and varied in motivation. While the reaction products of uranium oxide interaction with NO_x are not debated, there is disagreement on the structure of the UO_3 product resulting from reaction at temperatures greater than 100°C [71-75].

The reaction of current interest for advanced voloxidation methods is that of NO_2 with uranium oxides. However, other NO_x compounds are formed in equilibrium as a function of temperature. The two other oxides of greatest concentration in the temperature range of interest are N_2O_4 and NO_2. Intermediates such as NO_3, N_3O_6, and N_2O_2 are formed as well as other

products such as N_2O_3, NO, O_3, N_2, N_2O, and N_2O_5 [76]. The concentration of each of the three primary oxides is a function of temperature as shown in Figure 1.10.

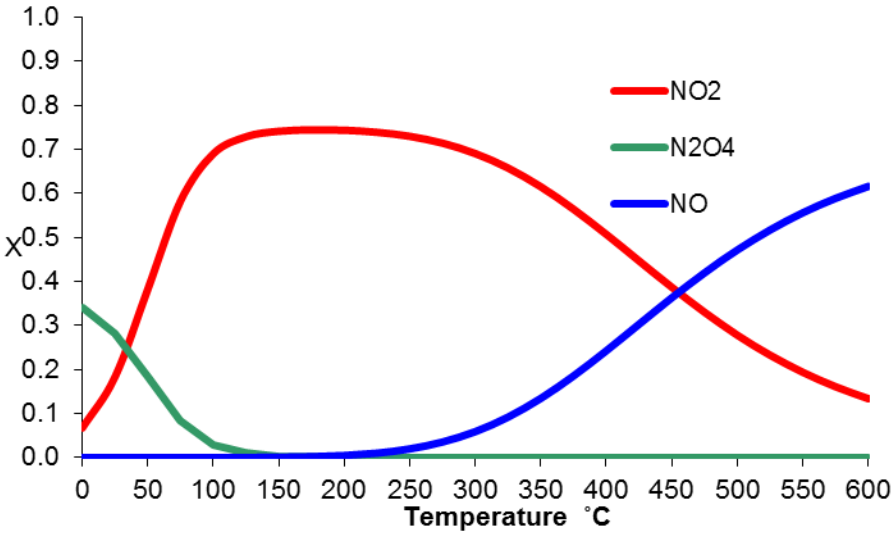


Figure 1.10. Equilibrium ratio of NO_x components at 1 atmosphere.

N_2O_4 dissociates at room temperature with a ΔH of reaction of 57.11 kJ mol^{-1} [76]. With increasing temperature, dissociation of N_2O_4 to NO_2 increases while the NO_2 formed begins to decompose to NO as shown in Equations 1.27 and 1.28.

$$N_2O_4(g) \leftrightarrow 2\ NO_2(g) \tag{1.27}$$

$$2\ NO_2(g) \leftrightarrow 2\ NO(g) + O_2(g) \tag{1.28}$$

Nitrogen dioxide is a paramagnetic compound as a result of the unbounded electron with C_{2v} point group symmetry. The molecule has a high oxidizing potential due to the weakly bonded

second oxygen. Nitrogen dioxide is a brown odorous gas while the NO and N_2O_4 are colorless and odorless.

The reaction of uranium oxides in a NO_x system can produce two products of interest, UO_3 and $UO_2(NO_3)_3NO$ [72, 74, 76-78]. The reaction of both UO_2 and U_3O_8 to UO_3 was studied with observation of the brick red colored UO_3. The UO_3 phase produced from reaction with NO_2 was later identified as ε-UO_3. The epsilon phase is one of six identified primary polymorphs, with others still possible as the structure of many of these phases is debated [69, 71, 75, 79-81].

The ε-UO_3 polymorph has been proposed to have a number of different structures including monoclinic, triclinic, and hexagonal [69, 73, 76, 82]. The complexity of the system, difficulty in forming single crystals, and formation of secondary phases has led to the varied reported structures. While these structures have been reported, atom positions have not been solved. The reaction to form ε-UO_3 is shown in Equation 1.29. The NO_2 can be regenerated from the reaction of NO product and O_2.

$$UO_2 + NO_2 \rightarrow UO_3 + NO \tag{1.29}$$

This reaction occurs within the temperature range of 100–350°C with uranyl nitrosyl nitrate formed with the UO_3 at temperatures below 180°C [72]. While the polymorph has been found to be stable up to 400–450°C, at 360°C the product is not observed. It is hypothesized that this is due to the transition of orthorhombic α-U_3O_8 to hexagonal β-U_3O_8 at 350°C, which may be less reactive [4, 72]. The conversion of ε-UO_3 above its transition temperature range was studied further, finding that rapid heating of the material yields decomposition to U_3O_8 while slow heating rates result in the formation of the γ-UO_3 phase, which is the most stable uranium

oxide [71]. This product was also reported by Kobets but was produced by increasing the pressure during reaction to greater than 0.5 MPa [76].

The oxidation of UO_2 with NO_2 was investigated further in a study at temperatures below 275°C and at NO_2 concentration at or below 1 vol.% NO_2 in air to simulate potential NO_2 concentrations from radiolysis [77]. As earlier studies had found, the NO_2 greatly increases the rate of oxidation as evidenced by the thickness of the oxide layer produced. It was found at temperatures >200°C, formation of U_3O_8 is observed, which then continues to oxidize and approaches UO_3. In the presence of NO_2 it has also been found that the intermediate U_3O_8 is formed twice as fast as in O_2/NO_2 mixtures at ~50 kPa [10, 83].

References

1. Goff, K.M. and M.F. Simpson, *Dry Processing of Used Nuclear Fuel.* INL/CON-09-15984, Battelle Energy Alliance, September 2009.

2. Song, K.C., *et al*., *Fractional release behavior of volatile and semivolatile fission products during a voloxidation and oreox treatment of spent PWR fuel.* Nuclear Technology, 2008. **162**(2): p. 158-168.

3. Herak, R., *Stress Induced a-U_3O_8-b-U_3O_8 Transformation.* Journal of Inorganic & Nuclear Chemistry, 1970. **32**(12): p. 3793.

4. Ackermann, R.J., A.T. Chang, and C.A. Sorrell, *Thermal-Expansion and Phase-Transformations of U_3O_{8-Z} Phase in Air.* Journal of Inorganic & Nuclear Chemistry, 1977. **39**(1): p. 75-85.

5. Park, J. and K. Howden, *Development of Voloxidation Process for Treatment of LWR Spent Fuel.* I-NERI Final Report Project 2004-004-K, INL-KAERI-ORNL, April 2007.

6. Park, G.-I., *et al*., *Thermo-Chemical Characteristics of Powder Fabricated by Oxidation of Spent PWR Fuel.* World Academy of Science, Engineering and Technology, 2010. **47**: p. 602-605.

7. Jahshan, S.N. and T.J. Mcgeehan, *An Evaluation of the Deployment of AIROX-Recycled Fuel in Pressurized-Water Reactors.* Nuclear Technology, 1994. **106**(3): p. 350-359.

8. Miller, J.R., *et al*., *AIROX Dry Pyrochemical Processing of Oxide Fuels - Proliferation Resistant Reprocessing Method.* Abstracts of Papers of the American Chemical Society, 1979(Apr): p. 126-126.

9. Takahashi, H., *et al*., *Analysis of the AIROX Process for LWR Fuel-Element Regenerated by Linear-Accelerator Reactor.* Transactions of the American Nuclear Society, 1979. **32**(Jun): p. 399-401.

10. McEachern, R.J. and P. Taylor, *A review of the oxidation of uranium dioxide at temperatures below 400°C.* Journal of Nuclear Materials, 1998. **254**(2-3): p. 87-121.

11. Higgs, J.D., *et al*., *Kinetics of precipitation of U_4O_9 from hyperstoichiometric UO_{2+x}.* Journal of Nuclear Materials, 2007. **366**(3): p. 297-305.

12. McCracken, D.R., *Oxidation of UO_2 at 400°C to 1000°C in Air and its Relevance to Fission Product Release.* AECL-8642, Chalk River Nuclear Laboratories, Atomic Energy of Canada Limited, July 1985.

13. Bae, K.K., *et al*., *Oxidation Behavior of Unirradiated UO_2 Pellets.* Journal of Nuclear Materials, 1994. **209**(3): p. 274-279.

14. McEachern, R.J., *et al*., *Determination of the activation energy for the formation of U_3O_8 on UO_2.* Journal of Nuclear Materials, 1997. **249**(1): p. 58-69.

15. Blackburn, P.E., J. Weissbart, and E.A. Gulbranson, *Oxidation of Uranium Dioxide.* Journal of Physical Chemistry, 1958. **62**(8): p. 902-908.

16. Walker, D.E.Y., *Oxidation of Uranium Dioxides.* Journal of Applied Chemistry, 1965. **15**(3): p. 128.

17. Rouyer, J., *et al*., *Modelling of the spent fuel oxidation: Toward the operational model.* Journal of Nuclear Materials, 2009. **395**(1-3): p. 89-98.

18. Idriss, H., *Surface reactions of uranium oxide powder, thin films and single crystals.* Surface Science Reports, 2010. **65**(3): p. 67-109.

19. Ishii, T., K. Naito, and K. Oshima, *X-Ray Study on a Phase Transition and a Phase Diagram in U_4O_9 Phase.* Solid State Communications, 1970. **8**(9): p. 677.

20. Gronvold, F., *High-Temperature X-Ray Study of Uranium Oxides in the UO_2-U_3O_8 Region.* Journal of Inorganic & Nuclear Chemistry, 1955. **1**(6): p. 357-370.

21. Willardson, R.K., J.W. Moody, and H.L. Goering, *The Electrical Properties of Uranium Oxides.* Journal of Inorganic & Nuclear Chemistry, 1958. **6**(1): p. 19-33.

22. Vaughan, D.A., J.R. Bridge, and C.M. Schwartz, *Comparison of Active and Inactive Uranium Dioxide-Oxygen Systems.* BMI-1241, December 1957.

23. Blackburn, P.E., *Oxygen Dissociation Pressures over Uranium Oxides.* Journal of Physical Chemistry, 1958. **62**(8): p. 897-902.

24. Aronson, S., J.E. Rulli, and B.E. Schaner, *Electrical Properties of Nonstoichiometric Uranium Dioxide.* Journal of Chemical Physics, 1961. **35**(4): p. 1382.

25. Schaner, B.E., *Metallographic Determination of the UO_2 -U_4O_9 Phase Diagram.* Journal of Nuclear Materials, 1960. **2**(2): p. 110-120.

26. Roberts, L.E.J. and A.J. Walter, *Equilibrium Pressures and Phase Relations in the Uranium Oxide System.* Journal of Inorganic & Nuclear Chemistry, 1961. **22**(3-4): p. 213-229.

27. Bannister, M.J. and W.J. Buykx, *Dilatometric Study of Solubility of U_4O_9 in UO_2.* Journal of Nuclear Materials, 1975. **55**(3): p. 345-351.

28. Saito, Y., *Nonstoichiometry in Uranium-Dioxide.* Journal of Nuclear Materials, 1974. **51**(1): p. 112-125.

29. Nakamura, A. and T. Fujino, *Thermodynamic Study of UO_{2+x} by Solid-State Emf Technique.* Journal of Nuclear Materials, 1987. **149**(1): p. 80-100.

30. Anthony, A.M., R. Kiyoura, and T. Sata, *Les Equilibres Des Composes Oxygenes De Luranium Entre 1500 Et 2000K.* Journal of Nuclear Materials, 1963. **10**(1): p. 8-14.

31. Kotlar, A., P. Gerdania, and M. Dode, *Determination of Phase Limits in System U-O by Oxygen Transfer.* Journal De Chimie Physique Et De Physico-Chimie Biologique, 1968. **65**(4): p. 687.

32. Kovba, L.M., *Phase Diagram of Uranium-Oxygen System.* Doklady Akademii Nauk Sssr, 1970. **194**(1): p. 98.

33. Vanlierd.W, J. Pelsmaek, and A. Lecocqro, *Phase Limits of U_4O_9.* Journal of Nuclear Materials, 1970. **37**(3): p. 276.

34. Markin, T.L. and R.J. Bones, *The Determination of Changes in Free Energy for Uranium Oxides Using a High Temperature Galvanic Cell. Part I.* AERE-R 4042, U.K.A.E.A., April 1962.

35. Peakall, K.A. and J.E. Antill, *Oxidation of Uranium Dioxide in Air at 350–1000°C.* Journal of Nuclear Materials, 1960. **2**(2): p. 194-195.

36. McEachern, R.J., *A review of kinetic data on the rate of U_3O_7 formation on UO_2.* Journal of Nuclear Materials, 1997. **245**(2-3): p. 238-247.

37. Quemard, L., *et al*., *On the origin of the sigmoid shape in the UO_2 oxidation weight gain curves.* Journal of the European Ceramic Society, 2009. **29**(13): p. 2791-2798.

38. Lefort, P., J. Desmaison, and M. Billy, *Behavior of Cubic Delta Niobium Nitride in Oxygen Atmosphere.* Materials Research Bulletin, 1979. **14**(4): p. 479-486.

39. Ferguson, I.F. and J.D.M. McConnell, *Heat of Adsorption of Oxygen on Uranium Dioxide at -183°C.* Proceedings of the Royal Society of London Series a-Mathematical and Physical Sciences, 1957. **241**(1224): p. 67-79.

40. Taylor, P., D.D. Wood, and D.G. Owen, *Microstructures of Corrosion Films on UO_2 Fuel Oxidized in Air-Steam Mixtures at 225°C.* Journal of Nuclear Materials, 1995. **223**(3): p. 316-320.

41. Taylor, P., *et al*., *Formation of Uranium Trioxide Hydrates on UO_2 Fuel in Air Steam Mixtures Near 200°C.* Journal of Nuclear Materials, 1989. **168**(1-2): p. 70-75.

42. Wasywich, K.M., *et al*., *Differences in Oxidation Behavior of Used CANDU Fuel during Prolonged Storage in Moisture-Saturated Air and Dry Air at 150°C.* Nuclear Technology, 1993. **104**(3): p. 309-329.

43. Taylor, P., *et al*., *Microstructures and phase relationships of crystalline oxidation products formed on unused CANDU fuel exposed to aerated steam and aerated water near 200°C.* AECL-10476, Atomic Energy of Canada Limited, November 1991.

44. Campbell, T.K., *et al*., *Oxidation Behavior of Nonirradiated UO_2.* Nuclear Technology, 1989. **85**(2): p. 160-171.

45. Dominey, D.A., *Oxidation of UO_2 by Oxygen at 66°C and 80°C.* Journal of Inorganic & Nuclear Chemistry, 1968. **30**(7): p. 1757.

46. Thomas, L.E., R.E. Einziger, and H.C. Buchanan, *Effect of Fission-Products on Air-Oxidation of LWR Spent Fuel.* Journal of Nuclear Materials, 1993. **201**: p. 310-319.

47. Tennery, V.J. and T.G. Godfrey, *Oxidation Properties of $(U,Pu)O_2$ Solid-Solutions.* Journal of the American Ceramic Society, 1973. **56**(3): p. 129-133.

48. Ishida, M. and Y. Korei, *Modeling and Parametric Studies of the Effect of Pu-Mixing Heterogeneity on Fission-Gas Release from Mixed-Oxide Fuels of LWRs and FBRs.* Journal of Nuclear Materials, 1994. **210**(1-2): p. 203-215.

49. Choi, J.W., *et al*., *The effect of fission products on the rate of U_3O_8 formation in SIMFUEL oxidized in air at 250°C.* Journal of Nuclear Materials, 1996. **230**(3): p. 250-258.

50. Kim, K.S., *et al*., *Oxidation Behavior of Unirradiated and Irradiated UO_2 in Air at 150-375°C.* Journal of the Korean Nuclear Society, 1997. **29**(2): p. 93-98.

51. Thomas, L.E., *et al*., *Microstructure Characterization of Low-Temperature Oxidized LWR Spent Fuel.* PNL-6640, Battelle Memorial Institute, Pacific Northwest Laboratory, December 1989.

52. Woodley, R.E., R.E. Einziger, and H.C. Buchanan, *Measurement of the Oxidation of Spent Fuel between 140°C and 225°C.* Nuclear Technology, 1989. **85**(1): p. 74-88.

53. Nakae, N., *et al*., *Irradiation Induced Lattice-Defects in UO_2.* Journal of Nuclear Materials, 1978. **71**(2): p. 314-319.

54. Nakae, N., Y. Iwata, and T. Kirihara, *Thermal Recovery of Defects in Neutron-Irradiated UO_2.* Journal of Nuclear Materials, 1979. **80**(2): p. 314-322.

55. Boase, D.G. and T.T. Vandergraaf, *Canadian Spent Fuel Storage Canister - Some Materials Aspects.* Nuclear Technology, 1977. **32**(1): p. 60-71.

56. Ohashi, H., E. Noda, and T. Morozumi, *Oxidation of Uranium-Dioxide.* Journal of Nuclear Science and Technology, 1974. **11**(10): p. 445-451.

57. Johnson, W.A. and R.F. Mehl, *Reaction Kinetics in Processes of Nucleation and Growth (Reprinted from Transactions of the American Institute of Mining & Metallurgical Engineers, vol 135, p. 416, 1939).* Metallurgical and Materials Transactions a-Physical Metallurgy and Materials Science, 2010. **41A**(11): p. 2713-2775.

58. Avrami, L., E. Dalrympl, and F. Schwartz, *Design of a Large Explosive Containment Capsule for Nuclear Reactor Irradiation.* Annals of the New York Academy of Sciences, 1968. **152**(A1): p. 773.

59. Aronson, S., R.B. Roof, and J. Belle, *Kinetic Study of the Oxidation of Uranium Dioxide.* Journal of Chemical Physics, 1957. **27**(1): p. 137-144.

60. Valdivieso, F., *et al*., *Oxidation behaviour of unirradiated sintered UO_2 pellets and powder at different oxygen partial pressures, above 350°C.* Journal of Nuclear Materials, 2006. **354**(1-3): p. 85-93.

61. Yagi, S. and D. Kunii, *Fluidized-Solids Reactors with Continuous Solids Feed .1. Residence Time of Particles in Fluidized Beds.* Chemical Engineering Science, 1961. **16**(3-4): p. 364-371.

62. Levenspiel, O., *Chemical Reaction Engineering*. 3rd ed. 1999, New York: John Wiley & Sons.

63. Jeong, S.M., *et al*., *A kinetic study of the oxidation of uranium dioxide.* Reaction Kinetics and Catalysis Letters, 2006. **89**(2): p. 269-275.

64. Jeong, S.M., J.M. Hur, and H. Lee, *Kinetic Modeling Study of a Voloxidation for the Production of U_3O_8 Powder from a UO_2 Pellet.* Nuclear Engineering and Technology, 2009. **41**(8): p. 1073-1078.

65. Jothimurugesan, K. and D.P. Harrison, *Reaction between H_2S and Zinc-Oxide Titanium-Oxide Sorbents .2. Single-Pellet Sulfidation Modeling.* Industrial & Engineering Chemistry Research, 1990. **29**(7): p. 1167-1172.

66. Kingery, W.D., H.K. Bowen, and D.R. Uhlmann, *Introduction to Ceramics*. 2nd ed. 1976: John Wiley & Sons.

67. Matzke, H., *Radiation-Damage in Crystalline Insulators, Oxides and Ceramic Nuclear-Fuels.* Radiation Effects and Defects in Solids, 1982. **64**(1-4): p. 3-33.

68. Kirkaldy, J.S., D.J. Young, and J.E. Lane, *Diffusion Profiles Associated with the Onsager Matrix in Nonequilibrium a-a-Star-Vacancy and a-B-Vacancy Solutions.* Acta Metallurgica, 1987. **35**(6): p. 1273-1279.

69. Allen, G.C. and N.R. Holmes, *A Mechanism for the UO_2 to a-U_3O_8 Phase-Transformation.* Journal of Nuclear Materials, 1995. **223**(3): p. 231-237.

70. Lewis, B.J., *et al*., *Thermodynamic and kinetic modelling of fuel oxidation behaviour in operating defective fuel.* Journal of Nuclear Materials, 2004. **328**(2-3): p. 180-196.

71. Hoekstra, H.R. and S. Siegel, *The Uranium-Oxygen System - U_3O_8-UO_3.* Journal of Inorganic & Nuclear Chemistry, 1961. **18**: p. 154-165.

72. Kobets, L.V. and G.N. Klavsut, *Behavior of U_3O_8 in Dissociating Gaseous Dinitrogen Tetroxide.* Soviet Radiochemistry, 1986. **28**(6): p. 657-660.

73. Kovba, L.M., L.M. Vidavskii, and É.G. Lavut, *Study of ε-UO_3.* Journal of Structural Chemistry, 1963. **4**(4): p. 573-574.

74. Ryabkova, N.V., *et al*., *Dissolution of UO_2 in the N_2O_4-H_2O system.* Radiochemistry, 2010. **52**(4): p. 399-402.

75. Cornman, W.R., *Preparation and Characterization of the Polymorphs of UO_3.* DP-749, Savannah River Laboratory, August 1962.

76. Kobets, L.V. and G.N. Klavsut, *Interaction of Uranium-Oxides with Dinitrogen Tetraoxide.* Uspekhi Khimii, 1990. **59**(8): p. 1251-1266.

77. McEachern, R.J., *et al*., *The influence of nitrogen dioxide on the oxidation of UO_2 in air at temperatures below 275°C.* Journal of Nuclear Materials, 1998. **255**(2-3): p. 234-242.

78. Gibson, G., C.D. Beintema, and J.J. Katz, *The Reaction of Uranium Oxides with Dinitrogen Pentoxide.* Journal of Inorganic & Nuclear Chemistry, 1960. **15**(1-2): p. 110-114.

79. Cordfunke, E.H.P. and E.F. Westrum Jr, *The thermodynamic properties of β-UO_3 and γ-UO_3.* Thermochimica Acta, 1988. **124**(0): p. 285-296.

80. Cordfunke, E.H.P. and P.C. Debets, *Preparation and Properties of a New Monohydrate of Uranium Trioxide e-UO_3 H_2O.* Journal of Inorganic & Nuclear Chemistry, 1964. **26**(10): p. 1671.

81. Sweet, L., *et al*., *Investigation of the polymorphs and hydrolysis of uranium trioxide.* Journal of Radioanalytical and Nuclear Chemistry, 2012: p. 1-6.

82. Tsvigunov, A.N. and L.M. Kuznetsov, *Low-temperature oxidation of uranium dioxide, uranium oxide (U_3O_8), and the U_3O_{8-x} phase by nitrogen dioxide.* Radiokhimiya, 1976. **18**: p. 411.

83. Anderson, J.S., L.E.J. Roberts, and E.A. Harper, *The Oxides of Uranium .Part VII. The Oxidation of Uranium Dioxide.* Journal of the Chemical Society, 1955: p. 3946-3959.

CHAPTER 2

OXIDATION OF SURROGATE AND USED NUCLEAR FUEL PELLETS

This chapter is a revised version of a paper (minor revisions due to its inclusion as a chapter in the dissertation) by the same title in preparation for a journal by: Jared A. Johnson, Barry B. Spencer, Robert M. Counce, and Guillermo D. Del Cul.

My contributions to this paper included: (1) all of the experiments, (2) analysis/modeling of data, and (3) all of the writing.

Abstract

The oxidation of UO_2 pellets to U_3O_8 was studied to develop an improved understanding of the reaction process and controlling phenomena. Studies to isolate specific phenomena were performed by varying such parameters as temperature, oxidant flow rate, oxidant concentration, and agitation. In addition, studies of the effect of cladding on the oxidation rate of UO_2 pellets were performed. From the data collected by thermogravimetric analyses along with qualitative information from cross-sectioned clad pellets, a reaction model is proposed.

2.1 Introduction

The oxidation of UO_2 to U_3O_8 has been studied extensively over the past six decades. In spite of an extensive research on this topic, there remains to be developed a model for reaction of pellets that is accurate and physically representative. Such a model is essential to voloxidation processes under development for head-end treatment of used nuclear fuel (UNF) for reprocessing or fuel preconditioning for storage. An accurate, experiment-based understanding of the phenomena occurring and controlling during reaction is required for process design and optimization.

In the standard voloxidation process, segmented clad fuel is heated to 450–600°C to oxidize the mostly monolithic UO_2 fuel to U_3O_8 [1-4]. The α-U_3O_8 product is a loose powder that

is easily segregated from the cladding hulls. Upon oxidation, the cubic (fluorite) UO_2 converts to orthorhombic U_3O_8 product, which results in a 36% crystalline volume change and up to a factor of five bulk volume increase [5-8]. Above 350°C, the U_3O_8 begins to transition to a hexagonal polymorph and upon cooling, when heated to <875°C, the structure converts to the orthorhombic phase [9]. The oxidation process releases volatile and some semi-volatile fission products from the fuel matrix, which can be trapped.

There have been a number of models developed for the oxidation of UO_2, but most have been focused on temperatures lower than those of interest for voloxidation. These studies have shown that below ~350°C the oxidation process consists of two distinct reactions.

$$UO_2 \rightarrow U_3O_7/U_4O_{9+y} \rightarrow U_3O_8 \quad (2.1)$$

First, the UO_2 oxidizes to intermediates U_3O_7 and/or U_4O_9 by a diffusion-controlled process before subsequent reaction to U_3O_8 by a nucleation and growth process typified by the models of Johnson-Mehl or Avrami [6, 10, 11]. Some researchers have concluded that above 350°C the reaction directly produces U_3O_8 with no observable intermediate formation [6]. While the majority of the studies have been focused on accident scenarios, there have been efforts to model the voloxidation reaction. However, these efforts were aimed at modeling unclad fuel and consisted of fitting curves to multi-parameter models which do not adequately describe the physical processes [12, 13].

In this work, parameter isolation was attempted to experimentally determine the rate-limiting phenomena as well as the general effects of the cladding on the oxidation processes. The effects of gas layer diffusion, product layer diffusion, oxidation kinetics, and other not previously

examined phenomena are studied. From the studies of the parameters that affect the oxidation rate of UO_2 at elevated temperatures, several important conclusions were made which allowed for reduction of scope for the reported studies. It has been found that the partial pressure of oxygen significantly affects the reaction rate for UO_2 pellets. The linear section of the sigmoidal reaction curve increases in slope with oxygen concentration; however, the incubation and final portion of the reaction curve have been found to be unaffected by oxygen concentration [1, 6, 14]. The effect of temperature variation within the range of interest, above 350°C, has also been studied previously. The reaction rate has been observed to increase with temperature up to ~550°C after which a reduction in reaction rate occurs as a result of self-sintering or agglomeration of the product layer as it is formed and is evidenced by an increase in particle size [14-16]. Furthermore, the incubation period of reaction decreases with increased temperature [6]. Therefore, the effects of various parameters on the linear portion of the reaction curve were the primary focus of these studies.

It is recognized that models developed with surrogates for nuclear material do not necessarily translate directly for irradiated fuel due to additional parameters that influence the oxidation rate, such as burn-up (composition and structure), age of the fuel (surface oxidation to hydrated UO_3), and radiation (vacancies in lattice) not being accounted for in the surrogates tested. However, at temperatures below 400°C, it has been concluded that there is little difference in overall reaction times of irradiated materials versus surrogates, while intermediate phases formed can be affected [6]. It is also believed the qualitative phenomena observed and found to control oxidation will translate independent of variations due to irradiation.

2.2 Experimental

Macro-thermogravimetric analysis was conducted on depleted uranium (UO_2) pellets to isolate those phenomena limiting the rate of reaction. This was achieved by varying specific conditions such as the presence of cladding, length of cladding, oxidant concentration, oxidant gas flow rate, and agitation for removal of product. After initial testing with surrogates to understand the system in more detail, a model was built and compared with the oxidation of a segment of used fuel, which was performed in a hotcell environment.

2.2.1 Surrogate Materials

Surrogate fuel experiments were conducted with depleted uranium oxide pellets (UO_2). The pellets had been pressed and sintered to a density of 10.44 g/cm^3 (95% of theoretical). The pellets used were 1.39 cm long and had a diameter of 0.68 cm, which corresponds to pressurized water reactor (PWR) fuel pellets. The average grain size in the sintered pellets was calculated to be 17.5 ±0.6 μm, determined by scanning electron microscope (SEM) imaging using a Hitachi S4800 at a magnification of 600x and by following the procedure of ASTM E112-10. Samples were polished using a final diamond suspension abrasive of 0.25 μm before a 10 *M* HNO_3 etchant was applied for three minutes. Figure 2.1 displays an SEM image of a cross-sectioned sample. Pellets used were treated at 500°C with an Ar/H_2 (volumetric ratio: 96/4) mix to reduce any surface oxidation. Pellets were uniform with minimal defects.

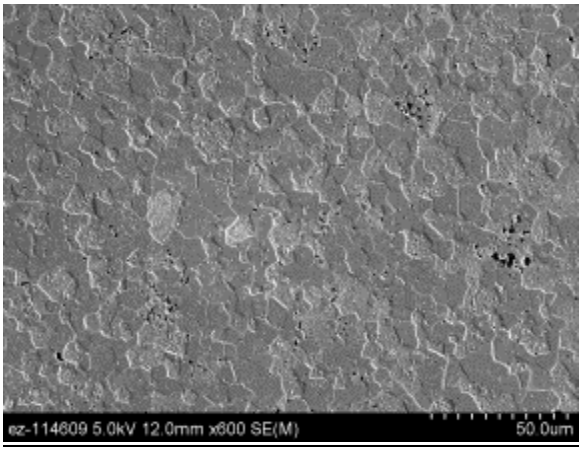


Figure 2.1. Scanning electron microscope image of cross-sectioned UO_2 pellet at 600x magnification.

For those clad samples, the cladding consisted of stainless steel cups with an inside diameter of 0.691 cm and were open on one end. The cladding was pretreated by heating to 500°C. The pellets fit tightly in the cups with a gap of 5.5×10^{-3} cm. The length of cladding used varied from 2 cm to 8 cm.

2.2.2 Experimental Equipment and Procedure

A macro-thermogravimetric analysis (TGA) system was custom fabricated from a box furnace with a digital balance below the furnace. A 2.54-cm-diameter hole was made in the bottom of the furnace through which a quartz tube was passed and on which a stainless steel stand was located. Reaction and purge gases were fed into the furnace and delivered to samples through a gas lens inside a shroud. The temperature was controlled using feedback from a thermocouple located on the inside of the shroud and the original thermocouple inside the furnace. A diagram of the system is shown in Figure 2.2.

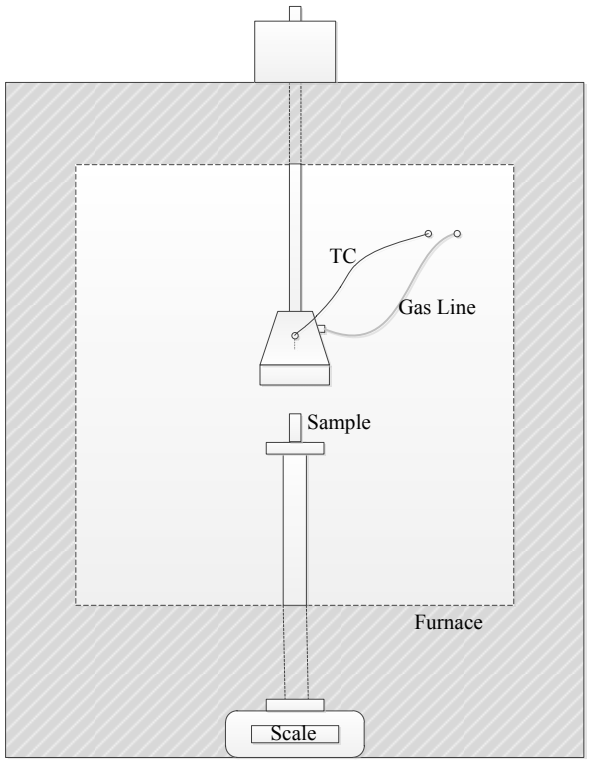


Figure 2.2. Sketch of macro-thermogravimetric analysis system for unagitated samples.

Before use, the scale was calibrated and data were collected for one hour to ensure readings were consistent. The sample was then placed on the stage, and the gas lens was positioned above the sample. Nitrogen was used to purge the furnace for 30 minutes at 750 sccm before heating was initiated. Balance readings were collected during heat-up until both the specified temperature and balance reading were constant. The feed gas was then initiated at the specified flow rate. Weight readings were taken every 30 seconds until the run was complete.

A second macro-TGA system that allowed for agitation of clad oxide pellets was fabricated. A schematic of the apparatus is shown in Figure 2.3. The system consisted of a 30.48 cm tube furnace with an inside diameter of 6.35 cm, which contained a quartz liner. A stainless steel rod, which holds the sample, was suspended in the vertical furnace with an adjustable

vibration device attached to the sample cross support rod. The clad pellet was attached to the suspended rod by threading on the bottom end of the cladding. A thermocouple extended down the line ending at the sample midpoint. A digital scale positioned below the furnace collects spalled product. Preliminary tests without agitation with a scale above (to measure weight of unreacted sample) and below (to measure the weight of spalled product) demonstrated no significant dead time between spallation and collection below, nor was entrainment of spalled product observed.

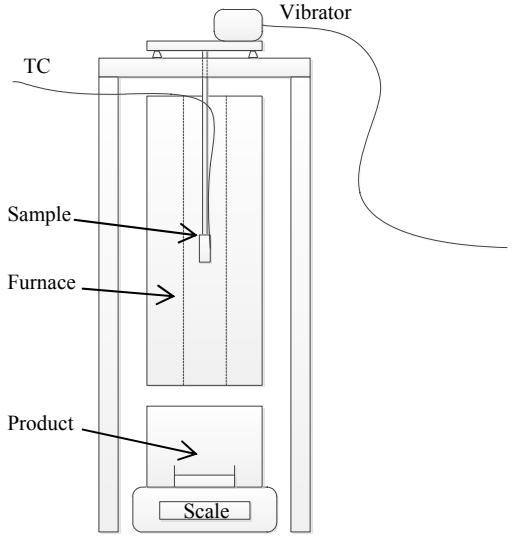


Figure 2.3. Sketch of macro-thermogravimetric system for agitated samples.

Samples were prepared by inserting the AgCu brazing powder into the 1.5-cm-long cladding before inserting a depleted uranium oxide pellet. The sample was then heated to 800°C under H_2/N_2 (4/96) to melt the braze and form a seal at the bottom of the pellet.

2.3 Results

2.3.1 Reaction Rates of Surrogates

2.3.1.1 Oxidation of Unclad Pellets

Unclad depleted UO_2 pellets were reacted in air to give a baseline for comparison and to compare the rates to previous studies for verification that the pellets used were characteristic and comparable to those in other studies. The reactions were conducted as described previously at three temperatures (450°C, 525°C, 600°C) in a macro-TGA unit without agitation. Weight gain data for the three specified temperatures is displayed in Figure 2.4. The reaction curve displays the characteristic sigmoidal shape, as expected, with little incubation period

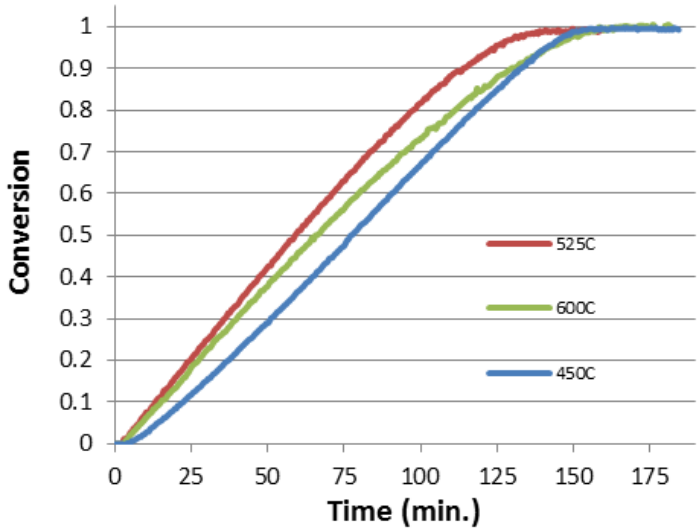


Figure 2.4. Reaction kinetics for unclad UO_2 pellet oxidation to U_3O_8.

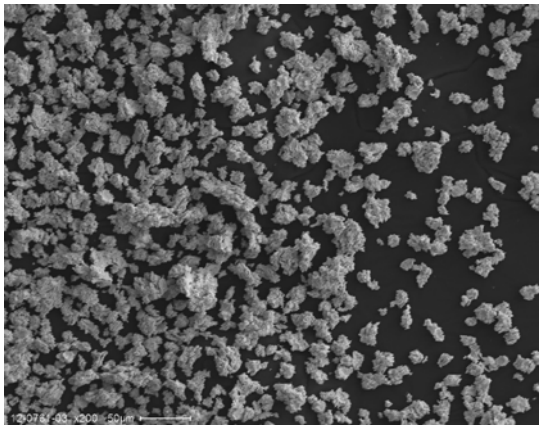
The expected dependence of reaction on temperature is also evident for the three reaction temperatures. The reaction rate increased from 450°C to 525°C but decreased at 600°C. Also, the incubation period decreased with increased temperature. Product from each reaction was

analyzed by X-ray diffraction (XRD) and the expected α-U_3O_8 was confirmed. Samples of the product were investigated by SEM for particle size and by Brunauer, Emmett, Teller (BET) analysis for surface area; the results are shown in Table 2.1.

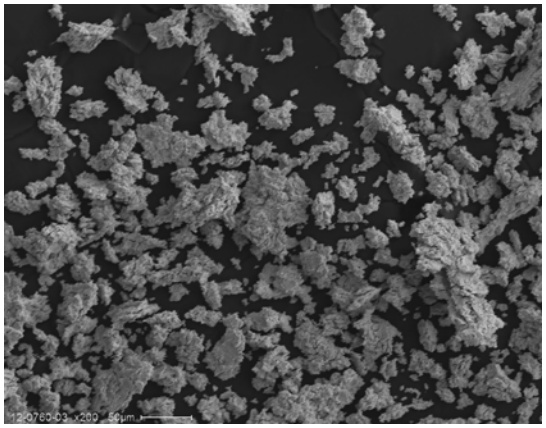
Table 2.1. Average particle size and surface area of U_3O_8.

	450°C	525°C	600°C
Average particle size (μm)	15.55	19.72	15.47
Surface area (m^2/g)	0.96	0.73	0.43

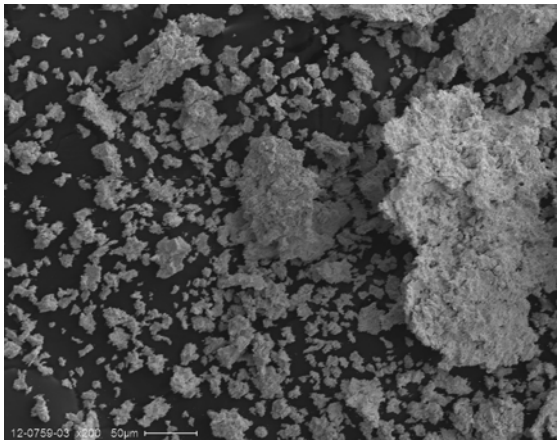
BET results showed the expected trend in surface area. Previous studies indicate an increase in particle size with increasing temperature [16]. Specific surface area is expected to decrease with increasing particle size. Results from the particle size analysis were within the range expected, but the smaller particle size for the product from oxidation at 600°C was unanticipated. Upon review of the data and images, it is believed that the method employed was biased for samples with a wide distribution in particle sizes. The particles measured were those not touching others on the perimeter, and images of the samples showed larger particles not measured as they are more probable to touch surrounding particles and therefore excluded from measurement. Images of the product powder are displayed in Figure 2.5(a-c).



(a)



(b)



(c)

Figure 2.5. Scanning electron microscope images of U_3O_8 product from reaction temperatures of (a) 450°C, (b) 525°C, and (c) 600°C.

2.3.1.2 Oxidation of Clad Pellets

Clad UO_2 pellets were oxidized under a variety of conditions. As described previously, pellets were clad with stainless steel tubing of varied length, closed at one end and open to the oxidizing atmosphere on the other. It was found that the length of cladding had little effect on reaction rate as compared to other parameters. It was observed that the product was influenced by the cladding mechanically giving it shape with stratified layers as shown in Figure 2.6.



Figure 2.6. U_3O_8 product growing out of cladding.

Reaction rates were found to be linear, verifying the bulk product does not contribute to the reaction resistance. If diffusion through the loose product layer was limiting, the reaction would slow with product formation. While the reaction demonstrated the characteristic curve observed for unclad pellets initially, for a number of samples, the reaction slowed with a parabolic transformation of the reaction curve, as shown in Figure 2.7.

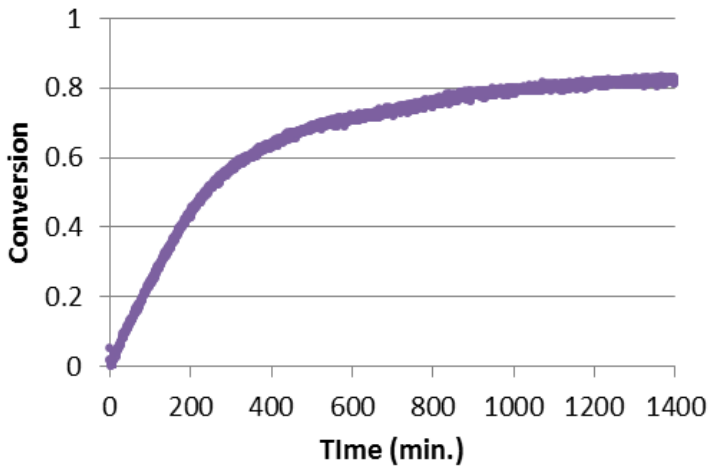


Figure 2.7. Oxidation of clad UO_2 pellet exposed to air at 525°C.

Upon inspection, the product was found to have densified at the reaction interface for those pellets which the reaction rate was greatly reduced. A number of the samples also showed evidence of cladding deformation and even rupture due to the stress induced. Several of the clad, partially reacted pellets were cross-sectioned for micrographs. The micrographs displayed a concave reaction interface as shown in Figure 2.8, which is believed to be an artifact of the stress distribution with greater internal stress at the cladding-uranium oxide interface. While plugging at the reaction interface was frequent, reaction rate differences in the linear section of the reaction curve were still measureable when oxidant concentration and agitation parameters were varied.

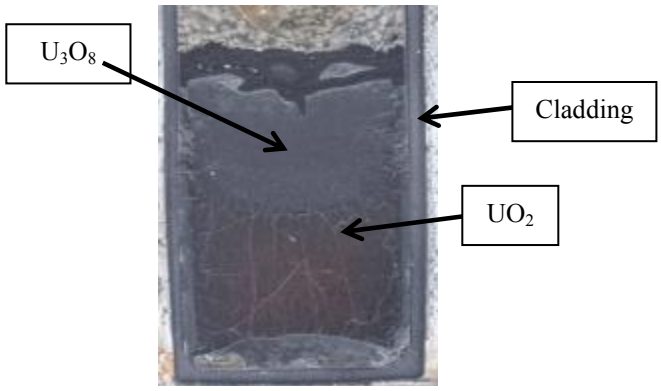


Figure 2.8. Cross-section of partially reacted pellet, which plateaued during reaction.

Experiments were conducted using flowing air and oxygen as oxidants with significant observed changes in reaction rate. The reacted pellets were clad with 8-cm-long cladding with an oxidant flow rate of 200 sccm. It was found, for the linear portion of the reaction rate, that the reaction proceeded at 0.64 cm/hr with 1 atm partial pressure of oxygen, while the observed reaction rate with air (0.21 atm partial pressure) was 0.10 cm/hr. The relative increase agrees with a study of Goode *et al*. for unclad irradiated pellets [1].

Reaction rate data for clad agitated pellets was also collected. Post reaction pellets were cross-sectioned to determine the effectiveness of the agitation for removal of the product from the reaction interface. An image of a partially reacted agitated clad pellet micrograph is shown in Figure 2.9 where very little product material is observed at the interface. The oxidation progression rate, up to 35% conversion for an agitated pellet under 0.21 atm oxygen at 525°C, is 0.17 cm/hr, which is comparable to an oxidation progression rate of 0.20 cm/hr for progression under oxygen for an unclad pellet, assuming the radius is the limiting dimension.

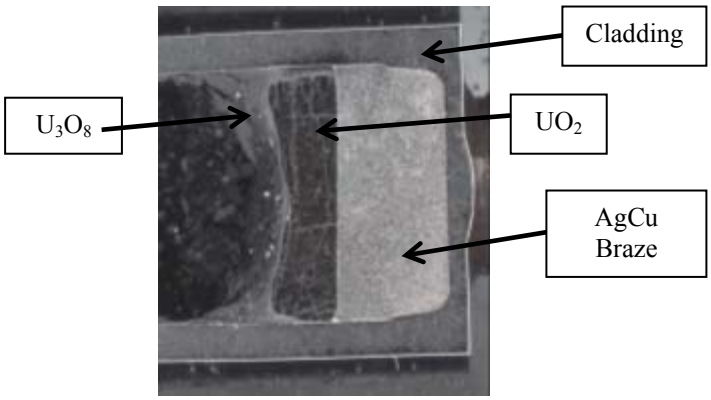


Figure 2.9. Cross-section of clad pellet, which was reacted with agitation.

The reaction rate data for clad, unclad, and clad vibrated samples are shown in Figure 2.10. The rate of reaction of the agitated sample in air was observed to be approximately 76% greater than the unagitated sample.

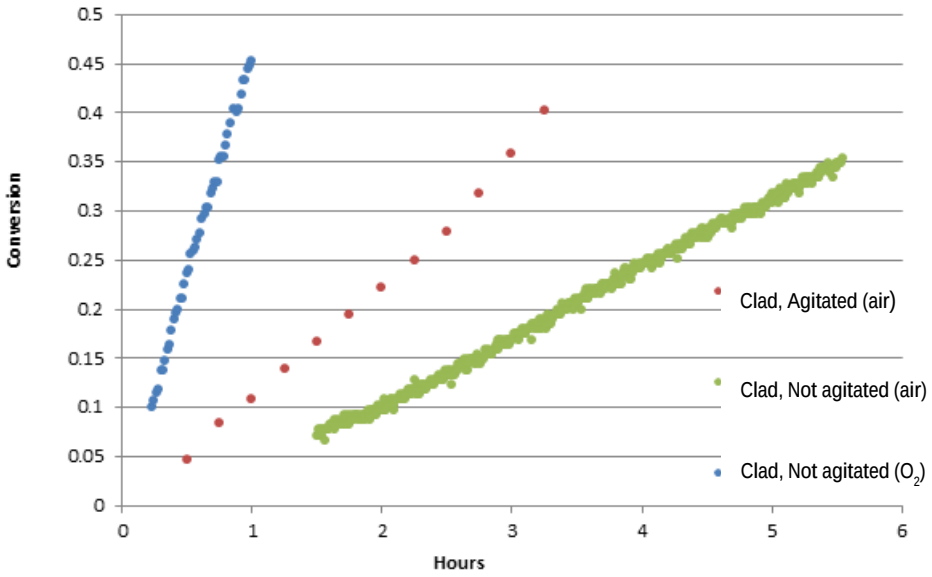


Figure 2.10. Conversion rate for clad UO_2 pellets to U_3O_8.

2.3.2 *Used Fuel Reaction Rate*

A 2-in. segment of used Dresden Boiling Water Reactor (BWR) Fuel (24GWD/MT burnup, 34-year decay) was oxidized in a hotcell environment at 525°C in a macro-TGA system. The segment was open on both ends unlike the surrogates, which were exposed to oxidant only on one face. A quartz bowl/stand was used to contain the oxidizing segment, which sat on a scale and within a tube furnace. A top plate was placed on the furnace, which had limited t ventilation. The thermocouple and gas delivery were implemented from the top plate with the thermocouple dipping down within an inch of the fuel. Before placing the fuel in the bowl, the system was brought to temperature with an air flow rate of 200 sccm. After the system remained at temperature for 30 minutes, the top plate was lifted and the segment of fuel was placed in the system. Initially, weight measurements were recorded every five minutes, and after the reaction had slowed, weight measurements were recorded every hour as can be observed in Figure 2.11.

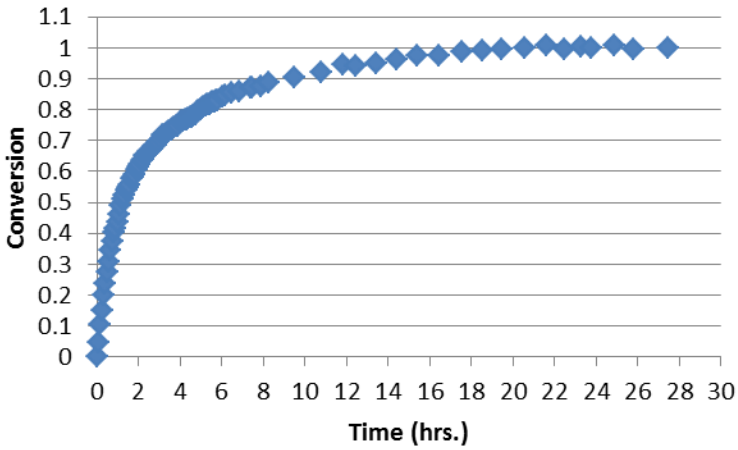


Figure 2.11. Conversion rate for a 2-in. clad Dresden fuel segment at 525°C in air (no agitation).

Initial oxidation was observed to be almost linear with no incubation period. An oxidation progression rate of 0.67 cm/hr was calculated based on the oxidation rate observed up to a conversion of 0.35 for each reaction front. The product of the oxidation process was examined and is shown in Figure 2.12. It was observed that a fraction of the product fell out of either end of the segment. It was also observed that the cladding had deformed with most of the observed swelling being located toward the middle of the cladding. The segment was agitated to remove the residue powder; however, it was evident that a large fraction of the product was tightly packed in the middle of the cladding and likely the cause of the deformed Zircaloy. Based on the observation gained in the surrogate experiments coupled with the reaction curve and evidence of plugged product, it is believed that the compacted product is the cause of the slow extended reaction as was the case in surrogate experiments.



Figure 2.12. Swollen Dresden used nuclear fuel segment, post reaction.

2.4 Model and Discussion of Results

2.4.1 Model Approach

A shrinking core model is thought to be the most appropriate for the case of oxidation of clad pellets. Such a model was first presented by Yagi and Kunii and has been adjusted by others such as Levenspiel [17, 18]. In the model, an unreacted core exists with a sharp reaction interface that recedes until the reactant is completely transformed. There are five proposed general potential controlling phenomena in the classical shrinking core model with any one, or combination of, phenomena controlling the reaction rate. The phenomena are listed below:

1) Diffusion of gaseous reactant through a gaseous film surrounding the surface
2) Penetration (diffusion) of reactant gas through the product or "ash" layer before meeting unreacted core
3) Reaction of gas with solid at core interface
4) Diffusion of gases back through "ash" layer
5) Diffusion of gases back through stagnant gas layer surrounding particle

From experiments performed in this work and other studies previously mentioned, it is believed that gas layer diffusion or mass transfer (Phenomenon 1) is not the controlling phenomenon for reaction. With no gaseous product, Phenomena 4 and 5 also do not warrant further consideration. Phenomena 2 and 3 were considered and models derived for the geometry of the system are shown in Figure 2.13 for cladded fuel with two exposed surfaces at either end of the segment. It was observed that the reaction fronts from either end receded toward the center

of the material until all UO_2 was converted to U_3O_8. The model is applied to the entire clad UO_2 segment and not for each grain. Model nomenclature is based on the following reaction.

$$A(gas) + bB(solids) \rightarrow \text{Solid Products}$$

$$O_2(g) + 3UO_2(s) \rightarrow U_3O_8(s) \quad (2.2)$$

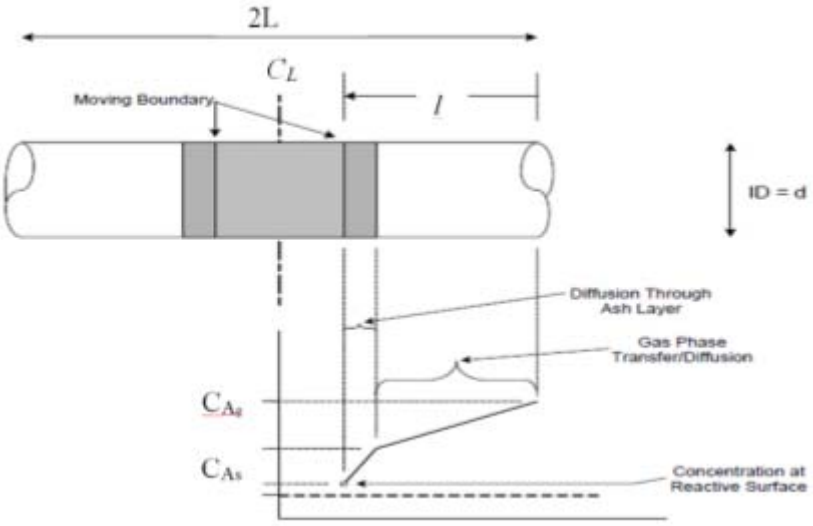


Figure 2.13. Schematic of clad UO_2 oxidation system with potential controlling reaction phenomena.

2.4.1.1 Diffusion through Product

The following derivation is for the standard case in which the diffusion of oxidant gas through a product layer is controlling. In this case, the product layer extends, at all times, to the end of the cladding, and the thickness of the product gas layer increases with the reaction as the reaction front recedes toward the center. An effective diffusivity is used, which is the product of

the gas phase diffusivity and a scalar, which represents the porosity (ε) over the tortuosity (τ). The model is based on Fick's first law in one direction with constant diffusivity. In the following, N_A represents moles of oxidant gas (O_2), Q_A represents the molar flux of O_2, r is the radius of the pellet inside the cladding, t is time, and l is the length at a given time.

$$-\frac{dN_A}{dt} = b\pi r^2 Q_A \tag{2.3}$$

$$Q_A = D_{eff}\frac{dC_A}{dl} \qquad D_{eff} = D_{A,B}\frac{\varepsilon}{\tau} \tag{2.4}$$

$$-\frac{dN_A}{dt} = b\pi r^2 D_{eff}\frac{dC_A}{dl} \tag{2.5}$$

$$-\frac{dN_A}{dt}\int dl = b\pi r^2 D_{eff}\int dC_A \tag{2.6}$$

Integrating from L (initial length) to l and from C_{As} to 0, where ρ_B is the molar density of UO_2,

$$-\frac{dN_A}{dt}(L-l) = b\pi r^2 D_{eff} C_{As} \tag{2.7}$$

$$-\pi r^2 \rho_B \int (L-l)dl = b\pi r^2 D_{eff} C_{As}\int dt \tag{2.8}$$

Integrating from L to l and from 0 to t,

$$t = \frac{\rho_B L^2 \left(\left(\frac{l^2}{L^2} \right) - \left(\frac{2l}{L} \right) + 1 \right)}{2bD_{eff} C_{A_s}} \tag{2.9}$$

Using the Chapman-Enskog theory for bimolecular diffusion, a diffusivity coefficient for oxygen/nitrogen system can be estimated by,

$$D_{A,B} = 0.0018583 \frac{\sqrt{T^3 \left(\frac{1}{M_A} + \frac{1}{M_B} \right)}}{p\sigma^2{}_{A,B}\Omega_{D,A,B}} \tag{2.10}$$

where M_A is the molecular weight of oxygen for this case, M_B is that for nitrogen, p is the absolute pressure, $\sigma_{A,B}$ is the "average collision diameter," and $\Omega_{D,A,B}$ is a collision integral based on the Lennard-Jones potential.

The application of the model using the diffusivity coefficient without the porosity and tortuosity give the case for a stagnant nitrogen layer to the end of cladding. For the limiting case in which a stagnant nitrogen layer extends to the end of the cladding, a reaction time for a 2.54 cm segment of fuel, open to both ends, of 37.8 minutes is predicted from the model. The character of such a reaction curve is shown in Figure 2.14.

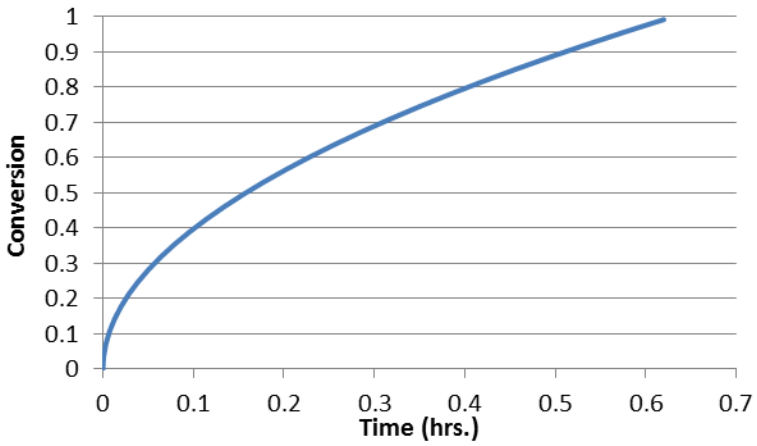


Figure 2.14. Diffusion model for gas layer diffusion reaction control at 525°C and 1 atm air.

2.4.1.2 Chemical Reaction

The rate of reaction based on molar rate of A or B reacting can, in some cases, be expressed based on the stoichiometry of the reaction equation:

$$-\frac{1}{S_{rx}}\frac{dN_B}{dt} = -\frac{1}{\pi r^2}\frac{dN_B}{dt} = -\frac{b}{\pi r^2}\frac{dN_A}{dt} = bk''(C_{A_S}) \tag{2.11}$$

where S_{rx} is the area of the reaction surface. In the case at hand, this would be the one open end of a pellet. The reaction is also assumed in this equation to be first-order with the reaction rate constant, k'', and C_{A_g} is the concentration of reactant gas at the reaction interface. Also, it should be noted that the units of k'' are length per time and the volume is denoted by V.

$$N_B = \rho_B V \tag{2.12}$$

$$-dN_B = -b \cdot dN_A = -\rho_B dV = -\rho_B \pi r^2 dl \tag{2.13}$$

$$-\rho_B \int dl = bk''(C_{A_g} - C_{A_s}) \int dt \tag{2.14}$$

By substitution and integration from L to l and 0 to t,

$$t = \frac{\rho_B (L - l)}{bk'' C_{A_g}} \tag{2.15}$$

2.5 Model/Data Comparison

Results obtained for oxidation of fuel surrogates demonstrated the potential reaction scenarios and influence of several variables. It was observed that oxidation of clad pellets without agitation can proceed by two different paths. The reaction rate was observed to be linear throughout for a minority of the samples, while more frequently the reaction of the samples would proceed by two stages. First, a linear reaction behavior is observed, which is followed by reaction slowing with a more parabolic character at some conversion, which varied with no obvious correlation with temperature or oxidant. The agitation of clad samples led to linear reaction through complete conversion without product plugging.

From the observations made from surrogate tests and application of the model, it is clear there are two distinct stages of reaction control for unagitated samples with product plugging. Initially, it is believed that the reaction proceeds by surface area/kinetic control during the initial linear portion of the reaction curve. Using the kinetic model previously derived, a reaction rate constant (cm/s) can easily be extracted. A kinetic constant of approximately 0.35 cm/s is estimated for the reaction of the clad Dresden used fuel segment.

The second stage was then modeled by the diffusion control case. From this model diffusion coefficients were solved but were not found to be constant. This, with the observation of a dense plugged layer of product, leads to the conclusion that the effective diffusivity is not constant, and it is likely that the porosity of the product changes with conversion. The relative change in tortuosity is thought to be negligible, as significant changes in grain size are not expected. The observation of the plugging taking place at some intermediate point other than the end of the cladding leads to a revised model, which accounts for changing porosity at some length L* as shown in the diagram in Figure 2.15 in which it is proposed there are three distinct zones.

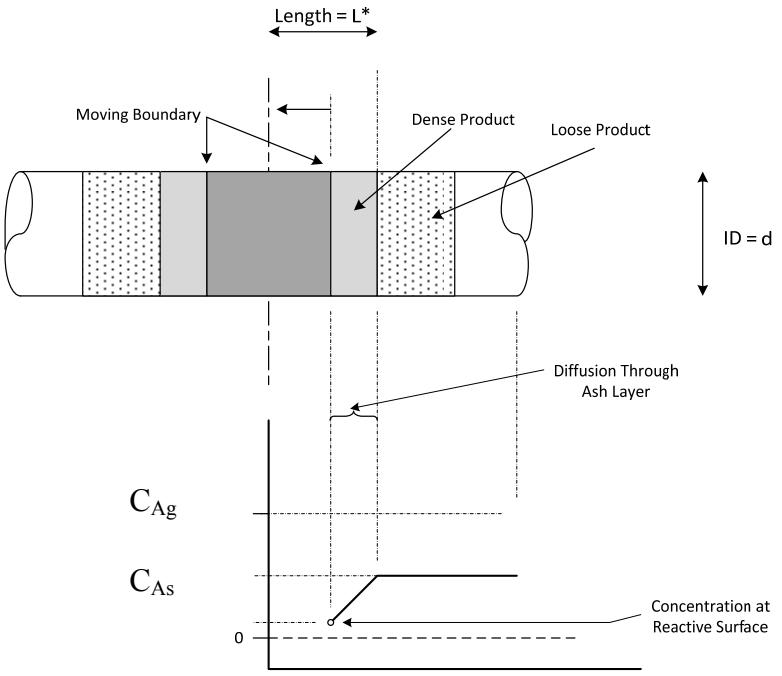


Figure 2.15. Schematic of clad UO_2 oxidation system with two product phases.

As the reaction front progresses, the product (U_3O_8) is forced into the dense U_3O_8 phase further compacting the material and causing it to approach its theoretical density. The

observation of cladding deformation is evidence of relieved stress from this densification. The result is reduction of void volume and, therefore, reduction of porosity. A mathematical representation of this process can be expressed as:

$$-\frac{dN_A}{dt} = b\pi r^2 \frac{\varepsilon(t)}{\tau} D_{A,B} \frac{dC_A}{dl} \tag{2.16}$$

$$\varepsilon = \frac{V_{Void}}{V_{Geometric}} \tag{2.17}$$

$$\varepsilon = \frac{V_{Void_o} - N_{product}\rho_{theo}}{\pi r^2 l(t)} \tag{2.18}$$

$$N_{product} = N_A \tag{2.19}$$

where V_{void} is the void volume, V_{Void_o} is the initial void volume at the time of plugging, $V_{Geometric}$ is the geometric volume of the dense U_3O_8 phase, and ρ_{theo} is the theoretical density of U_3O_8. By substitution,

$$-\frac{dN_A}{dt} = b\frac{V_{Void_o} - N_A\rho_{theo_P}}{l(t)} \frac{1}{\tau} D_{A,B} \frac{dC_A}{dl} \tag{2.20}$$

The model is integrated from L* to l and from time 0 to t. Time of diffusion-controlled reaction after plugging can be added to that of the kinetic model up to the transition conversion for an

overall time of reaction. A sketch of the reaction curve character of each of the controlling phenomena, individually, as well as the proposed step-wise process, which is thought to occur, is shown in Figure 2.16.

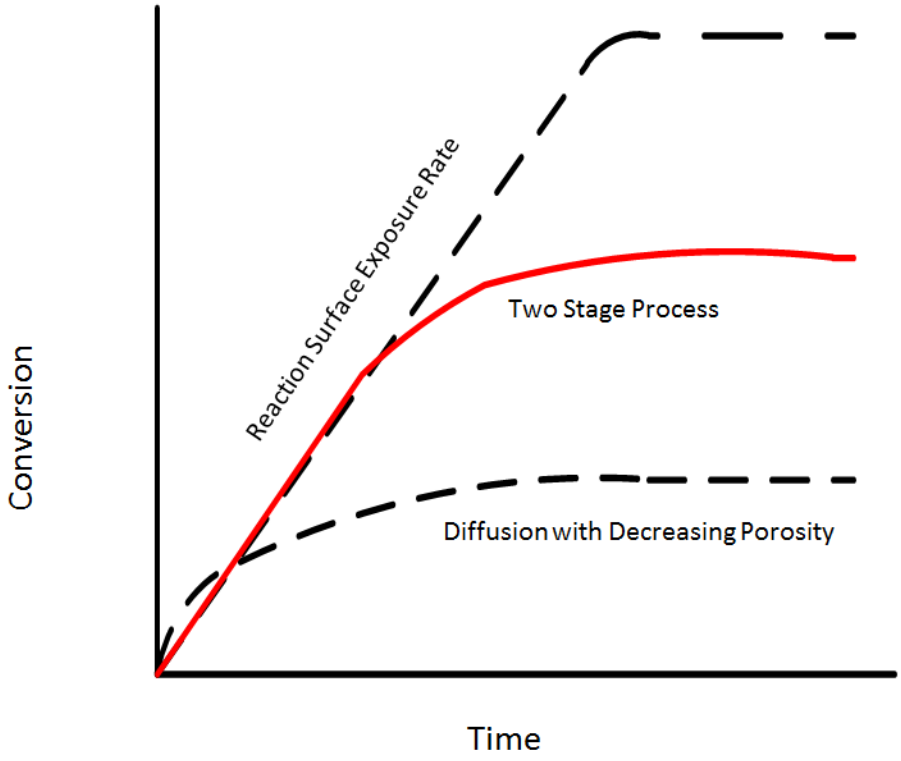


Figure 2.16. Reaction character of diffusion, reaction control, and hybrid.

From the curves in Figure 2.16, one can see how the combination of the surface exposure rate-limiting process and diffusion with changing porosity can be combined to describe the character, which has been observed for the reaction of clad pellets.

2.6 Conclusions

While various approaches to modeling the oxidation of UO_2 to U_3O_8 have been proposed and demonstrated, a physically accurate model developed from phenomenological studies that couples probing experiments with model development had yet to be shown. The work presented uses limited assumptions, due to parametric isolation experiments, and general experimental observations. This work confirms that a nucleation and growth reaction model, while it may fit the curve, is not accurate for the reaction of pellets either clad or unclad. This conclusion can be drawn from the observations of a moving reaction front, which stalls upon product plugging.

Parametric studies demonstrated the relative influence of temperature, oxygen partial pressure, and agitation. It was found that oxygen partial pressure was the most influential variable for reaction of unclad pellets and clad pellets during the linear portion of reaction. Agitation was found to aid in reaction for clad pellets with increased linear reaction rate and, most importantly, for avoidance of plugging, which was observed to occur for unagitated clad pellets, resulting in a reaction rate plateau. From the reaction kinetic data gathered and cross-sectioned clad samples for which the reaction plateaued, it was determined that the reaction was likely diffusion-controlled due to the formation of dense U_3O_8 product layer, which is pinned to the cladding wall. It is believed the continued reaction further compacts the product and reduces the diffusion rate.

The system was initially modeled with the base shrinking core model for which gas layer diffusion, product layer diffusion, and reaction kinetics were considered. It was found that, for unclad fuel and for agitated systems, this base model is appropriate, with rate of exposed surface/kinetics controlling the reaction with a moving sharp reaction interface. For the case of clad pellets without agitation, a two-stage model is thought to be accurate. In this model, the

reaction term controls while the reaction is linear, after which, diffusion control dominates upon plugging of the reaction product in the cladding for stage 2. For this second stage, a revised standard shrinking core model is proposed in which the changes affecting diffusivity are accounted for by varying porosity with product conversion. The model also accounts for the actual dense product layer thickness and is no longer based on the assumption that the product layer resisting diffusion extends at all times to the initial length of the reactant material. The oxidation studies presented provide needed insight into controlling phenomena for the voloxidation of clad UO_2 pellets. The proposed method to model the two typical cases of oxidation of clad UO_2 pellets can now be extended to larger scale models of voloxidation systems.

Acknowledgments

This research in part has been sponsored by the Laboratory Directed Research and Development Program of Oak Ridge National Laboratory (ORNL) which is managed by UT-Battelle, LLC. The work was performed at ORNL under the auspices of the Nuclear Security and Isotope Technology Division.

References

1. Goode, J.H., *Voloxidation - Removal of Volatile Fission Products from Spent LMFBR Fuels.* ORNL-TM-3723, Union Carbide Corporation, Oak Ridge National Laboratory, January 1973.

2. Goode, J.H., R.G. Stacy, and V.C.A. Vaughen, *Head-End Reprocessing Studies with H. B. Robinson-2 Fuel.* ORNL-TM-6037, Union Carbide Corporation, Oak Ridge National Laboratory, June 1978.

3. Goode, J.H., *et al*., *Comparison Studies of Head-End Reprocessing Using Three LWR Fuels.* ORNL-TM-7103, Union Carbide Corporation, Oak Ridge National Laboratory, June 1980.

4. Spencer, B.B., *et al*., *Voloxidation Processing of Kilogram Quantities of Used Nuclear Fuel*. in *Sixteenth Symposium on Separation Science and Technology for Energy Applications*. 2009. Gatlinburg, Tennessee.

5. McEachern, R.J., *et al*., *Determination of the activation energy for the formation of U_3O_8 on UO_2.* Journal of Nuclear Materials, 1997. **249**(1): p. 58-69.

6. McEachern, R.J. and P. Taylor, *A review of the oxidation of uranium dioxide at temperatures below 400°C.* Journal of Nuclear Materials, 1998. **254**(2-3): p. 87-121.

7. Bae, K.K., *et al*., *Oxidation Behavior of Unirradiated UO_2 Pellets.* Journal of Nuclear Materials, 1994. **209**(3): p. 274-279.

8. Quemard, L., *et al*., *On the origin of the sigmoid shape in the UO_2 oxidation weight gain curves.* Journal of the European Ceramic Society, 2009. **29**(13): p. 2791-2798.

9. Ackermann, R.J., A.T. Chang, and C.A. Sorrell, *Thermal-Expansion and Phase-Transformations of U_3O_{8-Z} Phase in Air.* Journal of Inorganic & Nuclear Chemistry, 1977. **39**(1): p. 75-85.

10. Johnson, W.A. and R.F. Mehl, *Reaction Kinetics in Processes of Nucleation and Growth (Reprinted from Transactions of the American Institute of Mining & Metallurgical Engineers, vol 135, pg 416, 1939).* Metallurgical and Materials Transactions a-Physical Metallurgy and Materials Science, 2010. **41A**(11): p. 2713-2775.

11. Avrami, M., *Kinetics of Phase Change. I General Theory.* The Journal of Chemical Physics, 1939. **7**(12): p. 1103-1112.

12. Jeong, S.M., J.M. Hur, and H. Lee, *Kinetic Modeling Study of a Voloxidation for the Production of U_3O_8 Powder from a UO_2 Pellet.* Nuclear Engineering and Technology, 2009. **41**(8): p. 1073-1078.

13. Jeong, S.M., *et al*., *A kinetic study of the oxidation of uranium dioxide.* Reaction Kinetics and Catalysis Letters, 2006. **89**(2): p. 269-275.

14. McCracken, D.R., *Oxidation of UO_2 at 400°C to 1000°C in Air and its Relevance to Fission Product Release.* AECL-8642, Chalk River Nuclear Laboratories, Atomic Energy of Canada Limited, July 1985.

15. Peakall, K.A. and J.E. Antill, *Oxidation of Uranium Dioxide in Air at 350-1000°C.* Journal of Nuclear Materials, 1960. **2**(2): p. 194-195.

16. Iwasaki, M., *et al*., *Oxidation of UO_2 Pellets in Air - Effect of Heat-Treatment of Pellet on Particle Size Distribution of Powders Produced.* Journal of Nuclear Science and Technology-Tokyo, 1968. **5**(12): p. 652.

17. Levenspiel, O., *Chemical Reaction Engineering*. 3rd ed. 1999, New York: John Wiley & Sons.

18. Yagi, S. and D. Kunii, *Fluidized-Solids Reactors with Continuous Solids Feed .1. Residence Time of Particles in Fluidized Beds.* Chemical Engineering Science, 1961. **16**(3-4): p. 364-371.

CHAPTER 3

PHASE MAPPING OF URANIUM OXIDES USING NEUTRON DIFFRACTION

This chapter is a revised version of a paper (minor revisions due to its inclusion as a chapter in the dissertation) by the same title in preparation for a journal by: Jared A. Johnson, Claudia J. Rawn, and Camden R. Hubbard.

My contributions to this paper include: (1) all of the experiments, (2) analysis/modeling of data, and (3) most of the writing.

Abstract

The oxidation of UO_2 pellets contained in 316 stainless steel cladding was studied. Depleted uranium oxide pellets within the cladding were partially reacted with exposure to an oxidant at one end. The partially reacted samples prepared at temperatures of 325, 450, 500, and 600°C were spatially mapped by neutron diffraction to determine phase distribution. Measurements were taken at the Oak Ridge National Laboratory (ORNL) High Flux Isotope Reactor (HFIR) on the HB-2B beam line, which is equipped with an automated sample positioning system and a collimated neutron beam. After neutron interrogation, the samples were cross-sectioned to allow for correlation of the data with micrographs. The study presented is novel in the use of spatial mapping by neutron diffraction to study uranium oxide phase distribution of spatially oxidized clad pellets and density gradient of the oxide product above the reaction interface.

3.1 Introduction

There have been numerous studies of various aspects of the oxidation of UO_2 as they apply to different applications such as accident scenarios and fuel reprocessing technologies *i.e.*, voloxidation, which is a process in which UO_2 is oxidized to enable the release of volatile and semi-volatile fission products [1-6]. In spite of the extensive research to date, there remain large

gaps in the understanding of the fundamentals of these oxidation reactions. Furthermore, the majority of these studies have been focused on oxidation reactions at lower temperatures of 350°C and below [7-10]. The work presented here is focused on reactions at higher temperatures and specifically investigating the phase distribution of oxides at the reaction interface of clad UO_2 oxide pellets. There have been limited studies of UO_2 oxidation processes by neutron diffraction and most of these have also focused on experiments carried out at lower temperatures [11, 12]. An understanding of the oxide phase distribution at the point of reaction is needed to determine if an effective multi-phenomena-based model beyond solely chemical reaction is required.

The reaction of UO_2 to U_3O_8 below a temperature of 350°C in an oxygen-rich environment is a two-step reaction process (Equation 3.1) [1].

$$UO_2 \rightarrow U_3O_7/U_4O_{9+y} \rightarrow U_3O_8 \tag{3.1}$$

The initial reaction to intermediate phases of U_3O_7 and/or U_4O_{9+y} is a diffusion-controlled process as evidenced by the observed parabolic shaped reaction curve [1]. At intermediate temperatures, close to 350°C, the parabolic reaction curve is still a result of the diffusion-controlled process. After U_4O_9/U_3O_7 forms, a sigmoidal reaction curve develops as the reaction proceeds to the formation of U_3O_8. The oxidation from the intermediate phases to U_3O_8 is known to proceed by a nucleation and growth process [1]. However, while some model the reaction of UO_2 pellets to U_3O_8 as a nucleation and growth process, using models such as Johnson-Mehl or Avrami, is physically inaccurate for dense pellets. While the reaction curve remains sigmoidal for pellets, the reaction to U_3O_8 of a pressed pellet is thought to be controlled by spallation and

cracking [3, 13, 14]. The cracking and subsequent spalling of the U_3O_8 product is the result of the drastic crystalline volume change of 36% resulting from the phase transformation from cubic (fluorite type) UO_2 to the orthorhombic U_3O_8 structure. Initial cracking at temperatures where the intermediates have been found is attributed to the slight density reduction (~2%) resulting from the formation of the U_4O_9/U_3O_7 [5, 15, 16]. The reaction temperatures of interest in this study are above 350°C, for which the majority of literature suggests no significant intermediate phases have been observed [17, 18]. This is likely due to the increased kinetics that causes the process to quickly pass through these phases and not due to their complete absence from the oxygen enrichment. However, the work of McCraken *et al*. suggests that at temperatures (above 400°C, there is a significant layer of intermediate phases (U_4O_9/U_3O_7) [19]. This work is intended to study this interface by spatially mapping the phases using neutron diffraction and combining the results with visual observations based on photo micrographs.

Because the reaction is believed to be surface area controlled, the reaction interface must be better understood. Previous studies have examined the exposed surface of the reaction as the material spalls [3, 14]. These studies have described and shown a step-wise process for oxidation and consequential spalling of the materials. However, the phases present at the reaction interface were not definitively determined. Other analyses, aimed at modeling the reaction as a multi-phenomenon process for fuel reprocessing techniques, have attempted to directly apply shrinking particle or shrinking sphere type models in which gas layer diffusion, product layer diffusion, and chemical reaction are modeled and then summed to give an overall reaction rate [20]. This model assumes a sharp reaction interface that has not been experimentally verified [21, 22].

The experiments reported here were aimed at mapping the phases of uranium oxide at the reaction interface to determine the length scale of the interface, and to determine if there exists a

mixture of uranium oxide phases over some significant depth, or discrete homogenous phases. To achieve this, neutron diffraction studies were carried out at the Oak Ridge National Laboratory (ORNL) High Flux Isotope Reactor (HFIR). The material at the interface was investigated and the d-spacings within the "unreacted" section of the pellets were mapped. The d-spacing profile provides an understanding of oxygen gradient for UO_{2+x} material that has not reacted to a U/O ratio required for initial phase change to intermediates.

3.2 Experimental

3.2.1 Sample Preparation

UO_2 pellets, pressed and sintered with a density of 10.44 g/cm^3, corresponding to 95% of the theoretical density were used for the oxidation reactions. The average grain size within the pellet was determined to be to 17.5 ± 0.6 μm. The sintered pellets were 1.39 cm long and had a diameter of 0.68 cm corresponding to the approximate size of pressurized water reactor (PWR) fuel pellets. The pellets were reduced under an Ar/H_2 (96/4) mix to minimize any surface oxidation. The treated pellets were loaded into stainless steel "cups" 8 cm deep with a 0.691 cm inside diameter and open on one end. The cladding was pretreated by heating to 500°C. The pellets fit tightly in the cups with a gap of 5.5×10^{-3} cm.

The oxidation reactions were carried out inside a macro-thermogravimetric analysis (TGA) unit. The clad pellets were brought to temperature under a helium purge during which no weight gain was observed. Once the TGA equilibrated, the reactant gas (O_2 or air) was initiated. The gas was delivered to the sample at a flow rate of 200 sccm. The weight gain was monitored, and at the selected extent of reaction, the gas feed was changed back to helium and the sample

was cooled to room temperature. The conditions under which each of the samples was prepared are summarized in Table 3.1.

Table 3.1. Sample listing with reaction conditions.

	Pellet 1	Pellet 2	Pellet 3	Pellet 4	Pellet 5
Feed Gas	O_2	O_2	O_2	O_2	Air
Temperature	500°C	450°C	325°C	600°C	500°C

The conditions chosen are those within the range typically employed in the voloxidation process but also correspond to potential accident scenario conditions. The reactions were stopped before complete oxidation of the UO_2 pellets in order to produce substantial quantities of the oxide product while leaving a significant fraction of unreacted UO_2 pellet.

After oxidation and neutron measurements were conducted, the clad pellets were mounted, cross-sectioned, and polished after the loose product powder was removed to allow for comparison of the micrographs relative to the position mapping data collected for each partially reacted pellet.

3.3 Diffraction Measurements

Aluminum tubes were used to contain the partially reacted stainless steel clad uranium oxide. The neutron diffraction measurements were conducted at the HB-2B beam line at the HFIR. An image of the sample, staged for measurement, is shown in Figure 3.1. The neutron beam was collimated to a height of 0.5 mm and a width of 5 mm, at the exit, after being passed through the silicon monochromator; however, the height at measurement is larger due to vertical

divergence of the beam. A wavelength of 2.67 Å was used. The instrument's monochromator allows for secondary harmonic energies that were observed and will be discussed later.



Figure 3.1. Clad, partially reacted, depleted uranium oxide samples in aluminum tubes loaded for neutron diffraction measurements.

The oxides within the concentric aluminum tubes and stainless steel cladding were mapped in 0.5 mm increments, initiated below the pellet moving up to the reaction interface and beyond. Count times between 3 and 40 minutes were employed depending on the observed intensities. The instrument utilizes seven detectors, and the data presented is the summation of the counts for all seven detectors. After scanning the samples along the length, step scans in 2θ were taken at what was determined to be the approximate reaction interface to determine if any additional phases other than U_3O_8 were present. Data were collected in two regions from approximately 84 to 90° 2θ and from 76.5 to 83° 2θ. These ranges were chosen because they are regions containing strong non-overlapping reflections for UO_2 (*i.e.*, the (220) reflection at approximately 87.30° 2θ and I/I_{max} = 100%) and U_3O_8 (*i.e.*, the (002) reflection at approximately 80.16° 2θ and I/I_{max} = 81.7%), respectively, based on calculated neutron powder diffraction

patterns using the 2.67 Å wavelength. Additionally, within these ranges the (808) refection of U_3O_7 with an I/I_{max} = 100% was calculated to be at 87.10° 2θ and the (808) reflection of the U_4O_9 with an I/I_{max} = 100% was calculated to be at 87.79° 2θ. Due to several contributing factors (*e.g.*, data collection time, density of interface material, etc.), it is difficult to state what the lowest quantitative amount of secondary phase could be; however, since the ranges of data collection contained the strongest peaks for possible secondary phases it is likely that they could be distinguished and identified. The location of the aluminum and stainless steel reflections was also considered when choosing the ranges. Step scans were compared to calculated patterns for all likely uranium oxide phases.

3.4 Results and Discussion

3.4.1 Neutron Diffraction Results

Neutron diffraction patterns were collected for each clad pellet in axial steps. Figure 3.2(a-e) shows the count rate for the (220) UO_2 peak versus the position from the bottom of each UO_2 pellet moving up each sample toward the open end of the 316 stainless steel cup. It can be observed from these plots that the intensity ranges from near zero to the maxima over approximately 1 to 1.5 mm, and the beam height at the sample position was approximately 1.5 mm. The bottom interface of the pellet and stainless steel cup is sharp, and the distance from minimum to maximum counts per minute is ~1.5 mm. Based on this observation, the data shows the reaction interface at the other end of the pellet to be just as sharp within the resolution of the measurements. This conclusion and the lack of clearly observable peaks at the locations discussed above for U_3O_7 and U_4O_9 suggests there is not a significant mixture of uranium oxide

phases over an extended depth. The data also shows no distinguishable difference in the interface as a function of temperature or oxygen partial pressure.

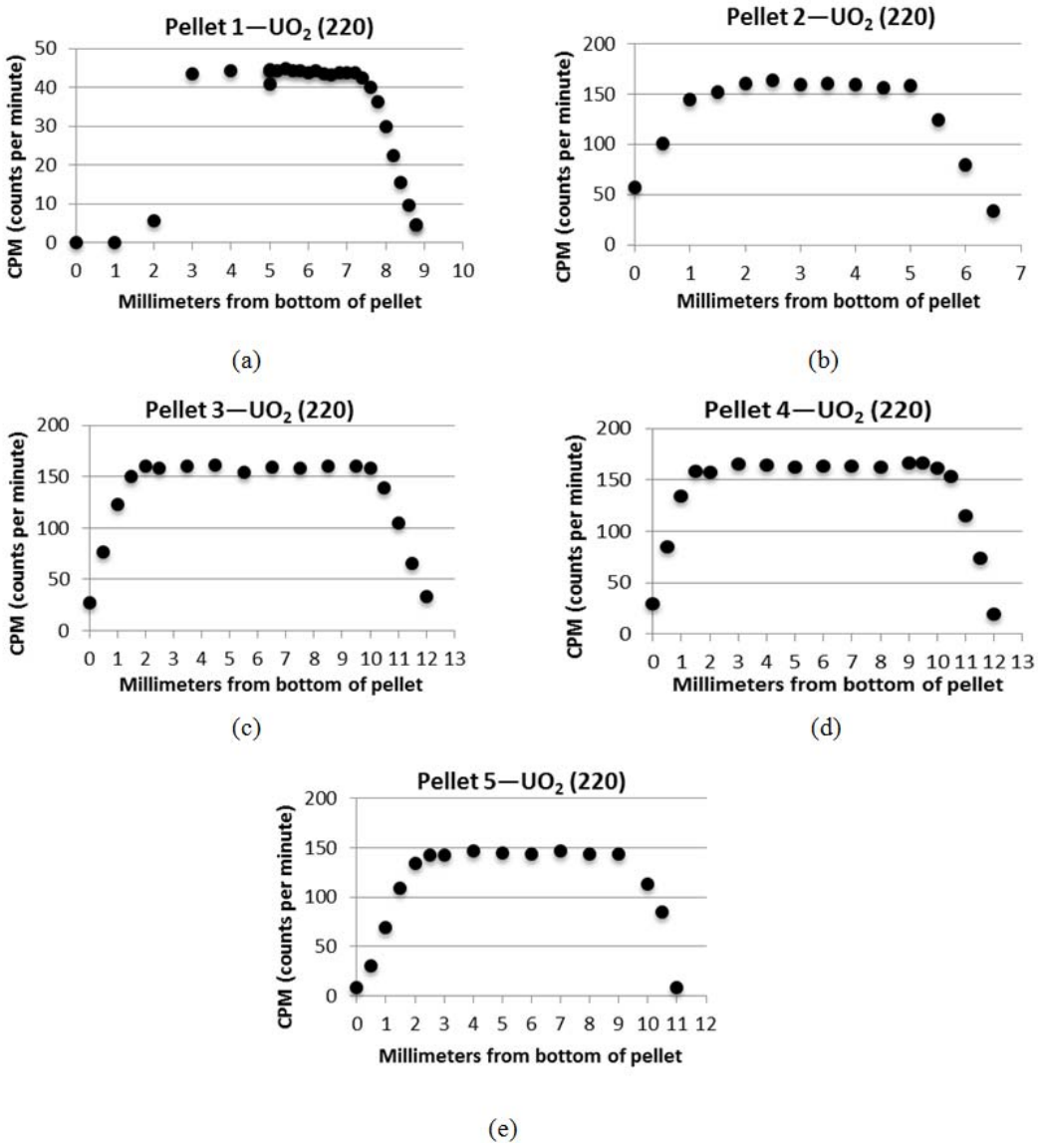


Figure 3.2(a-e). Neutron counts per minute summed for seven detectors for five partially reacted pellets as a function of height for the (220) peak for UO_2.

After axial spatial mapping using the 2θ range that included the UO_2 (220) reflection, data were collected within the 2θ range that included the α-U_3O_8 (002) reflection. The (002) reflection was evident and observed to increase in intensity from the position interpreted as the

UO_2/U_3O_8 reaction interface confirming the location and phase transition position. Longer count times of 40 minutes were needed due to the decreased density of the product powder compared to the UO_2 pellet (*i.e.*, the intensity is stronger when more sample is contained in the diffraction volume and the resulting U_3O_8 product is much less dense than the starting UO_2 pellet). Figure 3.3 shows an example of the raw data. The peak located at the higher 2θ position is the U_3O_8 (002) reflection and increases over distance. The peak located at the lower 2θ is the UO_2 (115) refection present due to the secondary harmonic energy resulting in a wavelength of 1.33 Å. This peak diminishes at the same rate as the previously observed (220) reflection in the 87.30° 2θ measurements.

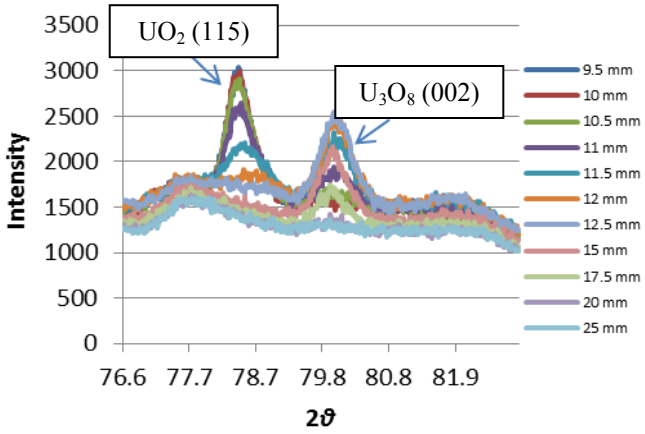


Figure 3.3. Raw data for 40-minute count times of "Pellet 3."

The intensity of the U_3O_8 (002) reflection is shown as a function of position in Figure 3.4. The U_3O_8 product at and just above the reaction interface has been found to be tightly packed in a dense powder when the sample cladding is emptied. The observation that the dense product is formed at the interface is supported by the data showing increased peak intensity that decreases with distance from the interface, which indicates less U_3O_8 material is in the diffracted volume.

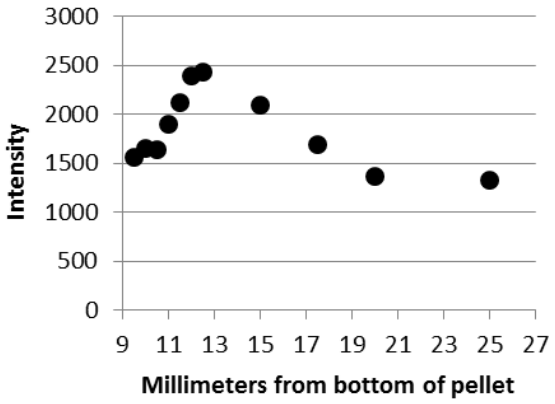


Figure 3.4. "Pellet 3" – U_3O_8 (002) reflection intensity as a function of distance.

Step scans were conducted at what was established to be the interface between UO_2 and U_3O_8 to determine if any intermediate phases such as U_3O_7 or U_4O_9 could be observed. No peaks associated with the intermediate phases were observed for any of the samples measured.

3.5 Comparison of Images to Diffraction Data

A comparison can be made correlating the diffraction data in Figure 3.2e to the cross-section pellet in Figure 3.5 of Pellet 5. The image confirms the position of the UO_2/U_3O_8 interface at approximately 10 mm from the bottom of the pellet. The image shows oxidation occurred primarily at the open end interface and shows a slight concave reaction front. From the image and data collected, it is determined ~29% of the pellet was oxidized. The image of Pellet 5 in Figure 3.5 is typical of each of the cross-sectioned samples. Images of the other four pellets were correlated to the data showing the data interpretation of the reaction interface to be accurate. Loose U_3O_8 product was removed before the samples were cross-sectioned and is not present in the micrograph.

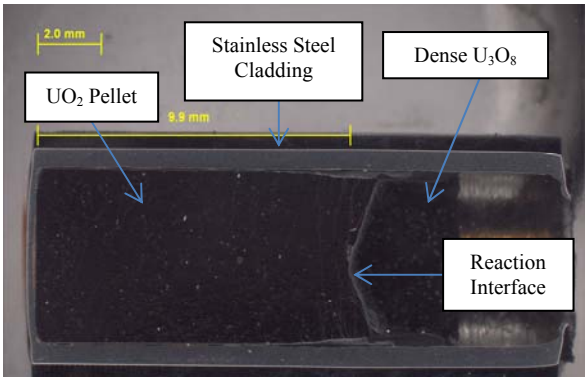


Figure 3.5. "Pellet 5" cross-sectioned post reaction and measurement.

3.6 Conclusion

Partially oxidized UO_2 pellets in stainless steel cups intended to simulate cladding were interrogated with neutrons to determine the phases present at the reaction interface and to determine the character of the interface. The experiments demonstrated the capability to do spatial mapping of the samples as well as step scan mapping at the full range of angles for depleted uranium oxide pellets in stainless cladding. The incident beam was found to be ~1.5 mm and the interface was found to be a sharp convergence of dense UO_2 and powder U_3O_8. The data collected showed no indication of intermediate phases present under any of the reaction conditions. This was expected as the majority of previous work suggests no intermediate phases are present at the temperatures of reaction studied here that are of interest for voloxidation processes. The observation of dense U_3O_8 product at the interface and the confirmation of the sharp interface with no significant quantity of intermediate oxides provide vital information for reaction model development.

Based on the capabilities demonstrated in this study, a variety of additional experiments are possible and would add value. The kinetics of the oxidation reaction could be studied by *in situ* reaction by measurements taken with the beam parallel with the clad pellets over the entire length. Additionally, the study of the oxidation of U_3O_8 to UO_3 with stronger oxidants such as NO_2 or O_3 is planned.

Acknowledgments

This research in part has been sponsored by the Laboratory Directed Research and Development Program of Oak Ridge National Laboratory (ORNL) which is managed by UT-Battelle, LLC. The work was performed at ORNL under the auspices of the Nuclear Security and Isotope Technology Division.

References

1. McEachern, R.J. and P. Taylor, *A review of the oxidation of uranium dioxide at temperatures below 400°C.* Journal of Nuclear Materials, 1998. **254**(2-3): p. 87-121.

2. McEachern, R.J., *et al*., *Determination of the activation energy for the formation of U_3O_8 on UO_2.* Journal of Nuclear Materials, 1997. **249**(1): p. 58-69.

3. Bae, K.K., *et al*., *Oxidation Behavior of Unirradiated UO_2 Pellets.* Journal of Nuclear Materials, 1994. **209**(3): p. 274-279.

4. Peakall, K.A. and J.E. Antill, *Oxidation of Uranium Dioxide in Air at 350-1000°C.* Journal of Nuclear Materials, 1960. **2**(2): p. 194-195.

5. McEachern, R.J., *A review of kinetic data on the rate of U_3O_7 formation on UO_2.* Journal of Nuclear Materials, 1997. **245**(2-3): p. 238-247.

6. Boase, D.G. and T.T. Vandergraaf, *Canadian Spent Fuel Storage Canister - Some Materials Aspects.* Nuclear Technology, 1977. **32**(1): p. 60-71.

7. Choi, J.W., *et al*., *The effect of fission products on the rate of U_3O_8 formation in SIMFUEL oxidized in air at 250°C.* Journal of Nuclear Materials, 1996. **230**(3): p. 250-258.

8. Blackburn, P.E., J. Weissbart, and E.A. Gulbranson, *Oxidation of Uranium Dioxide.* Journal of Physical Chemistry, 1958. **62**(8): p. 902-908.

9. Kim, K.S., *et al*., *Oxidation Behavior of Unirradiated and Irradiated UO_2 in Air at 150-375°C.* Journal of the Korean Nuclear Society, 1997. **29**(2): p. 93-98.

10. Rouyer, J., *et al*., *Modelling of the spent fuel oxidation: Toward the operational model.* Journal of Nuclear Materials, 2009. **395**(1-3): p. 89-98.

11. Desgranges, L., *et al*., *Neutron Diffraction Study of the in Situ Oxidation of UO_2.* Inorganic Chemistry, 2009. **48**(16): p. 7585-7592.

12. Higgs, J.D., *et al*., *Kinetics of precipitation of U_4O_9 from hyperstoichiometric UO_{2+x}.* Journal of Nuclear Materials, 2007. **366**(3): p. 297-305.

13. Valdivieso, F., *et al*., *Oxidation behaviour of unirradiated sintered UO_2 pellets and powder at different oxygen partial pressures, above 350°C.* Journal of Nuclear Materials, 2006. **354**(1-3): p. 85-93.

14. Quemard, L., *et al*., *On the origin of the sigmoid shape in the UO_2 oxidation weight gain curves.* Journal of the European Ceramic Society, 2009. **29**(13): p. 2791-2798.

15. Allen, G.C. and N.R. Holmes, *A Mechanism for the UO_2 to α-U_3O_8 Phase-Transformation.* Journal of Nuclear Materials, 1995. **223**(3): p. 231-237.

16. Thomas, L.E., *et al*., *Microstructure Characterization of Low-Temperature Oxidized LWR Spent Fuel.* PNL-6640, Battelle Memorial Institute, Pacific Northwest Laboratory, December 1989.

17. Walker, D.E.Y., *Oxidation of Uranium Dioxides.* Journal of Applied Chemistry, 1965. **15**(3): p. 128.

18. Ohashi, H., E. Noda, and T. Morozumi, *Oxidation of Uranium-Dioxide.* Journal of Nuclear Science and Technology, 1974. **11**(10): p. 445-451.

19. McCracken, D.R., *Oxidation of UO_2 at 400°C to 1000°C in Air and its Relevance to Fission Product Release.* AECL-8642, Chalk River Nuclear Laboratories, Atomic Energy of Canada Limited, July 1985.

20. Levenspiel, O., *Chemical Reaction Engineering*. 3rd ed. 1999, New York: John Wiley & Sons.

21. Jeong, S.M., *et al*., *A kinetic study of the oxidation of uranium dioxide.* Reaction Kinetics and Catalysis Letters, 2006. **89**(2): p. 269-275.

22. Jeong, S.M., J.M. Hur, and H. Lee, *Kinetic Modeling Study of a Voloxidation for the Production of U_3O_8 Powder from a UO_2 Pellet.* Nuclear Engineering and Technology, 2009. **41**(8): p. 1073-1078.

CHAPTER 4

MEASUREMENTS OF OXIDATION KINETICS FOR U_3O_8 TO ε-UO_3 WITH NO_2

This chapter is a revised version of a paper (minor revisions due to its inclusion as a chapter in the dissertation) by the same title in preparation for a journal by: Jared A. Johnson, Claudia J. Rawn, Barry B. Spencer, Roberta A. Meisner, and Guillermo D. Del Cul.

My contributions to this paper include: (1) all of the experiments, (2) analysis/modeling of data, and (3) all of the writing.

Abstract

The oxidation kinetics of U_3O_8 powder to ε-UO_3 in an NO_2 environment were measured by *in situ* X-ray diffraction (XRD). Experiments were performed using a custom designed and fabricated environmental sample stage at temperatures of 195, 210, 235, and 250°C. Data were refined for quantitative phase fractions using a newly proposed structure for the ε-UO_3 polymorph. The kinetics data was modeled using a shrinking core approach. A proposed two-step reaction process is presented based on the developed models.

4.1 Introduction

The NO_2 oxidation of uranium oxides is of interest to potentially serve as an alternative to oxygen oxidation in standard voloxidation processes. In standard voloxidation, monolithic flouritic UO_2 transforms to orthorhombic α-U_3O_8 powder to release volatiles and remove the pelletized used nuclear fuel (UNF) from cladding. The NO_2 oxidation process is thought to allow for additional release of volatile and semi-volatile fission products as well as possibly proceed with increased kinetics at

temperatures lower than those employed in standard voloxidation processes (*i.e.*, 450–600°C) [1-4].

The NO_2 oxidation of uranium oxide found in oxide UNF is believed to progress by the following reactions [5]:

$$3UO_2(s) + 2NO_2(g) \rightarrow U_3O_8(s) + 2NO(g) \quad (T \geq 350°C) \tag{4.1}$$

$$U_3O_8(s) + NO_2(g) \rightarrow 3UO_3(s) + NO(g) \quad (150°C \geq T \leq 350°C) \tag{4.2}$$

The UO_2 and U_3O_8 products are black in color while the ε-UO_3 is red in color. Oxidant recycle has been proposed in which additional oxygen is introduced to allow for regeneration of NO_2 from the NO product and resulting in a reduction of off-gas volume to be treated and released. Another proposed option for implementation is to use the stability limit of UO_3, which decomposes to U_3O_8 above 400°C–450°C, to further comminute the product by oxidation reduction cycling as has been proposed in the AIROX (Atomics International Reduction OXidation) and OREOX (Oxidation and REduction of OXide fuel) processes. These processes consist of oxidation and reduction cycling of UO_2 and U_3O_8 with the use of air/oxygen and hydrogen [6]. While the crystalline density change is thought to be minimal for the reaction of U_3O_8 to UO_3 as compared with the 36% crystalline volume change of UO_2 to U_3O_8, Brunauer, Emmet, Teller (BET) surface area analysis has shown an increase in surface area that is essential to the volatile and semi-volatile fission product removal. In addition, this cycling process does not require hydrogen reductant but instead relies on thermal cycling. Another

possible NO_2 oxidation process approach is the slow heating of ε-UO_3 above 400°C, which has been reported to produce the γ-UO_3 polymorph, instead of reduction to U_3O_8, resulting in greater density change and causing increased fracturing [7].

The second oxidation reaction of black U_3O_8 in the presence of NO_2 to red ε-UO_3 at temperatures less than 350°C is the focus of the current work. Studies of this oxidation reaction have been limited and consist of accident scenario studies for radiolysis-induced NO_x formation and research into extractions for UNF using liquid N_2O_4 as a solvent [8-11]. From previous work, several unit cells for ε-UO_3 with three different crystal systems have been proposed; however, atom positions for these phases have not been reported in the literature. A newly proposed structure of the ε-UO_3 polymorph is used for quantitative analysis of *in situ* data. The proposed unit cell determined using both X-ray and neutron diffraction data results in the triclinic crystal system space group $P\bar{1}$.

The objective of this study was to determine the oxidation rates of U_3O_8 to UO_3 in a NO_2 atmosphere as a function of temperature. *In situ* XRD was used to determine the kinetics by refinement of the phase fractions from the data collected at reaction temperatures of 195, 210, 235, and 250°C. Data were collected in a custom designed environmental sample stage fabricated out of reaction resistant materials which contain the reactive gas and depleted uranium and allow for X-ray penetration to the reaction interface. The collected data was modeled using both a standard first-order chemical reaction rate and a shrinking core model.

4.2 Experimental

Data were collected using a PANalytical X-ray diffractometer equipped with an X'celerator detector. Cu Kα radiation with a wavelength of 1.5406 Å was used. The strong oxidizing potential of NO_2 required an environmental sample stage system capable of containing the reactive gas without reaction. With no adequate stages commercially available for this specific system, a stage was designed and fabricated to meet the requirements for the reaction study of interest. A drawing of the custom stage used is shown in Figure 4.1. The base of the stage was constructed of 316 stainless steel. The stage was designed such that the inlet and outlet gas lines and a thermocouple are located within the reaction enclosure next to the well containing the powder samples. The containment dome was constructed of ~0.007-in.-thick nickel foil, which was annealed after being pressed into a dome shape. Nickel was chosen due to its relatively low atomic number allowing for X-ray penetration and its compatibility with NO_2. A thin rim on the stage mates with a collar which fits over the dome to create a seal. The stage was designed to be compatible with an Anton-Paar XRK 900 furnace and fits within the furnace enclosure. Proportional-Integral-Derivative (PID) settings were adjusted to maintain the temperature ±2°C. Gas lines in and out were heated to ensure NO_x delivered to system was in the form of gaseous NO_2.

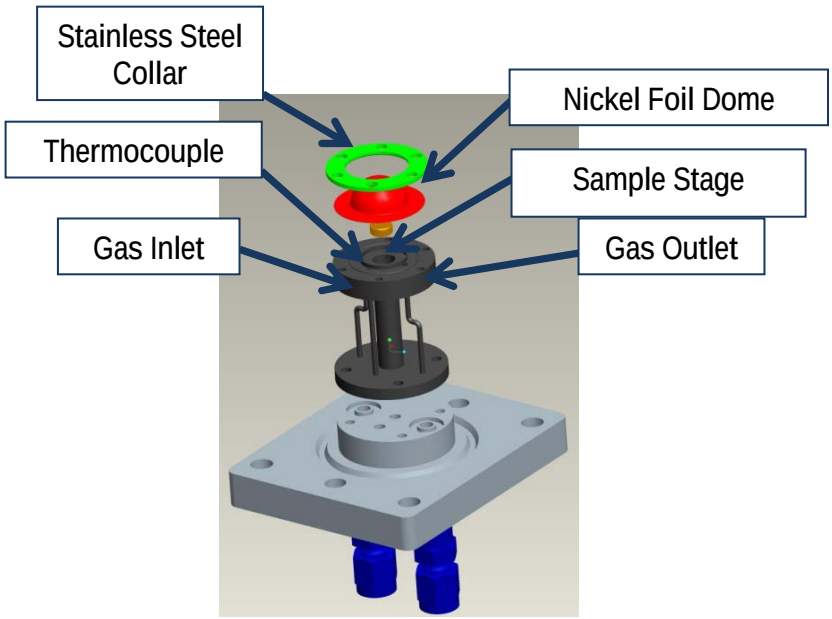


Figure 4.1. Custom designed environmental sample stage.

The U_3O_8 powder reactant was made by reacting depleted UO_2 pellets in air at 450°C for five hours. The starting α-U_3O_8 was characterized by XRD to ensure the product powder was single phase. The reaction product was characterized and found to have an average grain size of 15.6 μm by scanning electron microscope (SEM) imaging and BET specific surface area of 0.96 m^2/g. The product material was loaded into the sample holder and compressed gently to form a flat surface for diffraction. After insertion of the stage into the furnace, the system was brought to temperature in flowing N_2 at 50 sccm. After reaching the desired temperature, NO_2 was delivered at 50 sccm to the reaction enclosure and was subsequently scrubbed upon exiting the system.

In situ XRD measurements were conducted at temperatures of 195, 210, 235, and 250°C. Data were collected over time increments ranging between 2 and 10 minutes with the more frequent measurements being required for the more rapid reaction at higher

temperature. After reaction, the system was purged with nitrogen before cooling the system to avoid nitrate formation. An SEM image of the UO_3 product shows the particles' irregular shape (Figure 4.2).

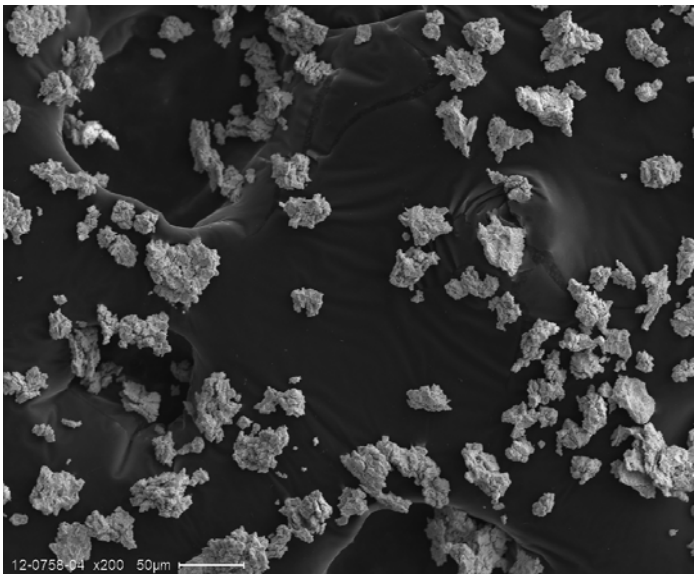


Figure 4.2. Scanning electron microscope image of ε-UO_3 product (200x).

4.3 Results and Discussion

Data were collected over a 2θ range of 20–40 degrees. Data was limited to this range due to both the background from fluorescent radiation and strong reflections from the nickel containment dome above a 2θ of 40 degrees. Within this 2θ range, there are several independent peaks for each phase. The collected patterns for the reaction of the α-U_3O_8 to ε-UO_3 in NO_2 at 195°C are shown in Figure 4.3.

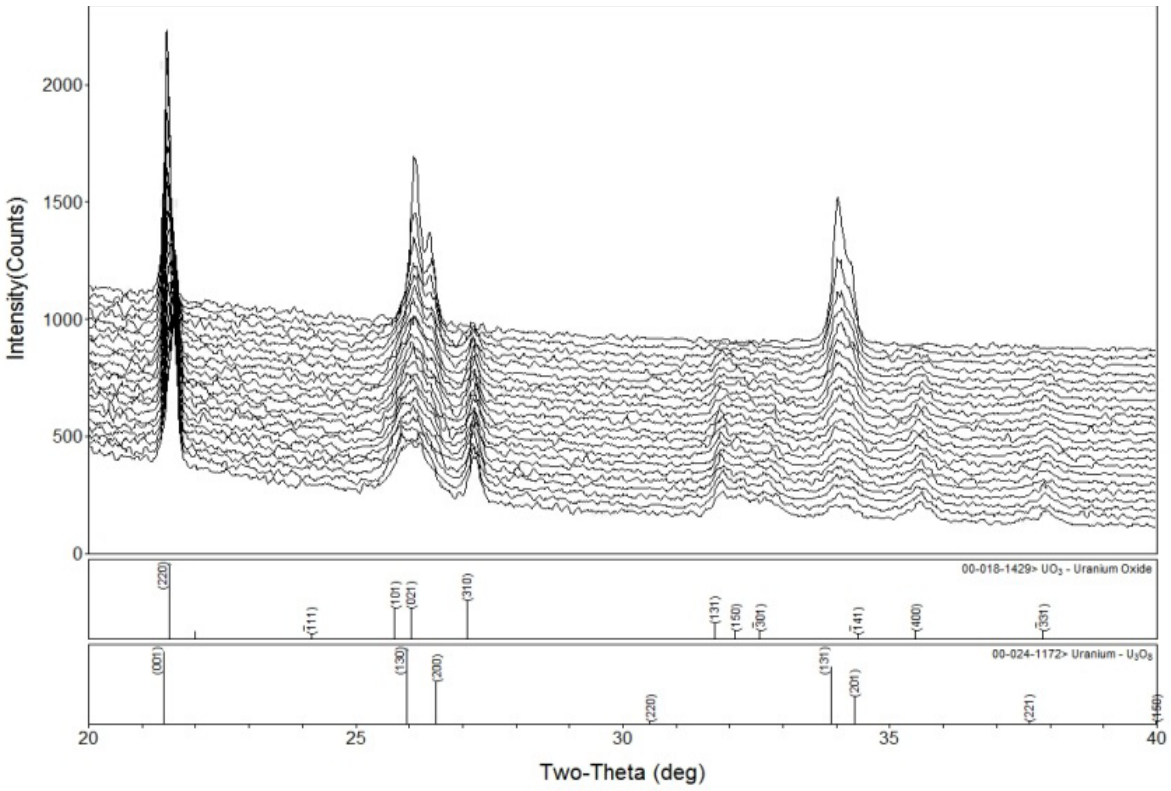


Figure 4.3. X-ray powder diffraction data showing the reaction of U_3O_8 to UO_3 at 195°C.

The Rietveld method was used to determine the refined phase fractions. Both the General Structural Analysis System (GSAS) [12] along with the EXPGUI [13] and the PANalytical software package Highscore were used for the Rietveld refinements. The starting U_3O_8 structure used for the refinements was that reported by Desgranges, *et al*. [14]. The UO_3 structure was determined from data collected from *ex situ* neutron and X-ray diffraction measurements. The triclinic UO_3 structure applied had lattice parameters of a = 4.0170(4), b = 3.8542(4), c = 4.1790(5) Å, α = 98.286(9), β = 90.42(1), and γ = 120.403(4)°. The refined phase fractions, as a function of time for each

conversion from α-U_3O_8, are shown in Figure 4.4. The initial reaction rate was observed to increase with temperature but conversion plateaued before reaching completion.

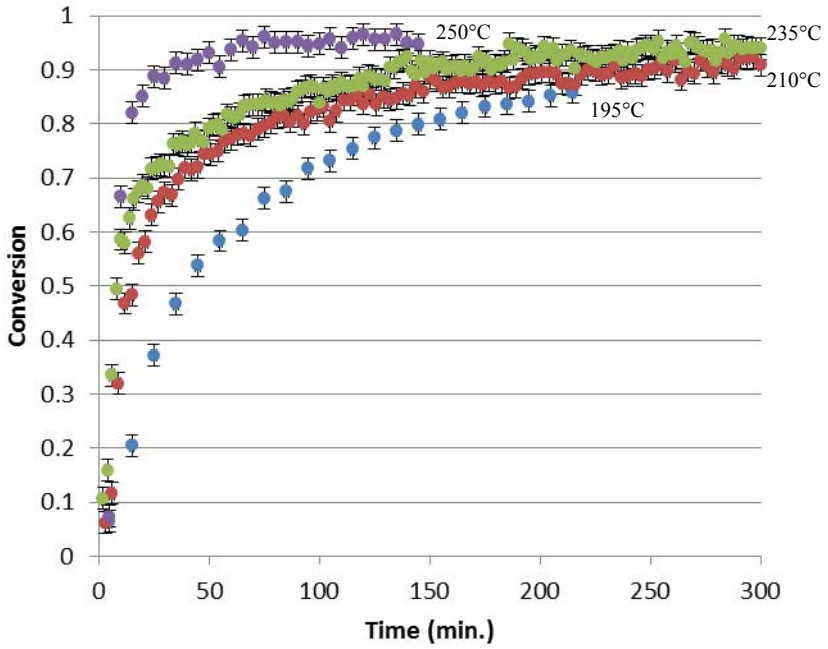


Figure 4.4. Refined UO_3 phase fractions at 195, 210, 235, and 250°C.

Initially, a first-order kinetic model was applied to the reaction curves as was proposed by Kobets and Klavsut. However, Figure 4.5 demonstrates a first-order kinetic model does not correlate with the data collected in this study, nor does it appear to correlate well to the raw data reported by Kobets and Klavsut [8]. However, from both Figure 4.5 and the conversion as a function of time plots, there appears to be two stages of reaction. As in other solid gas reactions, it is thought that initially the process may proceed by surface oxidation of the particles before a diffusion mechanism dominates [15, 16]. This diffusion of oxygen would be a result of the oxygen potential gradient

within the particles, which would induce the migration of oxygen into the particle from the surface.

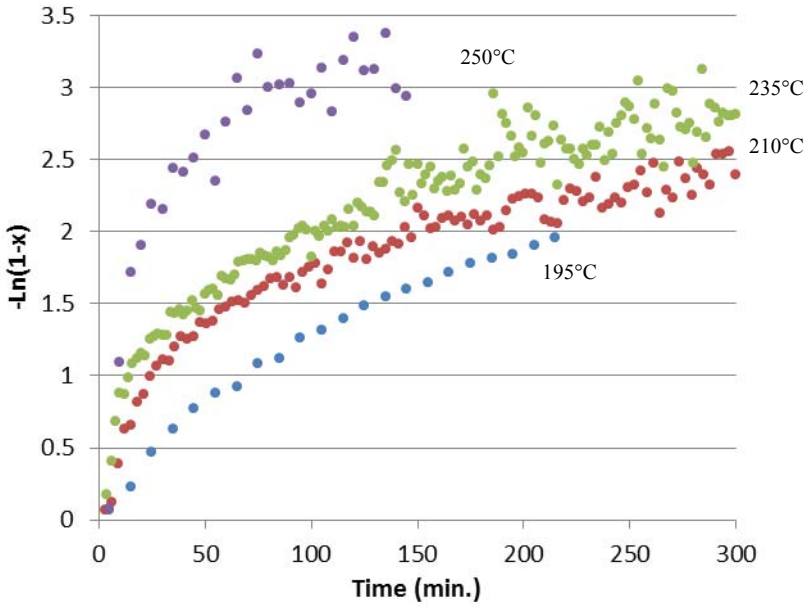


Figure 4.5. Semi-log plot to test for model plot for first-order kinetics for data collected.

Building from the two-stage model hypothesis, two modeling approaches were used. The reaction rate was modeled for the initial conversion range in which a first-order purely chemical reaction model fit. From this, an activation energy of 89.4 kJ mol^{-1} was estimated, which is within the error of the activation energies suggested for the overall reaction by Kobets and Klavsut [8]. While this result is in agreement with the previously reported activation energy, this model approach is not believed to be accurate for this gas-solid reaction. A shrinking core model is thought to be a more appropriate representation of the reaction process. As such, analysis of the data with this type of model approach led to the conclusion that the most suitable implementation is the use of

a kinetic model that accounts for the particle size, assumed to be spherical for the initial reaction, followed by a diffusion model. These models can be applied simultaneously if both phenomena are contributing significantly to limit the reaction rate; however, as previously described, surface reaction occurs quickly before the reaction plateaus and is controlled by diffusion of oxygen into the particles, thus simultaneous application is not appropriate. The reaction step-wise modeling, using the equations shown below, employs the convention where "A" is NO_2 and "B" is U_3O_8.

$$\text{A(fluid)} + b\text{B(solids)} \rightarrow \text{Products} \tag{4.3}$$

$$NO_2(g) + U_3O_8(s) \rightarrow 3UO_3(s) + NO(g) \tag{4.4}$$

The kinetic control model applies a first-order reaction rate but accounts for the surface area of the reactant particles where S_{rx} is the surface area, N is moles, r is radius of the particle, t is time, b is the solid reactant coefficient (1 in this case), and C is concentration. The reaction constant k'' is in units of cm/min.

$$-\frac{1}{S_{rx}}\frac{dN_B}{dt} = -\frac{b}{4\pi r^2}\frac{dN_A}{dt} = -bk''(C_A) \tag{4.5}$$

The diffusion model is derived similarly and employs Fick's first law in one dimension with an assumed effective diffusivity (D_{eff}) that does not change with conversion.

$$-\frac{dN_A}{dt} = b4\pi r^2 D_{eff}\frac{dC_A}{dr} \tag{4.6}$$

To determine the range over which each of these two mechanisms effectively control exclusively, the fractional time (t/τ) was analyzed, where τ is the time for complete reaction by a given mechanism, was used [16]. The ranges over which τ is constant can be used to determine where the respective mechanism is controlling. The dimensionless fractional time expressions are shown in Table 4.1 and τ for each mechanism where R is the initial average particle radius, r is the instantaneous radius, and x_B is the conversion.

Table 4.1. Model equations for surface and diffusion-controlled reaction.

Surface Reaction	Diffusion
$t = \frac{\rho_B}{bk''C_A}(R - r)$	$t = \frac{\rho_B R^2}{6bD_{eff}C_A}\left[1 - 3\left(\frac{r}{R}\right)^2 + 2\left(\frac{r}{R}\right)^3\right]$
$\tau = \frac{\rho_B R}{bk''C_A}$	$\tau = \frac{\rho_B R^2}{6bD_{eff}C_A}$
$\frac{t}{\tau} = 1 - (1 - x_B)^{\frac{1}{3}}$	$\frac{t}{\tau} = 1 - 3(1 - x_B)^{\frac{2}{3}} + 2(1 - x_B)$

The average effective diffusivities and reaction front progression rate k'' over the ranges identified were calculated for each of the reaction temperatures and are shown in Table 4.2.

Table 4.2. Effective diffusivities and front progression rates estimated by step-wise model approach.

	195°C	210°C	235°C	250°C
$D_{eff}(cm^2/s)$	$4.3\pm0.40 \times 10^{-8}$	$5.7\pm2.5 \times 10^{-8}$	$6.0\pm2.4 \times 10^{-8}$	$1.2\pm0.32 \times 10^{-7}$
k'' (cm/min)	$5.6\pm0.59 \times 10^{-6}$	$1.3 \pm0.33 \times 10^{-5}$	$3.0\pm0.54 \times 10^{-5}$	$3.3\pm0.83 \times 10^{-5}$

While there is a significant error introduced with the assumptions in this approach, the orders of magnitude and trends observed for both models are reasonable. Diffusivities of oxygen in other oxygen phases such as UO_{2+x} have been studied by more exact methods and found to have a significant dependence on oxygen content. Therefore, an exact comparison of the measured diffusivities is not possible. Diffusivity of O in UO_{2+x} has been reported to be 1.5×10^{-7} cm^2/s for diffusion at 727°C, while diffusivities in UO_2 for the same temperatures were on the order of 10^{-13} [17, 18]. Diffusivities for other oxide phases have been reported, such as for the formation of U_3O_7 where the diffusivity was found to be 9.85×10^{-9} cm^2/s [19]. A plot of the refined amount of conversion as a function of time along with the model prediction for reaction at 195°C is shown in Figure 4.6.

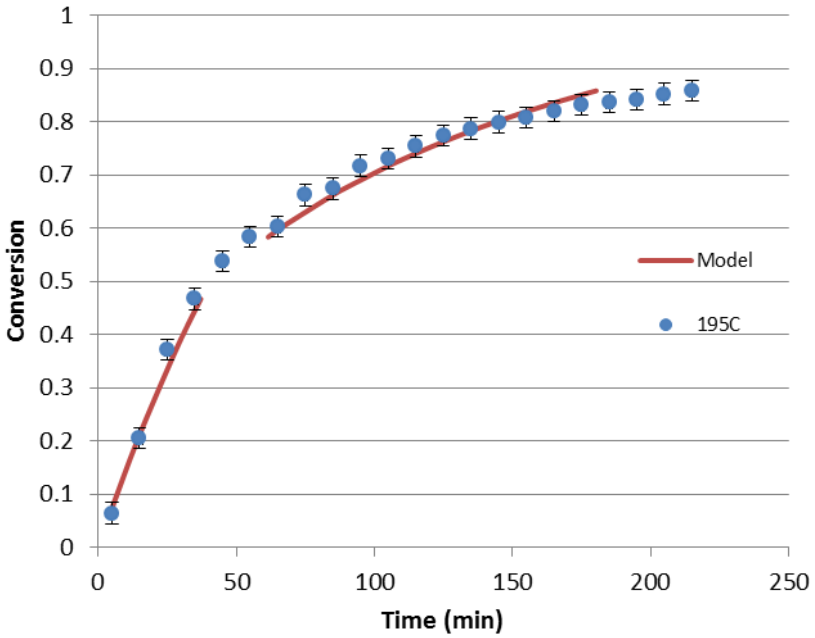


Figure 4.6. Refined amount of conversion as a function of time along with the model prediction for oxidation of U_3O_8 to UO_3 at 195°C.

Potential model improvements would include the use of a weighted particle size distribution and diffusion in multiple dimensions. Tests to aid in the verification of all assumptions used in the model are planned in which results from *ex situ* neutron diffraction experiments on partially reacted samples are compared with the results obtained using *in situ* XRD. These experiments will help to validate the existence of shrinking cores due to the ability of neutrons to penetrate through the bulk of the sample as compared with the surface measurements from the XRD technique. Additionally, reaction measurement experiments with sieved U_3O_8 powders of various particle sizes could help quantify the surface area dependence of reaction rate.

4.4 Conclusions

The use of a custom designed environmental sample stage to collect *in situ* XRD data, coupled with Rietveld refinements, allowed for the determination of quantitative phase fractions during the oxidation of α-U_3O_8 to ε-UO_3 by NO_2. The use of a triclinic unit cell and a newly proposed structure agreed well with the ε-UO_3 XRD pattern. The oxidation reaction of U_3O_8 to UO_3 using NO_2 as the oxidant cannot be accurately represented solely by a first-order chemical reaction rate model. Instead, a two-step reaction model, where the initial reaction is modeled by first-order kinetics with a surface area parameter and the subsequent step is represented using a diffusion model, is more suitable. From such an approach, the effective diffusivities and reaction front progression rates are estimated and found to increase with temperature, as expected. Future work to explore the kinetics at the stability limit may provide insight into the restructuring process.

Acknowledgments

This research has been sponsored in part by the Laboratory Directed Research and Development Program of Oak Ridge National Laboratory (ORNL) which is managed by UT-Battelle, LLC and by the U.S. Department of Energy through the Office of Nuclear Energy, Science and Technology's Fuel Cycle Research and Development Program. The work was performed at ORNL under the auspices of the Nuclear Security and Isotope Technology Division.

References

1. Goode, J.H., *Voloxidation - Removal of Volatile Fission Products from Spent LMFBR Fuels.* ORNL-TM-3723, Union Carbide Corporation, Oak Ridge National Laboratory, January 1973.

2. Goode, J.H., R.G. Stacy, and V.C.A. Vaughen, *Head-End Reprocessing Studies with H. B. Robinson-2 Fuel.* ORNL-TM-6037, Union Carbide Corporation, Oak Ridge National Laboratory, June 1978.

3. Goode, J.H., *et al*., *Comparison Studies of Head-End Reprocessing Using Three LWR Fuels.* ORNL-TM-7103, Union Carbide Corporation, Oak Ridge National Laboratory, June 1980.

4. Spencer, B.B., *et al*., *Voloxidation Processing of Kilogram Quantities of Used Nuclear Fuel*. in *Sixteenth Symposium on Separation Science and Technology for Energy Applications*. 2009. Gatlinburg, Tennessee.

5. Del Cul, G.D., *et al*., *Conceptual Design of a Simplified Head-End Process for the Recycling of Used Nuclear Fuel*. in *American Nuclear Society 2012 Annual Meeting*. 2012. Chicago, Illinois.

6. Song, K.C., *et al*., *Fractional release behavior of volatile and semivolatile fission products during a voloxidation and oreox treatment of spent PWR fuel.* Nuclear Technology, 2008. **162**(2): p. 158-168.

7. Hoekstra, H.R. and S. Siegel, *The Uranium-Oxygen System - U_3O_8-UO_3.* Journal of Inorganic & Nuclear Chemistry, 1961. **18**: p. 154-165.

8. Kobets, L.V. and G.N. Klavsut, *Behavior of U_3O_8 in Dissociating Gaseous Dinitrogen Tetroxide.* Soviet Radiochemistry, 1986. **28**(6): p. 657-660.

9. Kobets, L.V. and G.N. Klavsut, *Interaction of Uranium-Oxides with Dinitrogen Tetraoxide.* Uspekhi Khimii, 1990. **59**(8): p. 1251-1266.

10. McEachern, R.J., *et al*., *The influence of nitrogen dioxide on the oxidation of UO_2 in air at temperatures below 275°C.* Journal of Nuclear Materials, 1998. **255**(2-3): p. 234-242.

11. Katz, J.J. and D.M. Gruen, *Higher Oxides of the Actinide Elements - the Preparation of Np_3O_8.* Journal of the American Chemical Society, 1949. **71**(6): p. 2106-2112.

12. Larson, A.C. and R.B. Von Dreele, *General Structure Analysis System.* LAUR 86-748, Los Alamos National Laboratory, September 2009.

13. Toby, B.H., *EXPGUI, a graphical user interface for GSAS.* Journal of Applied Crystallography, 2001. **34**: p. 210-213.

14. Aykan, K. and A.W. Sleight, *Characterization of Mixed Uranium Antimony Oxides $USbO_5$ and USb_3O_{10}.* Journal of the American Ceramic Society, 1970. **53**(8): p. 427.

15. Yagi, S. and D. Kunii, *Fluidized-Solids Reactors with Continuous Solids Feed .3. Conversion in Experimental Fluidized-Solids Reactors.* Chemical Engineering Science, 1961. **16**(3-4): p. 380-391.

16. Levenspiel, O., *Chemical Reaction Engineering*. 3rd ed. 1999, New York: John Wiley & Sons.

17. Matzke, H., *Radiation-Damage in Crystalline Insulators, Oxides and Ceramic Nuclear-Fuels.* Radiation Effects and Defects in Solids, 1982. **64**(1-4): p. 3-33.

18. Matzke, H., *Diffusion-Processes in Nuclear-Fuels.* Journal of the Less-Common Metals, 1986. **121**: p. 537-564.

19. Aronson, S., R.B. Roof, and J. Belle, *Kinetic Study of the Oxidation of Uranium Dioxide.* Journal of Chemical Physics, 1957. **27**(1): p. 137-144.

CONCLUSIONS AND RECOMMENDATIONS

Conclusions

In order to develop an optimized voloxidation process, a more in-depth understanding of the oxidation mechanisms and the dependent parameters' relative effect on the rates of oxidation are needed. The research presented herein aid in closing a number of the gaps in our current understanding of oxidation processes associated with standard voloxidation and a voloxidation process implementing NO_2 as the oxidant. To accomplish this for standard voloxidation processes, parametric studies of the oxidation rate for clad and unclad UO_2 pellets were carried out using thermogravimetric analysis (TGA), X-ray diffraction (XRD), and neutron diffraction. Phenomenological models were developed to describe the reaction observations and allow for the extraction of specific physical parameters. From these studies, a number of conclusions can be drawn, with the most impactful being:

- The oxidation of UO_2 pellets at temperatures >350°C is controlled by the rate at which unreacted UO_2 is exposed from behind unspalled oxide product rather than solely by a nucleation and growth process.
- The oxidation rate of clad pellets has a linear reaction curve character if agitated; however, if not agitated, product (U_3O_8) plugging frequently occurs resulting in a significant reduction in reaction rate due to limiting oxygen diffusion to the reaction interface.
- For U_3O_8 plugging within cladding, the effective diffusivity decreases due to decreasing porosity as the reaction progresses.

- A two-stage model appears to be the best approach for modeling the case of unagitated clad UO_2 pellets that plug in which a first-order reaction rate is used for the initial linear segment, followed by a diffusion model with varying porosity.
- Oxygen concentration is the most impactful parameter on the oxidation rates at a given temperature, absent plugging of the cladding.
- Neutron diffraction can be used to axially map the reaction interface of partially reacted clad uranium oxide pellets and identify the position of the reaction interphase and its relative sharpness.
- No uranium oxide intermediates (U_4O_9/U_3O_7 or sub/hyper-stoichiometric variations) were observed at the reaction interface when investigated with a columnated neutron diffraction beam.

The study of the reaction of U_3O_8 with NO_2 by *ex situ* neutron and X-ray diffraction and *in situ* X-ray diffraction produced several impactful conclusions in the development and optimization of a NO_2 voloxidation process.

- A proposed triclinic ε-UO_3 structure was developed from neutron and X-ray diffraction data.
- A sample stage using a thin nickel foil containment dome can be effectively employed for the study of the reaction of uranium compounds with highly reactive gases.

- U_3O_8 converts to ε-UO_3 in a NO_2 environment at temperatures of 195, 210, 235, and 250°C with increasing kinetics and conversion with increasing temperature.
- The ε-UO_3 polymorph readily forms hydrates at room temperature.
- The reaction rate likely proceeds by a two-stage mechanism in which surface oxidation occurs to a temperature dependent depth, and is followed by diffusion of oxygen into the grains.

Recommendations

While these studies help in resolving particular questions regarding the oxidation process for voloxidation methods, there remains opportunity for further improvement and more detailed verification on these findings.

The work presented in Chapters 3 and 4 gives new insight into the controlling phenomena for standard voloxidation and their relative impact with variation of parameters; further testing with actual used fuel is necessary to define the impact of additional variables as well as to determine the variability among replicate samples. In addition, a verified model of the crystalline structure change-induced cracking, coupled with a model which accounts for the mechanical fracturing of the oxide at the interface, would likely prove to be the most useful simulation for voloxidation systems, as agitation would certainly be employed to avoid the diffusion-controlled reaction demonstrated in this work. For phase mapping, micro-XRD could likely provide greater resolution and clarification of the presence of intermediate uranium oxides at temperatures >400°C.

The studies reported in Chapter 5, where the oxidation rates and controlling phenomena are proposed for the reaction of U_3O_8 to ε-UO_3 by NO_2 oxidation, provide a foundation on which additional work can build. The proposed shrinking core process, by which the oxide is formed, could be further verified by neutron and XRD measurements of partially reacted samples as neutrons penetrate deeper into the grains than Cu Kα X-rays. Likely, this will be more conclusive for larger grain samples and Mo Kα measurement comparisons. It is also recommended that future studies determine the thermal precise stability range of ε-UO_3 and the exact decomposition products.

VITA

Jared Allen Johnson was born in Flint, Michigan, to Mark and Karen Johnson. Jared resided mostly in Michigan until 1993 when he moved with his parents and brother, Nick Johnson, to Spring Hill, Tennessee, where he graduated from Spring Hill High School in 2003 in the top 10 of his class.

Jared then attended the University of Tennessee where he majored in Chemical Engineering and minored in both Materials Science and Chemistry. While at the University of Tennessee, Jared conducted research in Dr. Robert Counce's, his main advisor, laboratory where he studied the thermodynamic modeling of liquid hydration for particular ions and the behavior of acetic acid formed from acetohydroxamic acid in organic solvents, as it applies to used nuclear fuel reprocessing. Jared was a Lead Co-op Ambassador while at Tennessee and co-oped for four semesters [Kimberly-Clark (3) and Dow Chemical (1)]. In his senior year, Jared served as president of the University of Tennessee chapter of the American Institute of Chemical Engineers (AIChE). Jared graduated Summa cum Laude from the University of Tennessee in 2008.

Upon graduation from the University of Tennessee, Jared accepted an offer to work at Oak Ridge National Laboratory (ORNL) as a radiochemical engineer in June of 2008. Jared currently works at the Radiochemical Engineering Development Center where he has supported and overseen a variety of projects in the areas of used nuclear fuel reprocessing and isotope production. While employed at ORNL, Jared received his Masters in Chemical Engineering in 2010 under the advising of Dr. Robert Counce.

Jared graduated with his Ph.D. in Chemical Engineering from the University of Tennessee, Knoxville in May of 2013.